Optimisation of the microstructure and mechanical properties of DP800 strip steel.

Yu, Xin

Optimisation of the Microstructure and Mechanical Properties of DP800 Strip Steel

Xin Yu

Master of Philosophy (MPhil) Thesis

Academic Supervisor: Dr. G. Fourlaris
Materials Research Centre
School of Engineering
University of Wales Swansea

Materials Research Centre
School of Engineering
University of Wales Swansea
Singleton Park
Swansea
SA2 8PP

DECLARATION

This work has not previously been accepted in substance for any degree and is not being concurrently submitted in candidature for any degree.

Signed _____ (Candidate)
Date _____

STATEMENT 1

This thesis is the result of my own investigations, except where otherwise stated.

Other sources are acknowledged by footnotes giving explicit references. A bibliography is appended.

Signed _____ (Candidate)
Date _____

STATEMENT 2

I hereby give consent for my thesis, if accepted, to be available for photocopying and for inter-library loans, and for the title and summary to be made available to outside organisations.

Signed _____ (Candidate)
Date _____

CONTENTS

ACKNOWLEDGEMENTS

I would like to express my deep and sincere gratitude to my supervisor, Dr. George Fourlaris. His wide knowledge and his logical way of thinking have been of great value for me. His understanding, encouraging and personal guidance have provided a good basis for the present thesis.

Special thanks to my colleague Mr S.W Ooi for his invaluable help in the use of experiment facilities.

Finally, I would like to express my thanks to my parents for their unselfish support and encouragement throughout my life.

LIST OF TABLES

LIST OF FIGURES

ABSTRACT

Dual phase strip steels are of interest to the automotive industry, due to the excellent combination of mechanical properties, attributed to their microstructure consisting mainly of ferrite and martensite. Dual phase steels are an excellent choice for applications, when low yield strength, high tensile strength, continuous yielding, and good uniform elongation are required. The soft ferrite matrix provides high elongation values, while the hard martensite dispersion offers a high tensile strength.

The present investigation was undertaken to study the effect of the annealing parameters (temperature, soaking time and cooling rate) on the microstructure and mechanical properties of DP800 dual phase strip steel and to quantify the effect of second phase formation on the mechanical properties. Finally, to assess the optimum heat-treatment parameters, which should be applied to optimise the microstructure and mechanical properties in DP800 strip steels.

Samples were annealed within the temperature range of 775°C to 875°C, for times ranging from 270s to 450s, followed by either water quenching, oil quenching or air-cooling.

The techniques used to study the presence of second phase formation and to fully characterise them involved light optical microscopy (LOM) and scanning electron microscopy (SEM). The mechanical properties, such as the tensile properties and hardness were subsequently measured on as received and heat treated samples.

The cooling rate from the intercritical annealing temperatures was found to be the most important factor influencing the microstructure developed during the heat treatment applied on DP800 samples. Higher intercritical annealing temperatures and longer soaking times can increase the volume fraction of the hard second phase as well as, causing a frequent occurrence of brittle fracture.

It was deduced that for DP800 samples intercritically annealed at 775°C for 330s, followed by water quenching, the optimum mechanical properties are obtained among

all tested samples. These intercritically modified DP800 samples exhibited a yield strength of 477MPa, a tensile strength of 816MPa, while retaining a reasonable elongation of 16% and a ratio of $\delta_{0.2\%}$/UTS of approximate 0.58.

1.0. INTRODUCTION

Advances in materials technology are allowing suppliers to meet three of the biggest concerns with carmakers--reducing vehicle weight, lowering costs and improving fuel efficiency [1-5]. This is achieved without compromising vehicle safety and overall performance. Dual phase steels provide carmakers with an opportunity to meet both targets. Dual phase strip steels are of interest to the automotive industry, due to their excellent combination of mechanical properties, a result attributed to their microstructure consisting mainly of ferrite and martensite. Dual phase steels are an excellent choice for applications where low yield strength, high tensile strength, continuous yielding, and good uniform elongation are required, permitting the down gauging of automotive components, resulting in lightweight vehicles (environmentally friendly automotives) [6-9]. The soft ferrite matrix provides high elongation values, while the hard martensite dispersion offers a high tensile strength. The name "dual phase" was coined to signify a ferrite-martensite microstructure, the martensite content usually being in the range of 15%-25%. Several commercial dual-phase steel grades deviate substantially though from a strictly ferrite-martensite combination and in fact the second phase is actually a complex mixture of martensite, retained austenite, and bainite [2, 10]. Generally, the martensite volume fraction in dual phase steel is retained at about 20% for good formability [11].

The dual phase microstructure is obtained by cooling steels with suitable composition from the intercritical temperature range (between A_{r1} and A_{r3}) at a rate sufficient for the transformation of austenite islands to martensite. Clearly, the chemical composition of the steel is of major importance in determining the thermal reference points, and in combination with kinetic factors, dictate the proportion of austenite formed at a particular intercritical temperature. The bulk composition will also contribute to the hardenability of the austenite phase formed. With this compositional flexibility, dual phase steels can be produced in cold rolled gauges by either

continuous and batch annealing in addition to a thermal production by controlled cooling on the hot mill run-out table [12].

The purpose of this thesis is to present results on the optimization of dual phase microstructures achieved with heat treatments and their effect on the mechanical properties of a dual phase grade with a nominal tensile strength of 800 MPa (DP800). Light optical microscopy (LOM) and scanning electron microscopy (SEM), using either secondary or back-scattered electron imaging were employed to fully characterize the modified via heat treatment microstructures. The mechanical properties of as received and modified via heat treatment material were assessed via hardness and tensile testing.

The modification of the DP800 microstructure could greatly affect the mechanical characteristics of dual phase strip steel grades. Samples were heat treated, for various periods of time, within the temperature range from 775°C to 875°C, followed by cooling to room temperature using a variety of cooling rates, such as water quench, oil quench and air cooling in order to study the effect of second phase formation and the influence of chosen heat-treatment parameters on the mechanical properties of DP800 samples. This study resulted in a series of modified DP microstructures. It has been possible by adopting relative simple heat treatment cycles to significantly modify the initial DP microstructure and produce an enhanced (in terms of its mechanical properties) DP800 strip steel product. The enhanced performance of the modified DP800 grade was attributed to the particular characteristics of the distribution of the second phase hard microconstituent in the predominant soft ferritic matrix.

2.0. AIMS

This study has been undertaken to achieve the following objectives,

1) To study the effect of the annealing parameters (temperature, soaking time and cooling rate) on the microstructures and mechanical properties of DP800 dual phase strip steel.

2) To quantify the effect of second phase formation on the mechanical properties of heat-treated DP800 strip steel.

3) To define the optimum heat-treatment parameters, which should be applied to optimize the microstructure and mechanical properties in DP800 strip steels.

3.0. LITERATURE REVIEW

3.1. Historical Developments

For the last 70 years, mild steel was the king of the hill. But today, it is getting to be a horserace between materials [13].

The last thirty years has seen a dramatic increase in the utilization of high strength steels in the automotive industry, while more recently, increased safety awareness has led to the use of high strength steels for improvements in crashworthiness. In view of accessories, cars become more equipped with antilock braking systems, air conditioning, air bags, etc., so a reduction of the total weight can only be obtained by a weight optimization of the structural parts by lightweight construction [5]. To achieve this demanding target different mechanisms for strengthening of the ferrite matrix are used separately or in combination, such as solid solution hardening, precipitation hardening, and grain refinement.

3.2. Dual Phase Steels

When the first patent of dual-phase steel was filed in the USA in 1968, it did not attract significant attention from the metallurgy industry in the USA. The great potential of dual-phase steels only was reestablished in 1975, arising from Furukawa's comprehensive research report on the microstructures, chemical compositions, and mechanical properties of dual-phase steels. In the subsequent years, variable grades of dual-phase steels were produced in the USA and Japan, involving continuous annealing and batch annealing technology, for the down gauging of body-in-white structures of automobiles [14]. Dual-phase steel is currently a material of commercial interest for key automotive applications. It's a new class of high-strength low-alloy steel characterized by a microstructure consisting of a dispersion of hard martensite

particles in a soft, ductile ferrite matrix. The term "dual phase" refers to the presence of essentially two phases, ferrite and martensite, in the microstructure, although small amounts of bainite, pearlite, and retained austenite may also be present. The interest originates from the demand for lighter, more fuel-efficient vehicles and the fact that the dual-phase steels combine higher strength and higher ductility as compared with ferritic–pearlitic steels, as can be seen in Fig 3.1. These are produced by intercritical annealing followed by quenching to transform the austenite to martensite. The carbon either free or combined with iron represents a major factor, which affects the strength of ferrite and martensite in dual-phase steels [15].

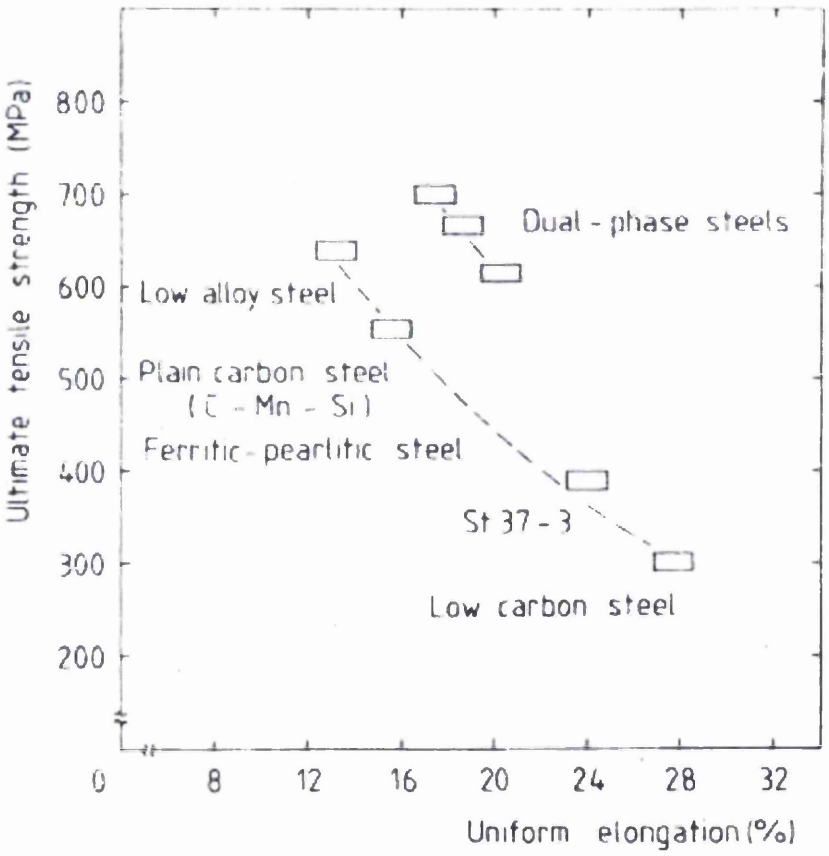

Fig.3.1: Strength-ductility relationship of dual-phase steels as compared with ferritic-pearlitic steels [15].

Dual phase strip steels have a number of unique properties, which include (1) continuous yielding behavior (no yield point), (2) a low 0.2% offset yield strength, (3) a high tensile strength, (4) a high work-hardening rate, and (5) an unusually high uniform and total elongation [9]. The high work-hardening rate, combined with the high uniform elongation of these steels, gives them formability equivalent to that of much lower strength sheet steels. Balliger et al. [16] consider that optimum properties are obtained in DP products when the ratio of proof stress and tensile strength is around 0.6. As a result of their interesting characteristics, DP steel grades are an attractive material for weight-saving applications in automobiles [6, 16].

The absence of a yield point phenomenon in DP grades is due to the combination of high residual stresses and a high mobile dislocation density causing plastic flow to occur easily at low plastic strains [17-19]. Since plastic flow begins simultaneously at many sites throughout the specimen, discontinuous yielding is suppressed [20].

Large scale production of ferritic-martensitic dual-phase steels involves annealing of a cold-rolled ferritic-pearlitic steel at 800°C ("intercritical annealing") and then quenching to room temperature, also referred to as intermediate quenching [21].

3.2.1. Creation of the Dual Phase Microstructure

The dual phase microstructure is produced by cooling steels with a suitable composition from the two-phase ($\alpha+\gamma$) region at a sufficient rate to transform the austenite island dispersions to martensite [3]. It may be produced by one of three routes. In the first, the dual phase structure is produced directly in the as-hot rolled coil without requiring further heat treatment. But the steel composition required consists of silicon, manganese, chromium, molybdenum additions to generate a specific CCT (Continuous Cooling Transformation) behavior. Alternatively, the structure is produced by continuously annealing either hot or cold rolled strip at a temperature in the two-phase ($\alpha+\gamma$) region followed by suitably cooling at a sufficient

rate to ensure that austenite present at the intercritical annealing temperature transforms substantially to martensite rather than to pearlite or bainite. The third approach is using the batch annealing sequence. This requires steel compositions to provide the possibility of forming martensite upon slow cooling from the batch annealing temperature [16]. Most recent industrial production has concentrated on using continuous-annealing techniques, since this results in higher production rates, better uniformity of properties, and the possibility to use lower alloy steels. However, batch annealing has also been considered where continuous-annealing facilities are not available.

From the lever rule, as can be seen in Figure.3.2, for a given carbon content, the amount of austenite will increase with increasing intercritical temperature, becoming equal to 100 percent at the Ar3 temperature. Similarly, for any given intercritical temperature, the amount of austenite will increase with increasing carbon content, becoming equal to 100 percent at a carbon content corresponding to the ($\gamma/\alpha+\gamma$) phase boundary.

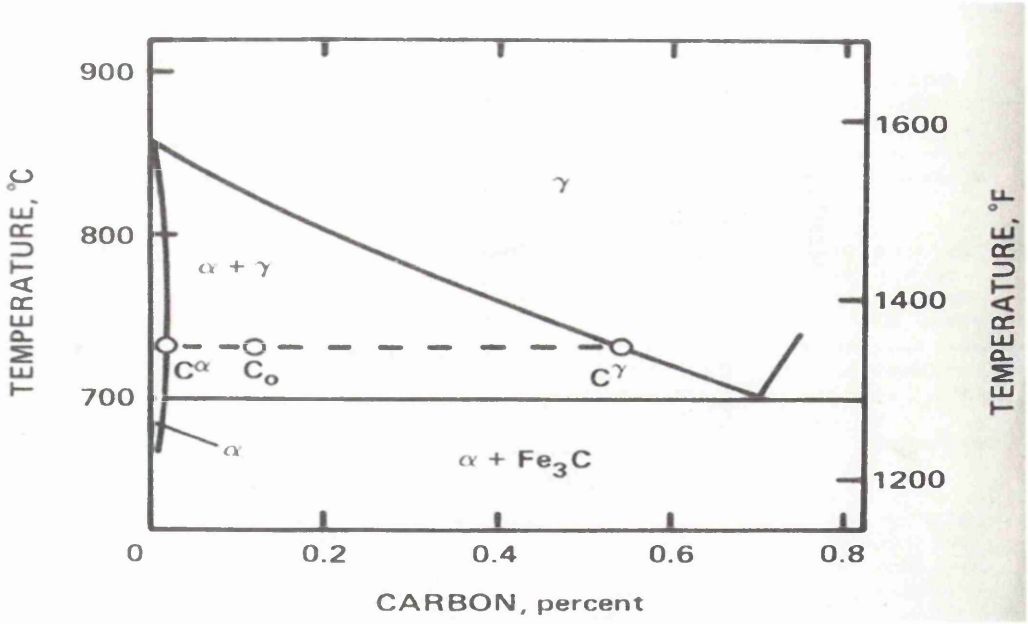

Fig.3.2: Phase diagram for 1.5M steel (paraequilibrium conditions) [6].

The transformation of austenite following intercritical annealing is controlled by the annealing temperature, the soaking time and the cooling path. The effects of annealing temperature and cooling rate are shown in Figure 3.3, where it can be seen that, at high cooling rates, virtually all austenite transforms to martensite, while as the cooling rate lowers, the proportion of non-martensitic transformation products increases. Martensite forms in the austenite grains upon quenching from the annealing temperature, maintaining the matrix-inclusion topology, i.e. martensite inclusions embedded in a matrix of ferrite. By varying the cooling rate following the intercritical annealing, the amount of martensite can be adjusted.

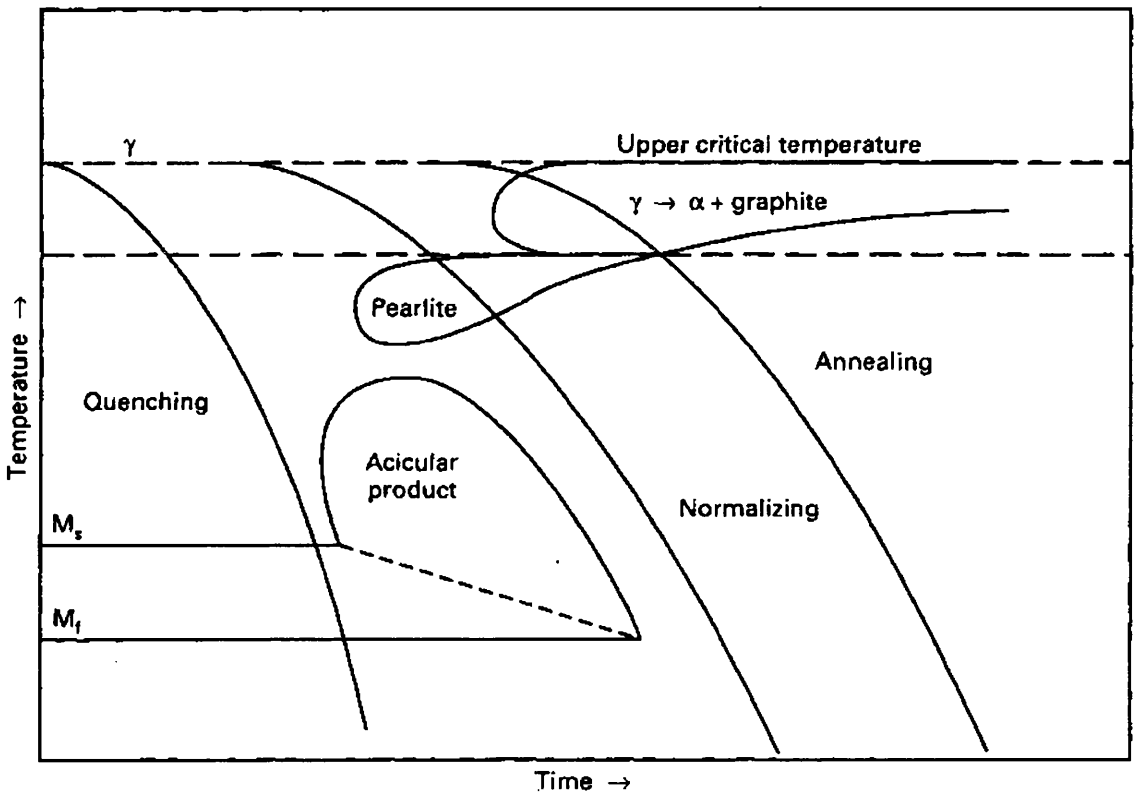

Fig.3.3: CCT diagram showing annealing, normalizing, and quenching. M_s, martensite start; M_f, martensite finish [22].

The start temperature of martensitic transformation M_s, which describes the thermodynamic stability of retained austenite is defined by the empirically developed

formula of Andrews [23]:

M_s=539-423C-30.4Mn-17.7Ni-12.1Cr-7.5Mo

The lower the M_s temperature, the more stable the retained austenite is.

3.2.2. Production and Processing of Dual Phase Steels

Dual-phase steels can be produced by intercritical heat treatment with either continuous-annealing or box-annealing techniques, and in the as-rolled condition. The composition of a dual phase product is selected on the basis of the production facility available which dictates the cooling pattern available for the production of the desired microstructure e.g. batch annealing will only allow very slow cooling (~20°C/hr) from the intercritical temperature, whereas continuous annealing allows more rapid cooling (50-1000°C/s) [6].

3.2.2.1. Continuous-annealing Processing of Dual Phase Strip Steels

In the continuous-annealing approach, the steel is heated for a short time into the intercritical temperature region to form ferrite-austenite mixtures, soaked for a sufficient time, and then followed by accelerated cooling (e.g. water quenching) to transform the austenite phase into martensite. The heating and soaking time are decided by the shape of the steel, which may affect the heat transform, as well as the soaking temperature. The actual cooling rate is dependent on the composition of the steel and also its thickness. In Figure.3.4, these terms are illustrated on a TTT diagram and a "window" of cooling rates at which dual phase microstructures can be produced is shown.

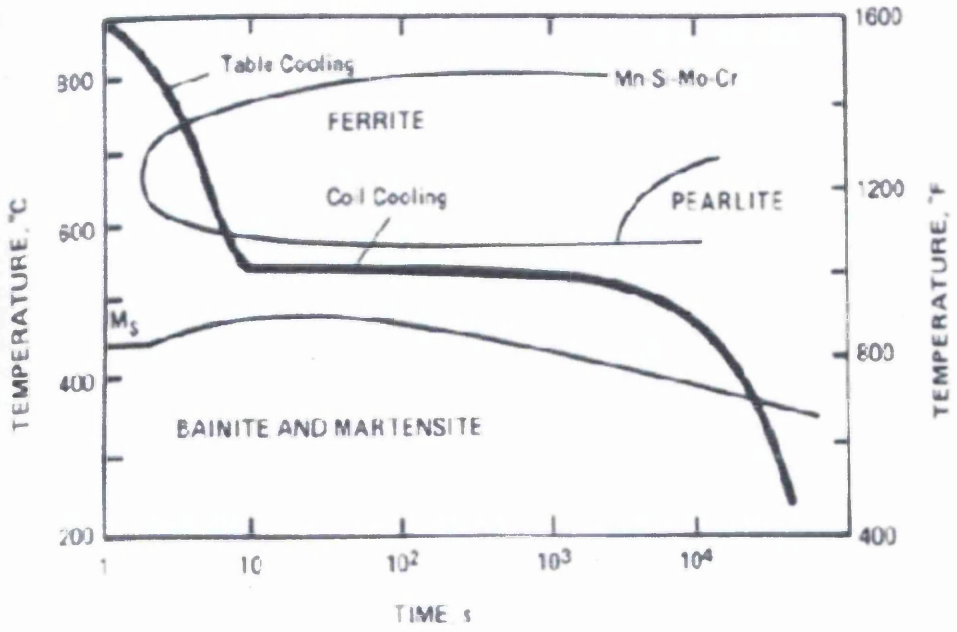

Fig.3.4: Time-Temperature-Transformation curve of a typical as hot rolled dual phase steel [6].

3.2.2.2. Batch-annealing Processing of Dual Phase Strip Steels

In the batch-annealing approach, a similar heat treatment is performed, but the annealing times are much longer (~3h) and the cooling rates are much slower (~20°C/h). For this slow cooling rate, much higher alloy steels are required to achieve the desired hardenability and transform kinetics.

3.2.2.3. As-Rolled Dual Phase Steels

The possibility of obtaining the dual phase microstructure without heat treatment is attractive with respect to energy savings. Therefore, in addition to the use of

intercritical heat treatment, dual-phase steels have been produced in the as-rolled condition by carefully controlling the continuous-cooling transformation characteristics of the steel. This generally requires the addition of substantial amounts of Si, Cr, and Mo in addition to about 1.0%wt Mn. A typical as-rolled dual-phase-steel composition is given in Table 3.1.

Table 3.1: Typical Dual-Phase Steel Compositions (wt %) [24].

Production Technique	C	Mn	Si	Cr	Mo	V	Al	N	S	P	Other
Continuous Annealing, Hot-Rolled gauges	0.12	1.55	0.61	-	-	0.06	0.05	0.007	0.006	0.015	Rare Earth
	0.11	1.43	0.58	0.12	0.08	-	0.04	0.007	0.012	0.015	-
Continuous Annealing, Cold-Rolled gauges	0.11	1.20	0.40	-	-	-	0.04	-	0.005	0.015	-
Box Annealing	≤0.13	≤2.20	≤1.50	≤1.00	-	-	<0.08	-	≤0.020	≤0.02	Rare Earth
As-Rolled	0.06	0.90	1.35	0.50	0.35	-	0.03	-	0.010	0.010	Rare Earth

3.2.3. Applications and Limitations of Dual Phase Steels

Currently these steels are most commonly used in structural applications where they have replaced more conventional HSLA steels. They offer a great opportunity for part weight reduction. The improved formability, capacity to absorb crash energy, and ability to resist fatigue has driven this substitution. Today's applications include front and rear rails, crush cans, rocker reinforcements, b/c pillar reinforcements, cowl inner/outer, back panels, cross members, bumpers, and door intrusion beams [24]. Naturally the more expensive use of dual phase steels is within the automotive sector. They are quickly becoming one of the most popular and versatile materials in today's automotive industry.

Limitations to the adoption of dual phase steels arise partly from the need for capital investment in versatile continuous annealing facilities in order to produce reliable, lean chemistry, dual phase steels. This was a particular problem in the USA and Europe at the end of the intensive development phase of the late seventies and early eighties where recession prevented heavy investment. Conversely, in Japan, where continuous annealing facilities were available at that time, a proliferation of commercial dual phase grades exists today. Batch annealed dual phase steels can be produced using very high Mn levels (>2.5wt %) but these have inherent property variability. As-rolled dual phase steels can also be produced but this incurs the problems of expensive alloying, tighter control of hot rolling conditions, variability in properties due to mill temperature control and the restriction to hot rolled gauges [12].

3.3. Role of Alloying Elements in Dual Phase Steels

Alloying additions will modify the relative amounts and compositions of the ferrite and martensite phases. In addition, they will modify the morphology of second phases.

Each alloying element has a specific effect on the properties of DP steels. They may prevent the precipitation of cementite, affect carbon partition, or raise the austenite non-recrystallization temperature and stabilize austenite.

3.3.1. Silicon

Silicon strongly slows down or completely prevents the precipitation of cementite, which would usually occur during the bainite formation and therefore leads to a high carbon content in retained austenite [4, 25]. This may stabilize the retained austenite. Indeed, the austenite carbon content increases in both steels up to a level that corresponds to the T_0-curve. Once this upper limit is attained, the bainite transformation cannot further proceed, and the transformation is said to be 'incomplete'. This behavior corresponds to the typical behavior of high silicon steels in which cementite precipitation is totally inhibited. Si can increase carbon concentration in the retained austenite when the Si content is set at critical value. M. H. Saleh, et al. [3] reported, increase in silicon content between 0.24 and 1.44% wt increased the amount of retained austenite significantly. When this certain value is passed in one chosen steel, further increase in addition Si will directly reduced the stability of the retained austenite. Meanwhile, high Si content could give difficulties in the welding process [26]. The increase in yield strength with increasing silicon content is believed to be due to solid solution hardening of ferrite [7].

3.3.2. Aluminum

In order to reduce surface quality problems during strip galvanizing, silicon is partially replaced by aluminum, which has a similar but weaker effect concerning the inhibition of cementite formation, and additionally strongly increases the bainite formation kinetics [27]. As calculated by thermodynamic modeling software for a C content of 0.2wt%, the austenitic phase region even disappear for a total substitution of Si by Al [7]. Therefore, the Si content can only be partially replaced by Al.

3.3.3. Phosphorus

Solid solution hardening by aluminum of DP steels is significantly lower than that of silicon. Therefore, phosphorus, which also inhibits cementite formation, is added since it has a strong solid solution hardening effect on ferrite [7].

3.3.4. Manganese

Manganese is added to slow down the pearlite formation, thus allowing a lower critical cooling rate to be applied. Manganese additions also stabilize austenite among the bainite transformation [28]. Moreover, manganese, which concentrates in austenite via partitioning, leads to a significant solid-solution hardening [29]. However, when Mn is added over an optimum level, the retardation of ferrite transformation would take place, resulting in a decrease of the soluble carbon and in the destabilization of retained austenite [7]. The complete effect of manganese partitioning on the mechanical properties of dual-phase steels is hard to define, since the variation of its partitioning with the annealing temperature and time also results in a change in martensite volume fraction and ferrite grain size. It is true though to say that manganese partitioning is beneficial to the strength and ductility of dual-phase steel.

Steel sheets containing high Mn find limited use for automobile components due to their low weldability [30].

3.3.5. Niobium

Niobium was originally added to steel to raise the austenite non-recrystallization temperature and enable the steel to be processed by a variety of temperature routes [31]. It is also well known that solute Nb increases austenite hardenability and decreases the M_s temperature by solid solution strengthening of the parent austenite. Therefore, for a given heat treatment cycle, austenite with more Nb in solution has a higher propensity to be retained or stabilized. This can be firstly related to the

inhibiting effect on the pearlite transformation and, secondly, through the presence of dissolved Nb leading to solid solution strengthening in the austenite, therefore reducing the M_s temperature [32].

3.3.6. Molybdenum

Molybdenum is also a ferrite former and lowers the bainitic start temperature [30, 33]. Addition of molybdenum has been found to be particularly beneficial in suppressing the pearlite transformation without preventing the formation of polygonal ferrite during cooling, over a wide rage of cooling rates [6].

3.3.7. Copper

The addition of copper is expected to contribute to the enhancement of formability of C-Si-Mn cold-rolled steel sheets, since copper, an austenite stabilizing element, works favorably for the formation of retained austenite, together with additional effects of solid solution strengthening of ferrite grains via precipitation strengthening through precipitation of a few nanometer sized ϵ-copper particles [34].

3.4. Role of Heat Treatment Parameters

3.4.1. Intercritical Temperature

During intercritical annealing, the formation of austenite has been studied in detail for carbon manganese steels and is found to occur in three stages [6]. Firstly, almost instantaneous nucleation of austenite takes place on pearlite or grain-boundary cementite particles, followed by rapid growth, until the carbide phase is dissolved. The austenite then grows slowly into ferrite at a rate controlled by austenite carbon

diffusion at high temperatures (~850°C) and manganese diffusion within ferrite or grain boundaries at low temperatures (~750°C). Finally, very slow final equilibrium of austenite and ferrite takes place, at a rate controlled by the diffusion of manganese in austenite. Since the formation of austenite from ferrite is diffusion-controlled phase transformation, the volume fraction of austenite and its coarseness increase with increasing soaking temperature and time. Partitioning of alloying elements does not approach equilibrium due to the inherently slow diffusion rates [1]. Carbon diffusion, on the other hand, is considerably more rapid but local concentration gradients may exist due to the effect of alloying inhomogeneity on diffusivity rates. The volume fraction of austenite formed is controlled by annealing temperature and time until equilibrium is reached.

When the intercritical annealing temperature is high, it is easier to get a higher volume fraction of austenite with sufficient annealing time. However, martensite forming upon cooling would be coarser. This could have an adverse effect on the mechanical properties.

3.4.2. Annealing Time

When the annealing time is not sufficient to establish equilibrium between austenite and ferrite, the amount of these two phases will change according to the time. However, a suitable annealing time must be chosen suitable for commercial purpose, which should be as short as possible, but long enough for the required phase transformation. Long annealing times are normally required to obtain complete manganese partitioning in order to increase the strength of the austenite phase and subsequently the martensite phase.

3.4.3. Cooling Rate

The required cooling rate can be obtained from the relevant TTT diagram (Fig.3.4). The cooling rate should cross the M_s temperature so as to obtain the desired

microstructure. The kinetic aspects of phase transformations are quite important. The metastable phase martensite can generally form with comparatively rapid cooling to ambient temperature, that is, when the diffusion of carbon and alloying elements is suppressed or limited to a very short range. Uninterrupted, rapid cooling is necessary to prevent decomposition of the austenite by diffusion processes, which would form such products as ferrite or pearlite. This mode of transformation kinetics is referred to as athermal (without thermal activation) to differentiate it from isothermal kinetics that characterize thermally activated diffusion-controlled transformations.

3.4.4. Tempering

Sometimes, intercritical annealing is followed by a tempering stage in the bainite transformation temperature range. During this tempering, part of the austenite transforms to bainite, whereas residual austenite may become sufficiently stabilized by carbon rejection from bainitic ferrite, preventing transformation to martensite during the final quenching to room temperature. Indeed, it is well known that a significant amount of austenite can be retained in bainitic steels, highly alloyed with silicon [35]. Normally the yield stress of DP grades increases with increasing tempering time, while the tensile strength decreases with increasing tempering time [33].

4.0. EXPERIMENTAL PROCEDURES

4.1. Experimental Materials

The experimental material used in the present study is an experimental DP800 dual phase steel having a strip thickness of 2mm. The chemical composition of the steel is presented in Table 4.1. Samples for heat treatments were cut into both small square coupons (25 x 25 x 2mm) suitable for subsequent optical and electron microscopy examination, while larger coupons (40 x 200 x 2mm) were prepared for subsequent tensile testing.

Table 4.1: Chemical composition (wt %) of DP800 dual phase steels studied.

C	Si	Mn	P	Ni	Al	Cr	Fe
0.112	0.445	1.52	0.012	0.039	0.043	0.027	97.802

4.2. Sample Preparation

4.2.1. Heat Treatments

Samples were annealing within the temperature rage of 775°C to 875°C, for times ranging from 270s to 450s, followed by either water quenching, or oil quenching or air-cooling.

4.2.2. Mounting

Following the various heat treatments, samples were subsequently mounted for metallographic observation. Standard cylindrical mount holders were used. Samples of larger width sufficiently balance as to be free standing were mounted without further support, whilst samples with thinner width were held in a small stainless steel clip to support and to ensure the surface to be examined remain parallel to the grinding plane during the mounting process. Castable materials consist of a resin and a hardener. The resin used was MetPrep Kleer-Set Type FF (Product code: 111081) and the hardener was MetPrep Kleer-Set Hardener (Product code: 111089)

4.2.3. Grinding

Grinding was performed initially using 240-, 320-, 600- then 1200- grit silicon carbides papers water-cooled. Before proceeding to the next grinding paper, the sample should be rotated 90°C between each step. In order to obtain and maintain a flat surface over the entire area, equal pressure was applied on the samples and avoiding any rocking motion that would produce uneven surface flatness on the surface, especially since grinding is being carried out by hand. Samples were carefully cleaned between each grinding steps to avoid contamination at the next step.

4.2.4. Polishing

After grinding, samples were rough polished using 6 and followed by 1 μm diamond impregnated polishing cloth. Polishing using the 1 μm diamond impregnated polishing cloth is the final step in producing a surface that is flat, scratch free and mirror-like in appearance. Such a surface is essential for subsequent accurate metallographic interpretation, both qualitative and quantitative. A lubricant compatible with the diamond abrasive is used to moisten the polishing cloth and reduce drag. Since polishing was carried out by hand, pressure applied should be moderate and firm to avoid any sample rocking and maintaining the surface flatness.

Samples are subsequently rinsed in flowing water and ethanol and dried under a stream of hot air. Samples should be carefully cleaned between each rough and final polishing step to avoid contamination at the next step.

4.2.5. Etching

A solution of 2% Nital was used to etch the specimens. The freshly prepared 2% Nital solution was poured carefully into a clean petri-dish and subsequently the mounted steel samples were immersed into the solution, using tongs to hold the sample securely. The etching was terminated when the surface of the samples appeared to be slightly dull. For most of the DP800 samples, the etching time is around 24 seconds. When the etching was completed, the sample was rinsed in flowing water and then rinsed with ethanol and dried under a stream of hot air.

4.3. Microstructural Characterization

4.3.1. Light Optical Microscopy (LOM)

After etching, all microstructures were examined on a Reichart (MeF3) Light Optical Microscope (LOM). Light optical microscopy was used to initially study the obtained microstructures by analysing the polished and etched surfaces. Light optical micrographs were then digitally recorded.

4.3.2. Scanning Electron Microscopy (SEM)

When the resolution of the light optical microscopy was insufficient for classification of the obtained microstructures, the scanning electron microscope (SEM) was employed, using either secondary or back-scattered electron imaging. The samples for the scanning electron microscopy were extracted from the mounting material used for optical metallography to avoid any charging effects. A Philips XL30 scanning electron

microscope was employed for the SEM examination.

4.4. Mechanical Testing

4.4.1. Tensile Testing

Tensile properties were measured on samples cut longitudinally from the rolling direction. Tensile testing was performed at room temperature using a 50KN Hounsfield tensile machine employing a cross head speed of 1mm/min. Tensile samples were prepared according to BS EN 10 002 – 1: 1990 (Tensile Testing of Metallic Materials-part 1: Method of Test at Ambient Temperatures). The tensile samples were machined into the required shape having a gauge length of 40mm and a width of 20mm.

4.4.2. Hardness Testing

Vickers hardness testing was carried out for the as received and heat treated samples using a 20kg load. The instrument uses a diamond square-based pyramid of 136° angle as the indenter, which gives geometrically similar impressions under differing loads. A square indent was thus produced, and the average diagonal lengths were measured and the hardness value was displayed in the control panel (Hv) of the instrument.

5.0. RESULTS AND DISCUSSION

5.1. Actual Time and Soaking Temperature

Experimentation has been carried out to define the minimum required time, at a given soaking temperature, for establishing an intercritical annealing temperature regime (Fig.5.1). In addition, the cooling rates in air, oil and water for a soaking temperature of 800°C (Fig.5.1) have been established.

It has been confirmed that the minimum time at a soaking temperature should be 210s, at which the samples' temperature is within 10°C less than the intended heat treatment temperature. Therefore, for experiments of a nominal duration of 270s the actual soaking time is 60s at the annealing temperature. Moreover, for nominal soaking times of 300s, 330s or 450s, the actual time at the soaking temperatures are 90s, 120s, and 240s respectively. The average soaking temperature is 747°C for a soaking temperature of 775°C. When the temperature is set to 800°C, 825°C, 850°C or 875°C, the actual temperature is 788°C, 791°C, 842°C or 860°C, respectively (The error is $\pm$ 5°C). However, when the soaking temperature was increased, the actual soaking time would be longer since a higher heating rate is required.

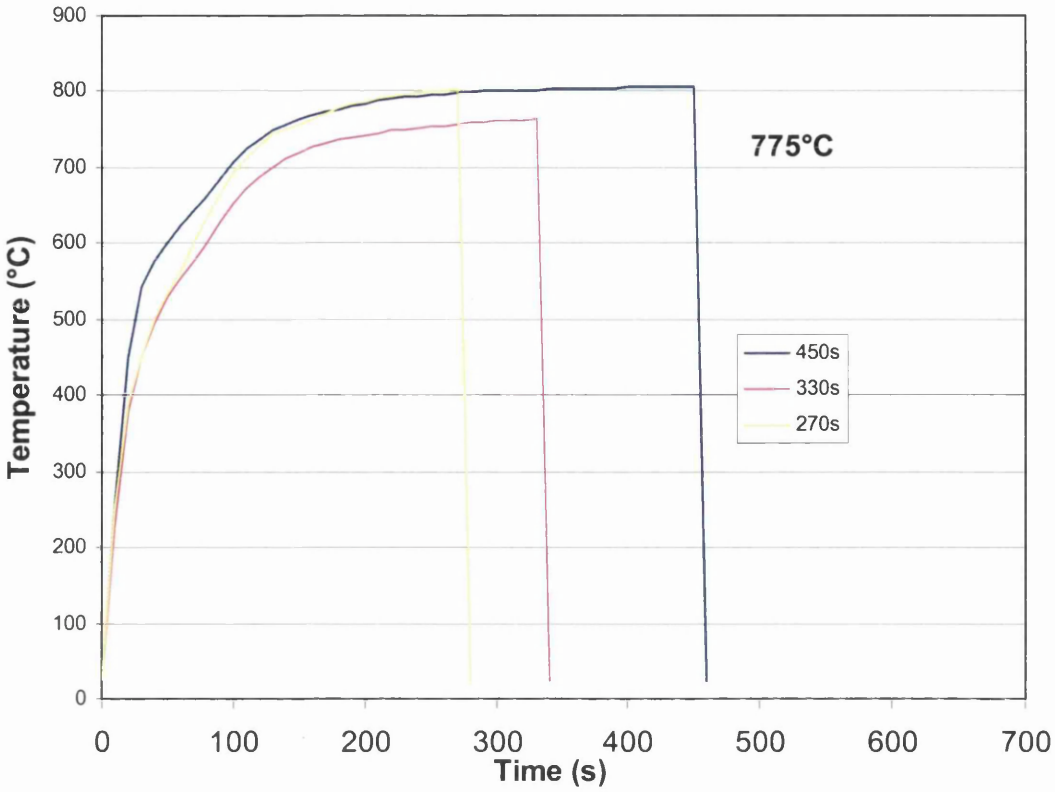
775°C
450s
330s
270s
Temperature (°C)
Time (s)
0
100
200
300
400
500
600
700
800
900

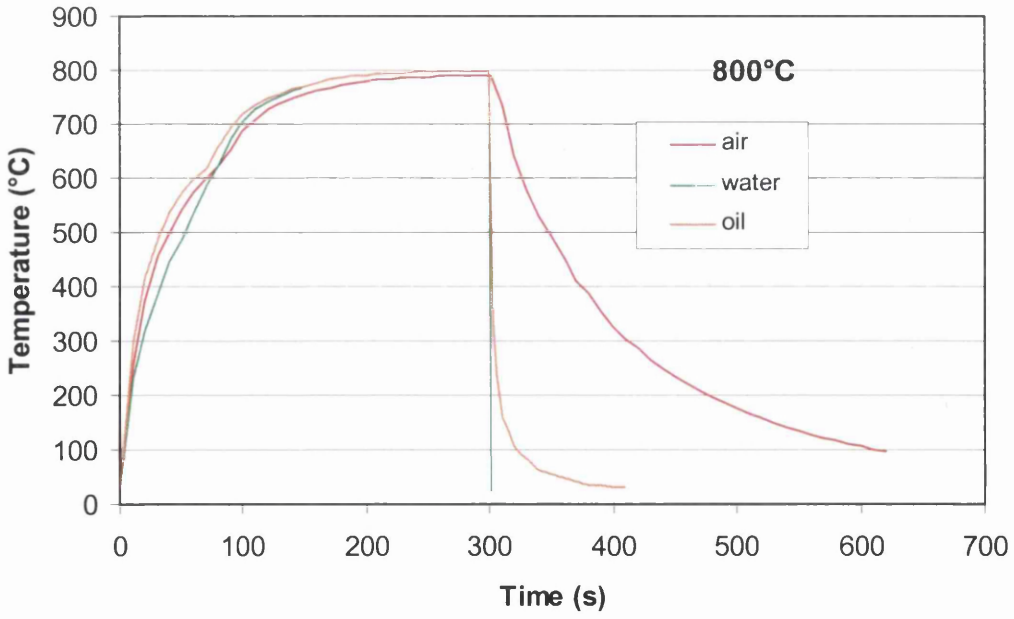
800°C
air
water
oil
Temperature (°C)
Time (s)
0
100
200
300
400
500
600
700
800
900

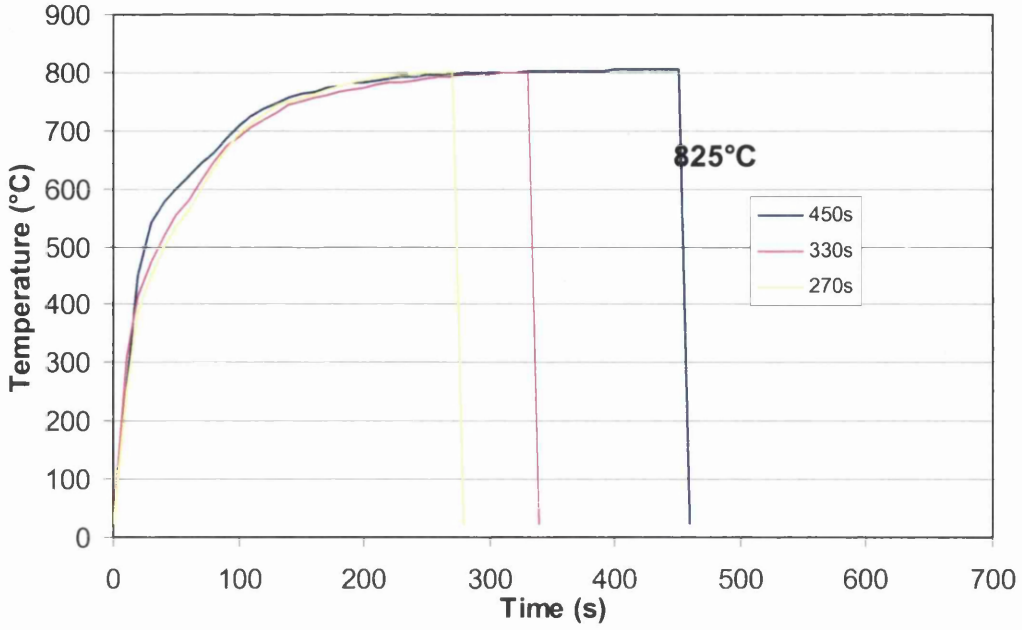
900
800
700
600
500
400
300
200
100
0
Temperature (°C)
825°C
450s
330s
270s
0
100
200
300
400
500
600
700
Time (s)

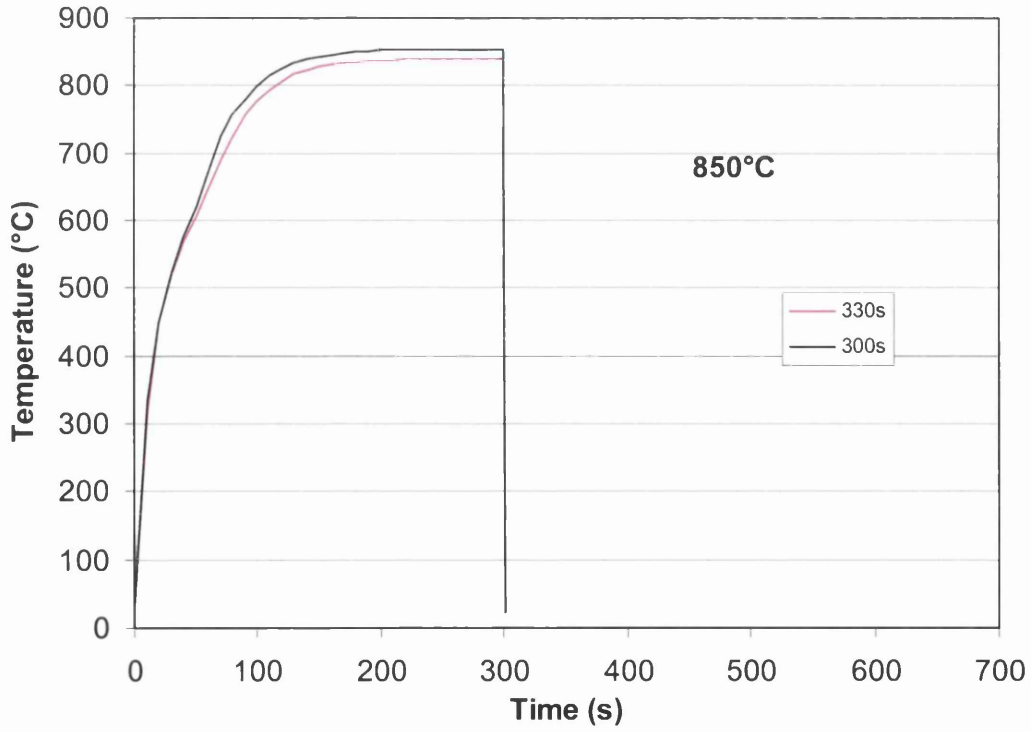
900
800
700
600
500
400
300
200
100
0
Temperature (°C)
850°C
330s
300s
0
100
200
300
400
500
600
700
Time (s)

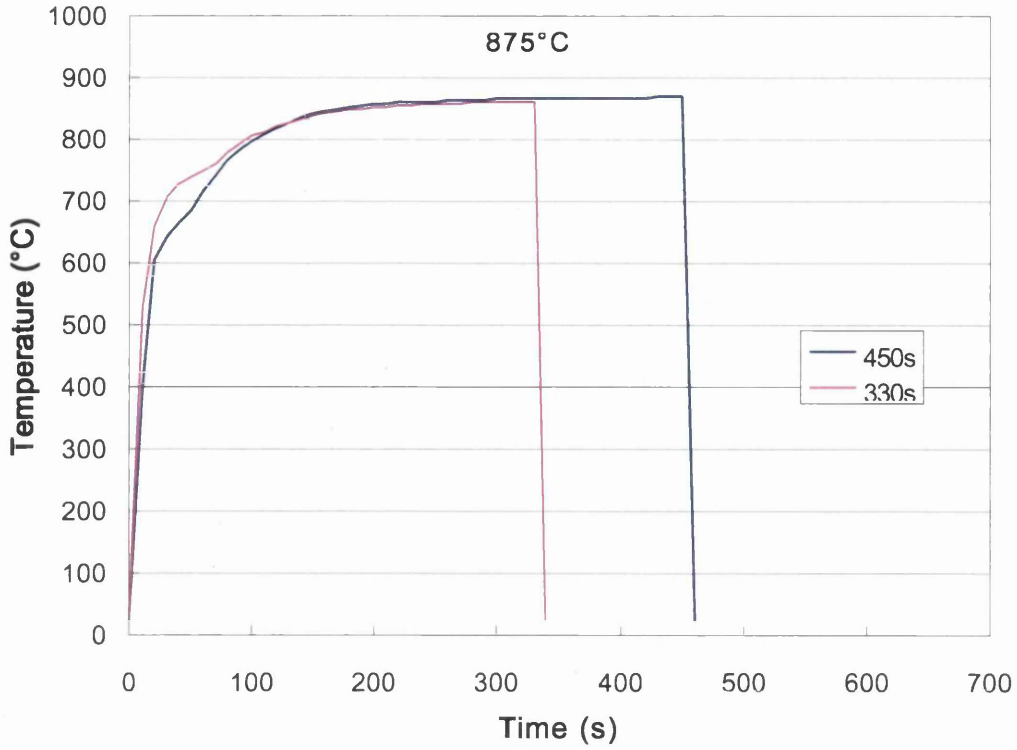

Fig.5.1: Temperature and time curves at the soaking temperatures of 775°C, 800°C, 825°C, 850°C and 875°C.

5.2. Light Optical Microscopy of Heat Treated DP800 Samples

The initial LOM characterization, performed on samples heat treated at the three soaking temperatures of 800°C, 850°C and 875°C previously reported, indicates that the obtained water quenched microstructures appear to be the coarsest (Figs. 5.2, 5.3, 5.4).

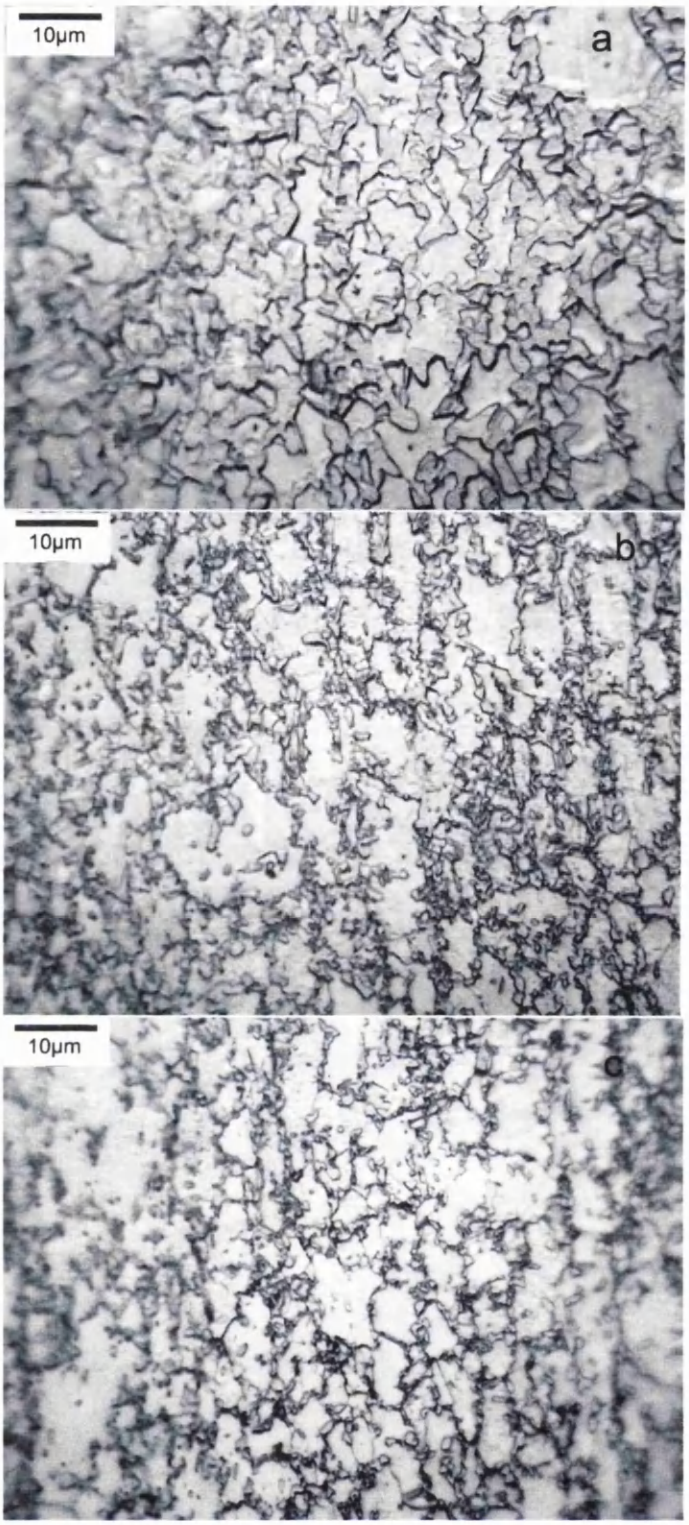

Fig 5.2: Intercritical annealing at 800°C for 300s followed by (a) Water quenching (b) Oil quenching and (c) Air cooling.

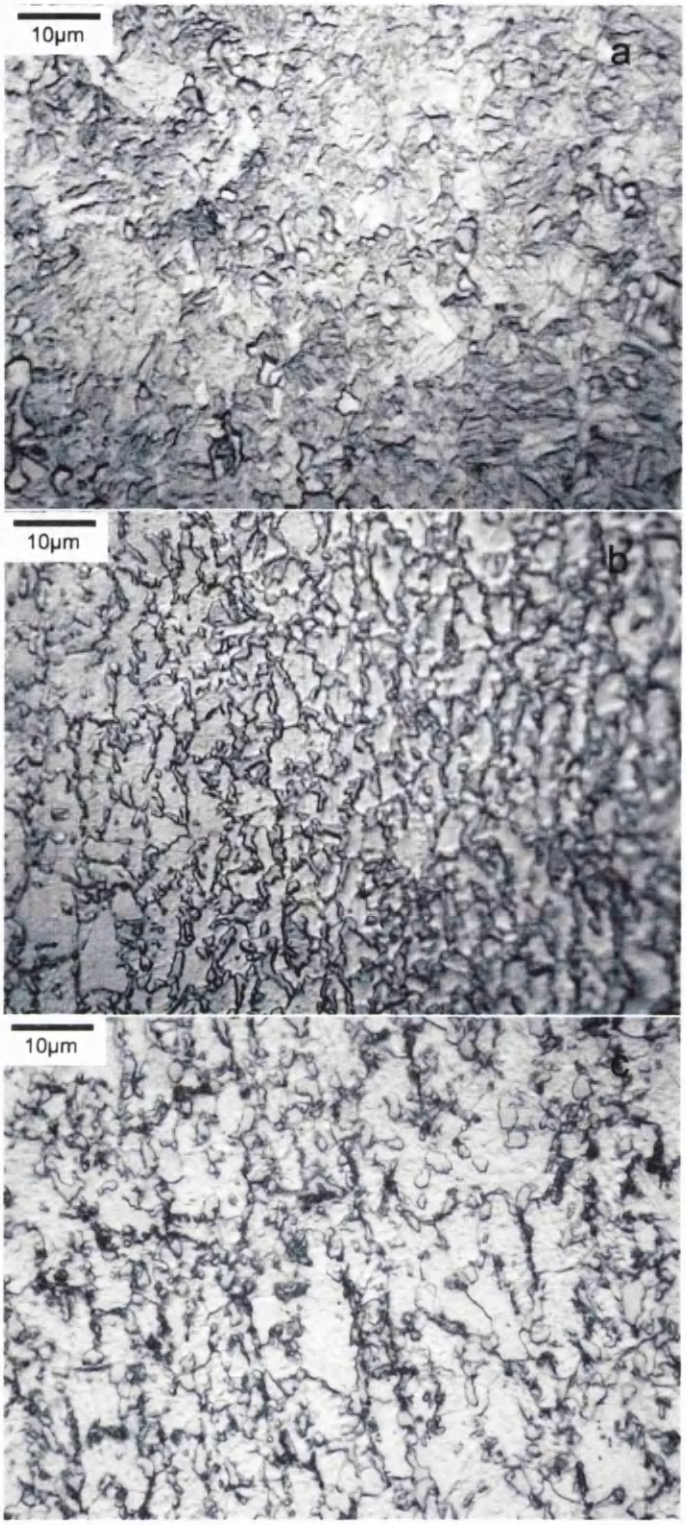

Fig 5.3: Intercritical annealing at 850°C for 300s followed by (a) water quenching (b) oil quenching and (c) air cooling.

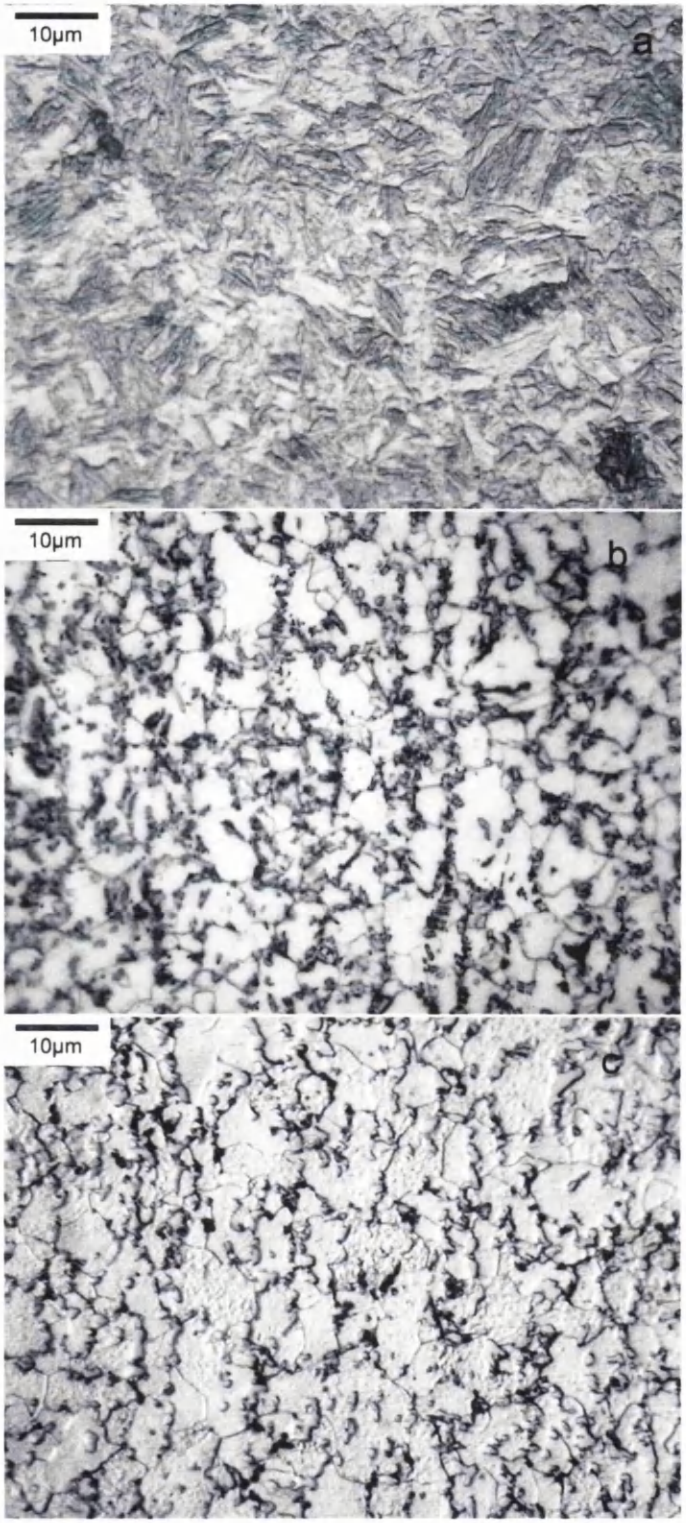

Fig 5.4: Intercritical annealing at 875°C for 330s followed by (a) water quenching (b) oil quenching and (c) air cooling.

At the higher temperatures of 850°C and 875°C, that involve water quenching, ferrite cannot even be identified among the second phase constituents.

However, for a given soaking temperature, samples that have been subjected to identical cooling rates develop similar microstructures, although perhaps with different volume fractions, despite their different soaking times at the temperature (Figs.5.5, 5.6). Therefore, it seems the cooling rate is the main factor to influence the microstructures, followed by the soaking temperature and the soaking time.

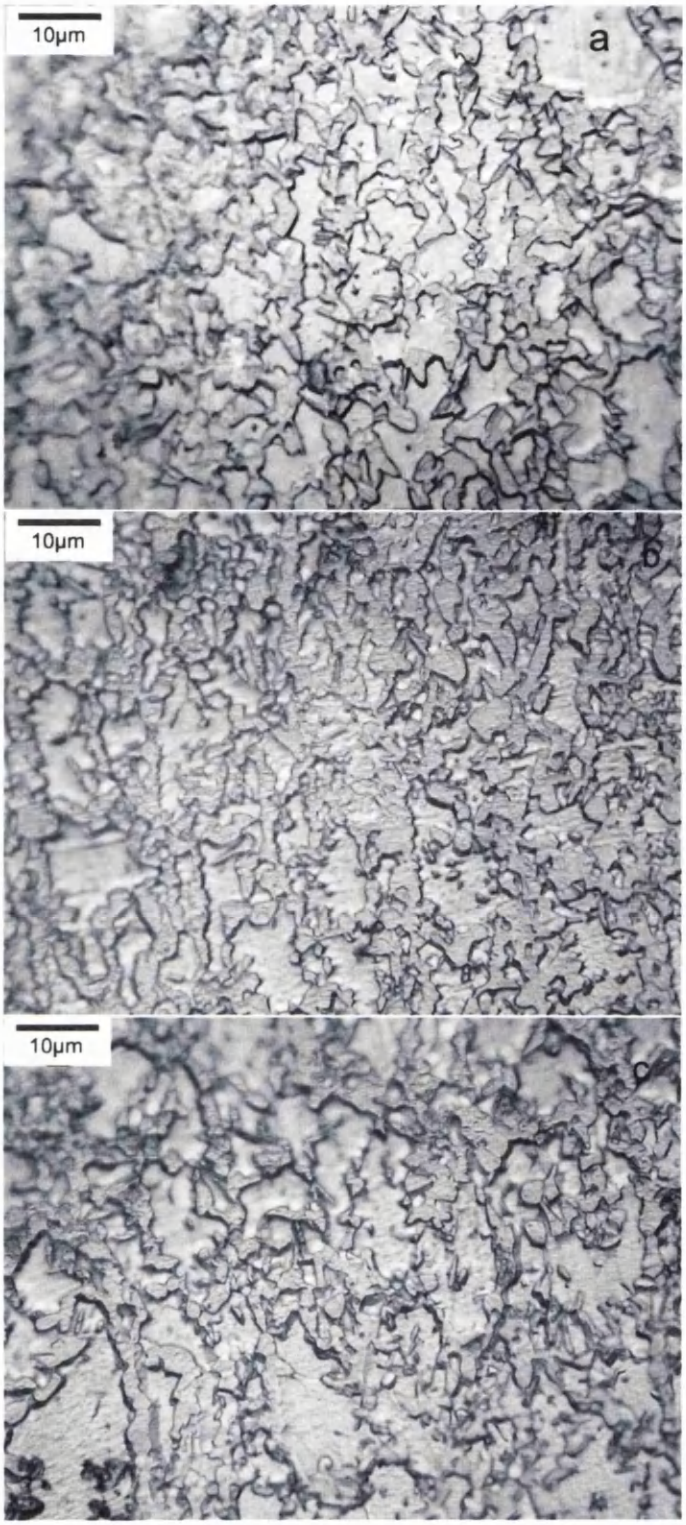

Fig 5.5: Intercritical annealing at 800°C, for (a) 300s, (b) 330s, (c) 450s, followed by water quenching.

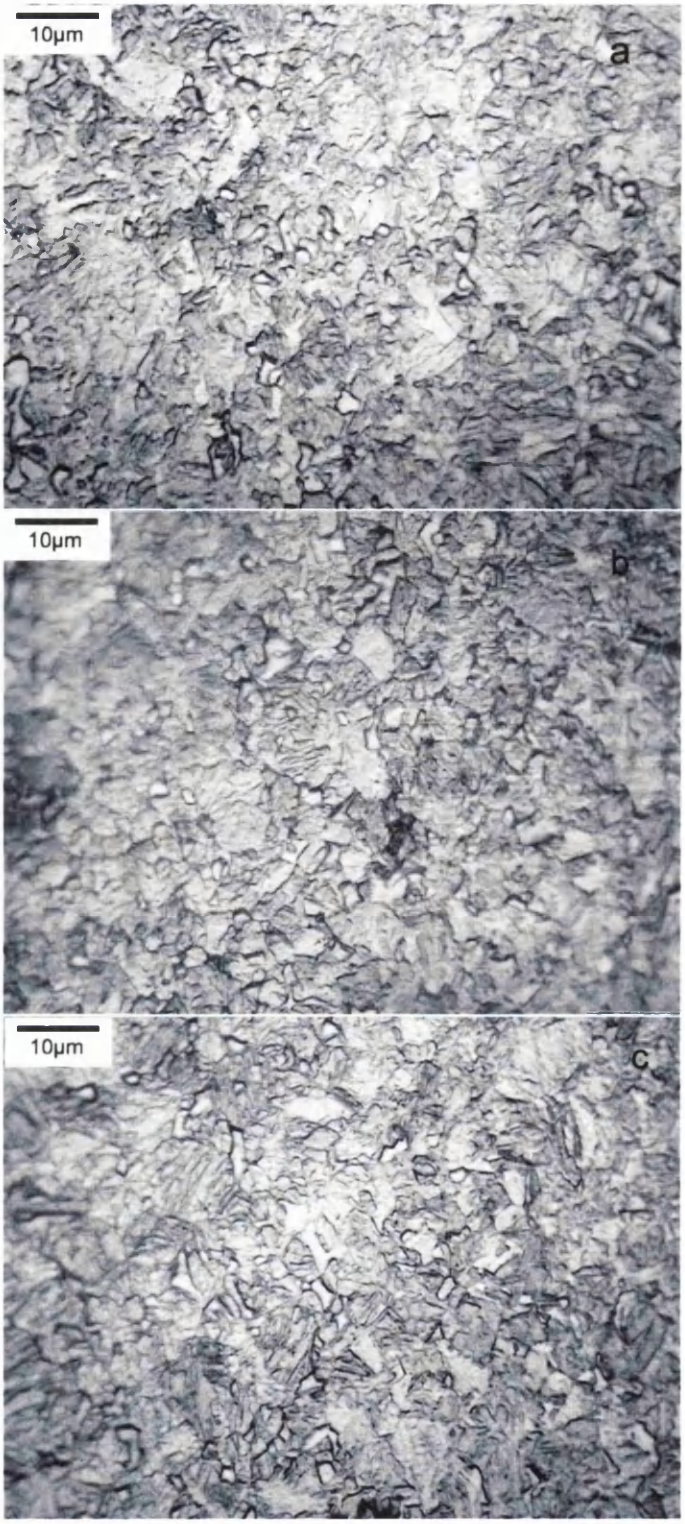

Fig 5.6: Intercritical annealing at 850°C, for (a) 300s, (b) 330s, (c) 450s, followed by water quenching.

The coarser microstructures develop when the higher soaking temperatures are employed. Therefore, when the soaking temperature is set at 800°C, when the microstructures are not so coarse, we can easily identify the ferrite matrix from second phase constituent present. However, for a soaking temperature of 875°C, the microstructures are quite coarse (Fig.5.7). Compared with the microstructures of the as received samples (Fig.5.8), even the microstructures obtained at the lowest soaking temperature of the three (800°C) appear to be coarser.

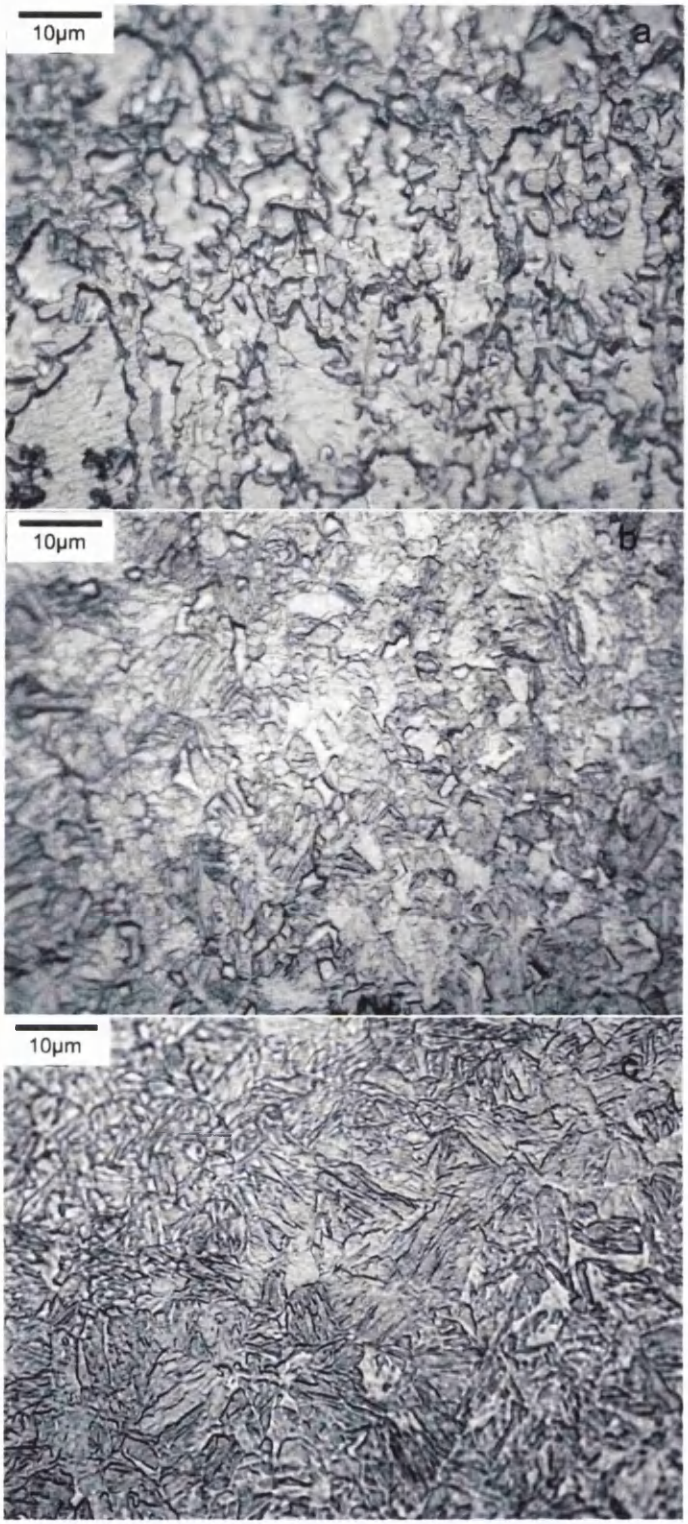

Fig 5.7: Intercritical annealing experiments performed at (a) 800°C, (b) 850°C, and (c) 875°C for 450s, followed by water quenching.

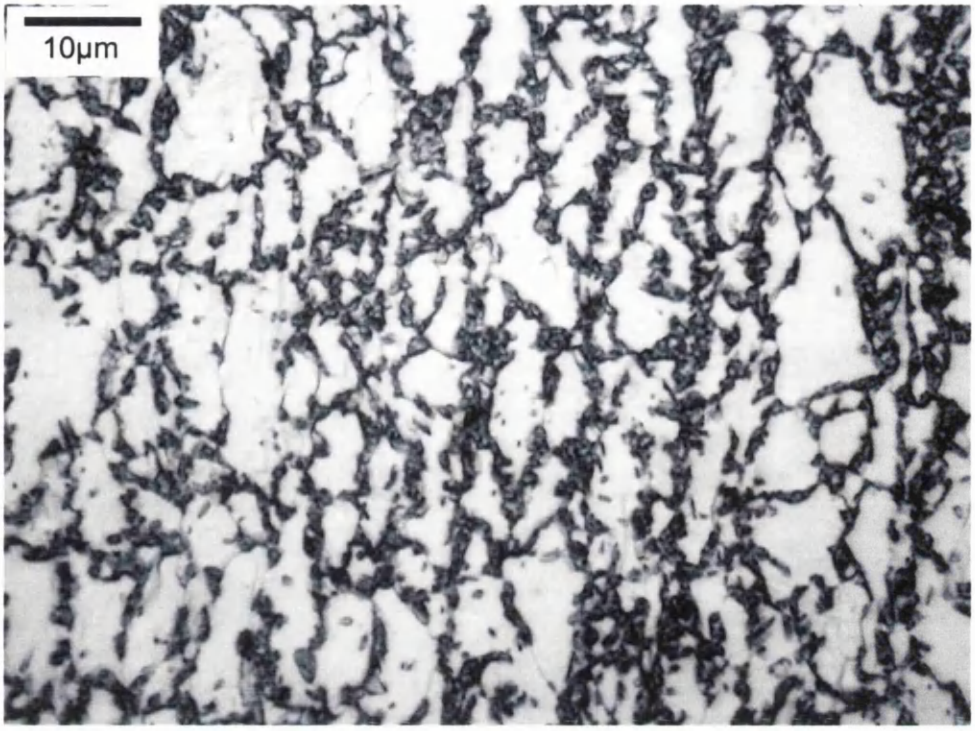

Fig.5.8: Microstructure of the as received DP800 samples.

5.3. SEM Characterisation

5.3.1. Secondary Electron Imaging of Water-Quenched Samples

For a soaking temperature of 775°C, the obtained microstructures appear similar when the soaking time is increased. These are second phase islands dispersed in ferrite, ferrite being the major constituent (Fig.5.9). The second phase volume fraction increases as the soaking time increased at this intercritical temperature. For a soaking time of 270s, the second phase volume fraction is only 23±3%, it increased to 37±3% when the soaking time was increased to 330s, while for a soaking time of 450s, it is more than 40±3% (Fig.5.10). This indicates that at this temperature the austenite transformation is not completed at soaking times of 330s or less. When the soaking temperature was increased to 800°C, martensite appears coarser. However, the evolution of second phase volume fraction looks the same as the previous one. The second phase volume fraction has increased from 32±3% to more than 48±3% (Figs.5.10, 5.11). For the same soaking time, and same cooling rate, the second phase

volume fraction of the samples soaked at the higher temperature is higher than that soaked at the lower temperature.

For the other higher intercritical annealing temperatures, samples that have been subjected to identical soaking time almost have approximately the same second phase volume fraction, such as the ones annealed at 825°C and 850°C. No marked change on the microstructure can be seen between these annealing condition. For the soaking temperatures of 825°C and 850°C, the second phase volume fraction is around 42±3% and 82±3% respectively (Figs.5.10, 5.12, 5.13). This can be understood as at this temperature, the soaking time of 270s is sufficient long for complete austenite transformation to take place. While, when the soaking time is set to 875°C, only austenite appears to be present (Fig.5.14). However, the microstructures of the as received DP800 samples are quite fine (Fig.5.15), and the volume fraction of second phase (i.e. martensite) is the smallest among all DP samples studied at approximately 21±3% (Fig.5.10).

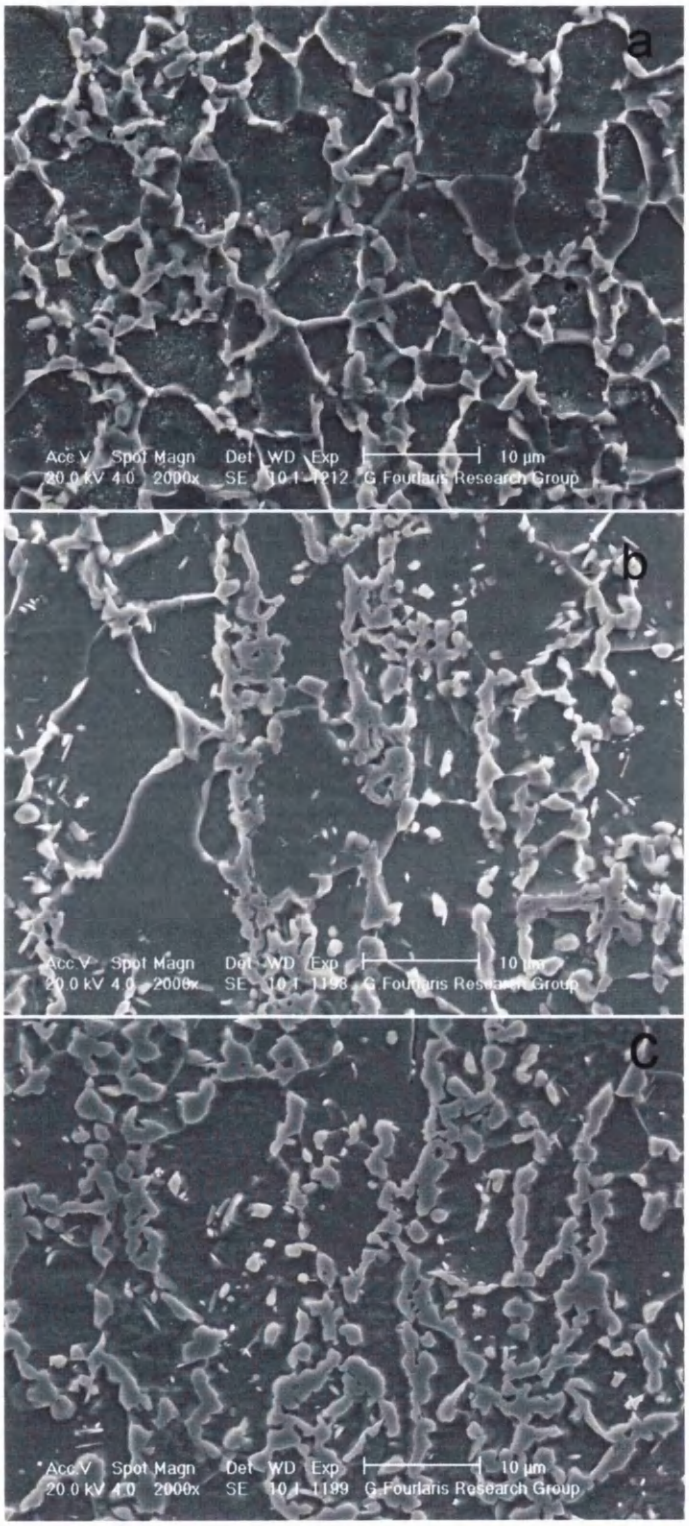

Fig.5.9: Secondary Electron micrographs of the DP800 samples intercritically annealed at 775°C for soaking times of (a) 270s, (b) 330s, and (c) 450s, followed by water quenching.

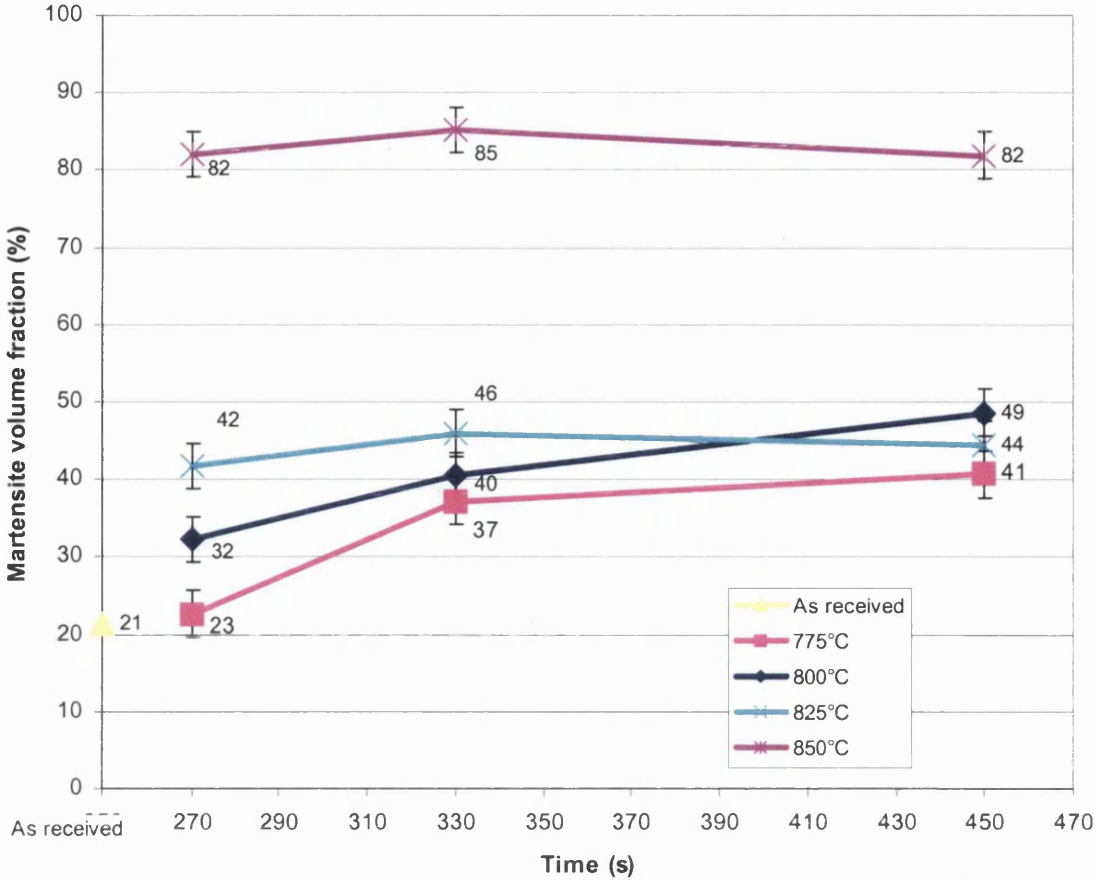

Fig.5.10: Evolution of second phase volume fraction of water-quenched samples for soaking temperatures of 775°C, 800°C, 825°C and 850°C.

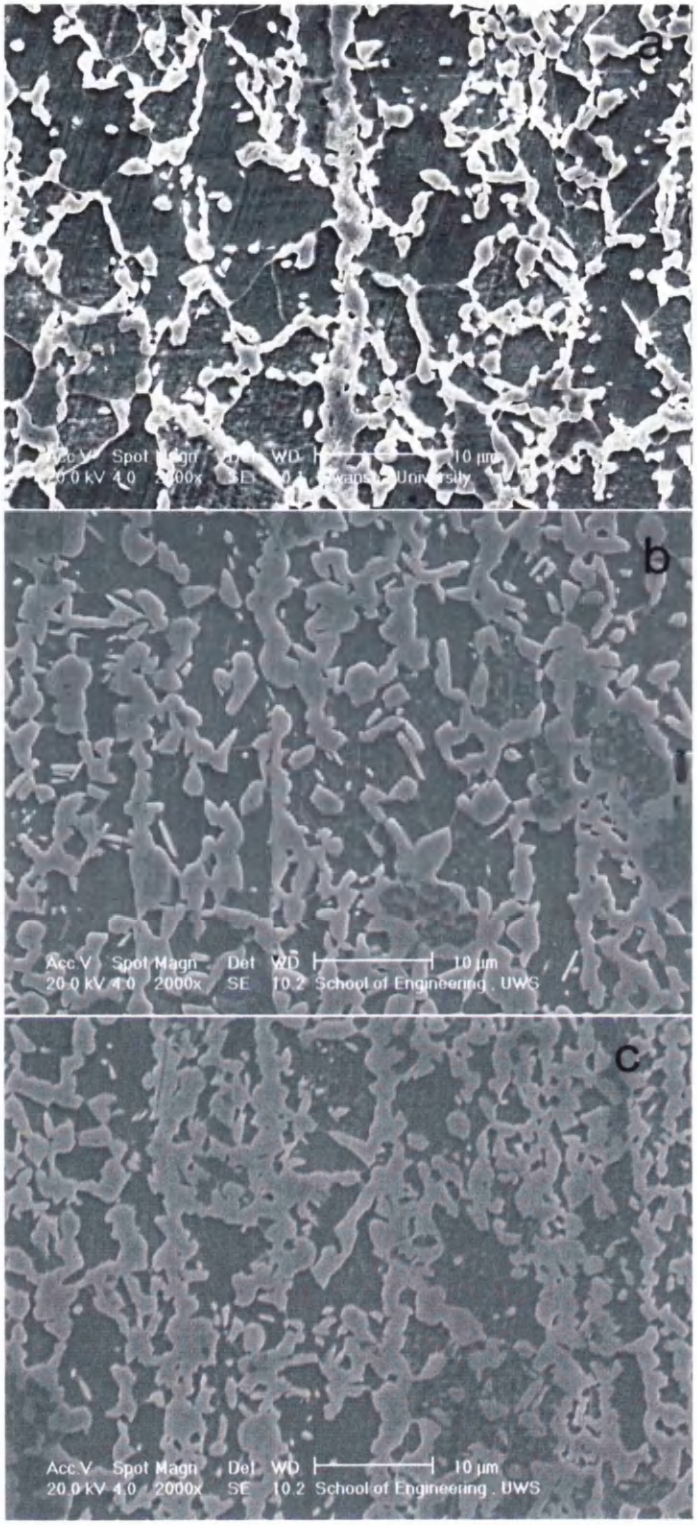

Fig.5.11: Secondary Electron Micrographs of the DP800 samples intercritically annealed at 800°C for soaking times of (a) 270s, (b) 330s, and (c) 450s, followed by water quenching.

Fig.5.12: Secondary Electron Micrographs of the DP800 samples intercritically annealed at 825°C for soaking times of (a) 270s, (b) 330s, and (c) 450s, followed by water quenching.

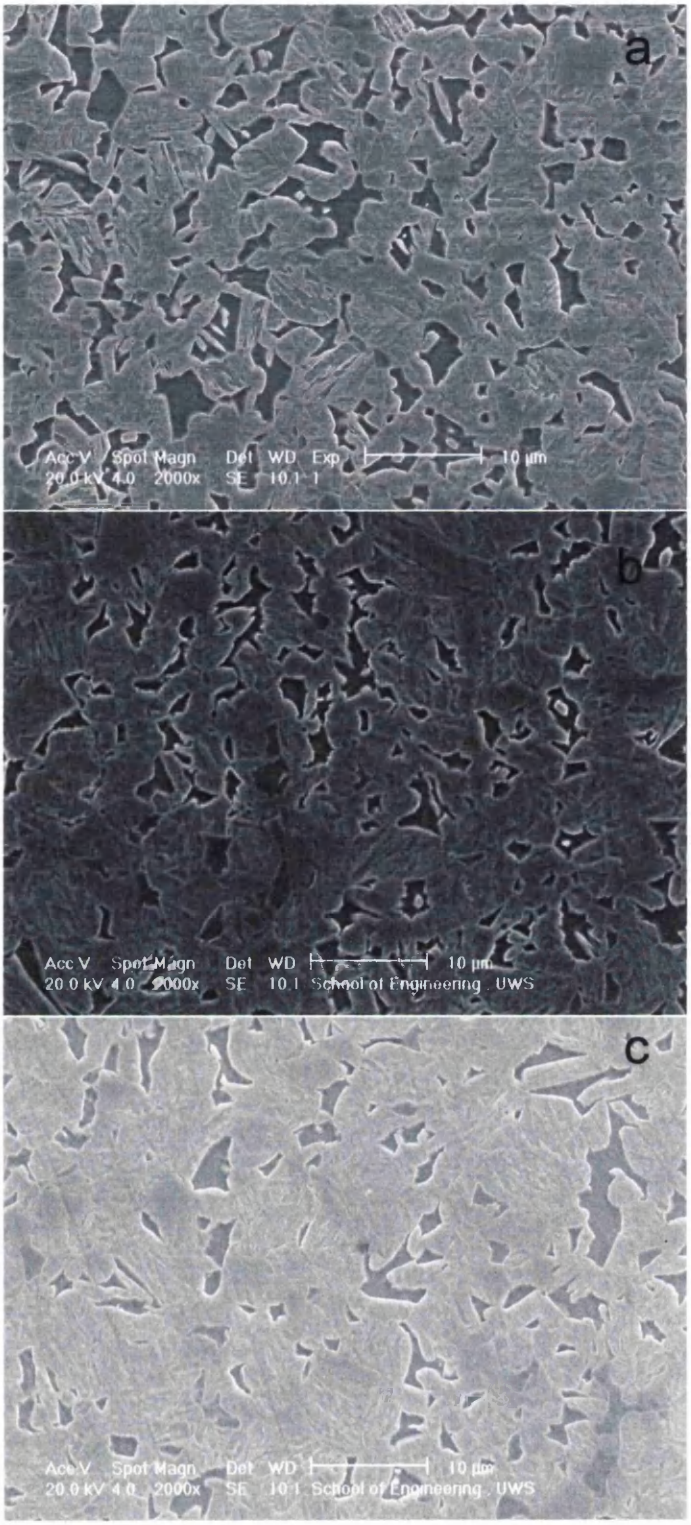

Fig.5.13: Secondary Electron Micrographs of the DP800 samples intercritically annealed at 850°C for soaking times of (a) 270s, (b) 330s, (c) 450s, followed by water quenching.

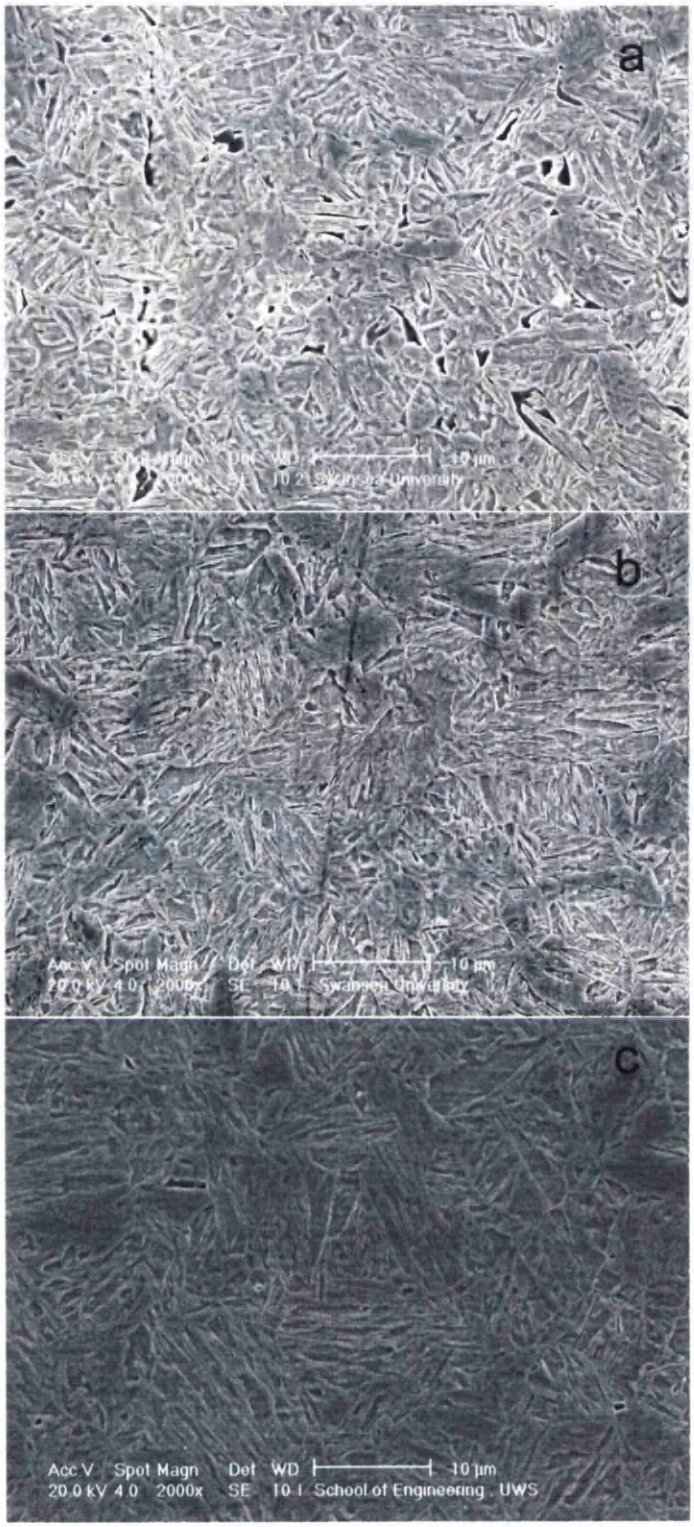

Fig.5.14: Secondary Electron Micrographs of the DP800 samples intercritically annealed at 875°C for soaking times of (a) 270s, (b) 330s, (c) 450s, followed by water quenching.

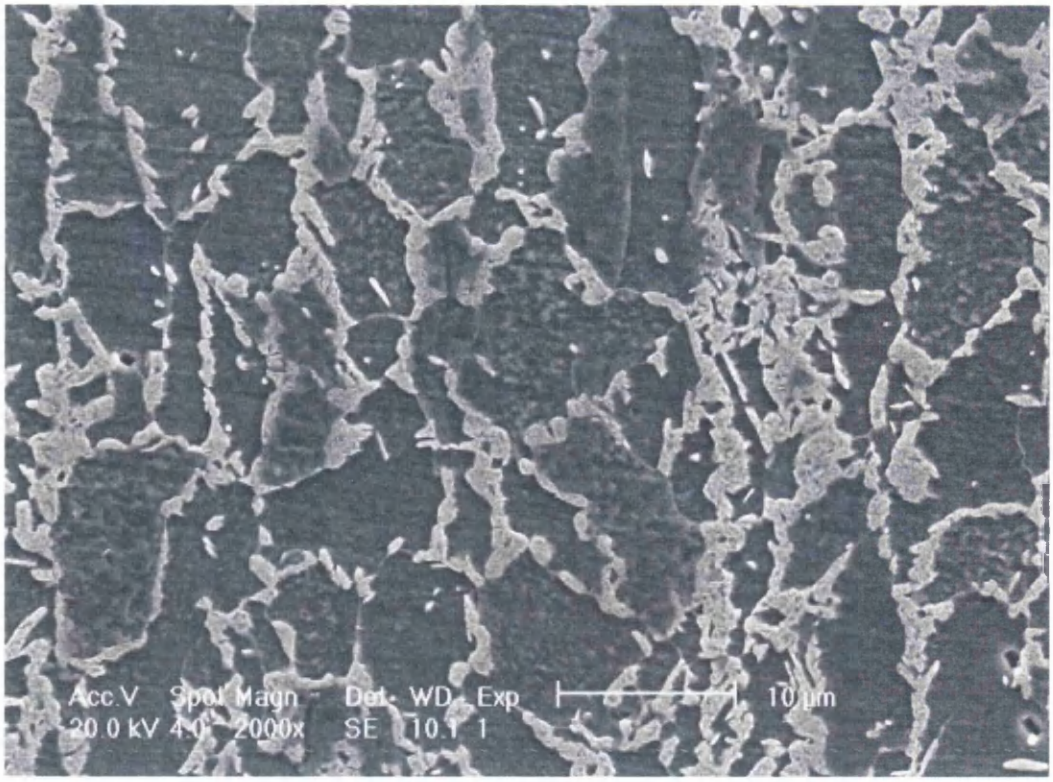

Fig.5.15: Secondary Electron Micrograph of an as received DP800 sample.

Comparing the Secondary Electron Micrographs of the heat-treated DP800 samples with those of the sample as received, samples which were soaked at temperatures above 825°C do not fall within the definition of a DP800 grade. Therefore, future research activities described on this thesis focus on annealed DP800, heat treated at temperatures less than 825°.

5.3.2. Backscattered Electron Micrographs

All the Backscattered Electron Micrographs have similar contrast. Non-metallic inclusions are the most likely explanation for the "dark-contracted" particles visible in the micrographs (Fig.5.16). No significant composition difference among the second phase can be found from those micrographs.

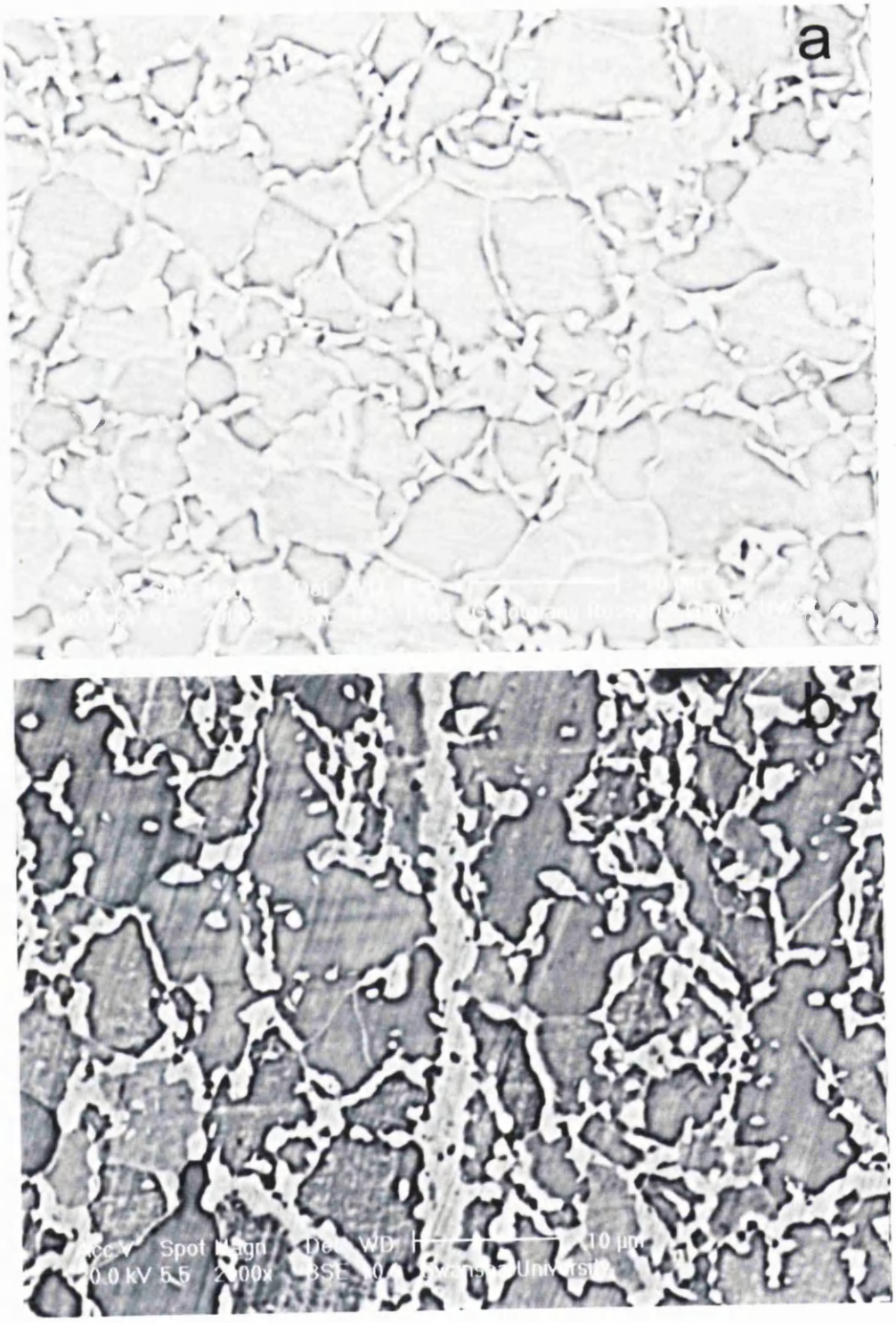
a
b

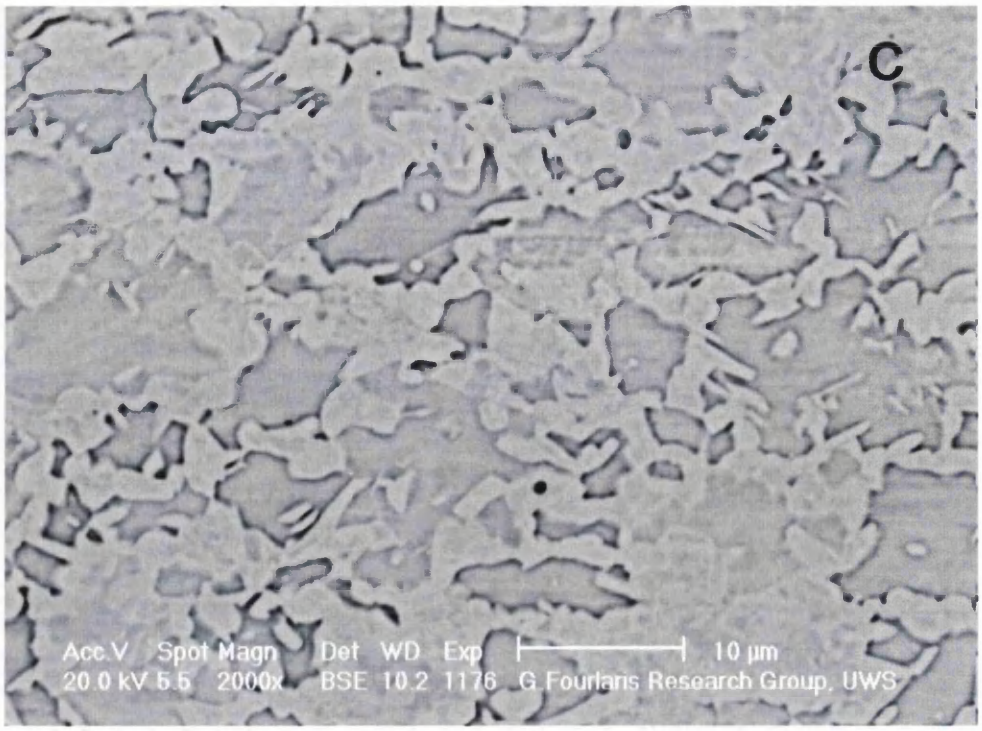
c
Acc.V Spot Magn Det WD Exp 10 µm
20.0 kV 5.5 2000x BSE 10.2 1176 G.Fourlanis Research Group, UWS

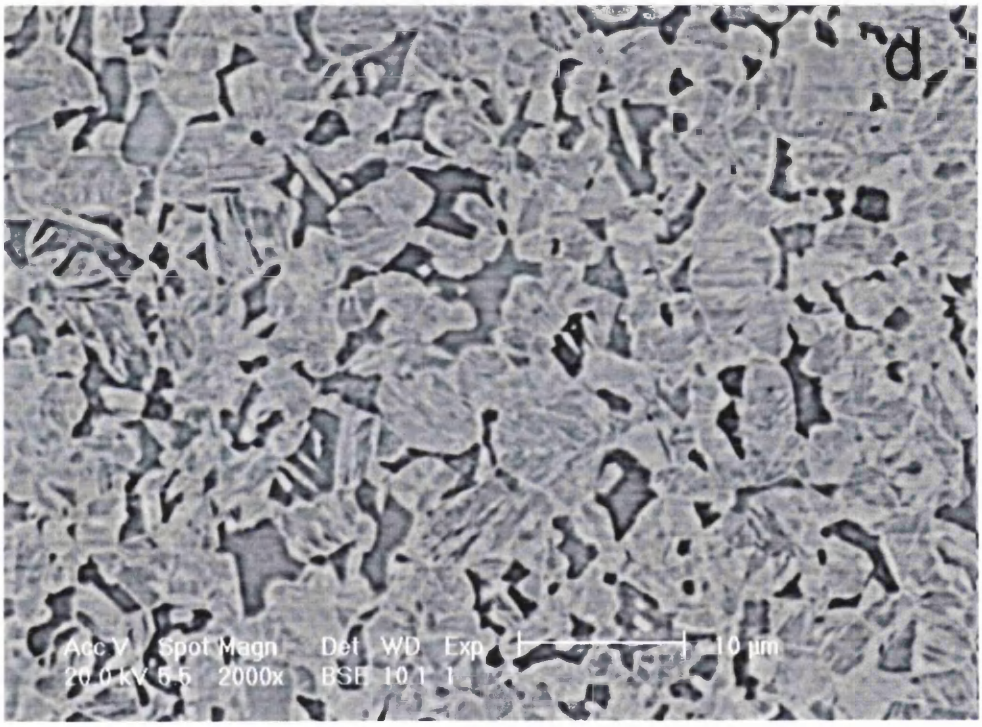
d
Acc.V Spot Magn Det WD Exp 10 µm
20.0 kV 5.5 2000x BSE 10.1 1

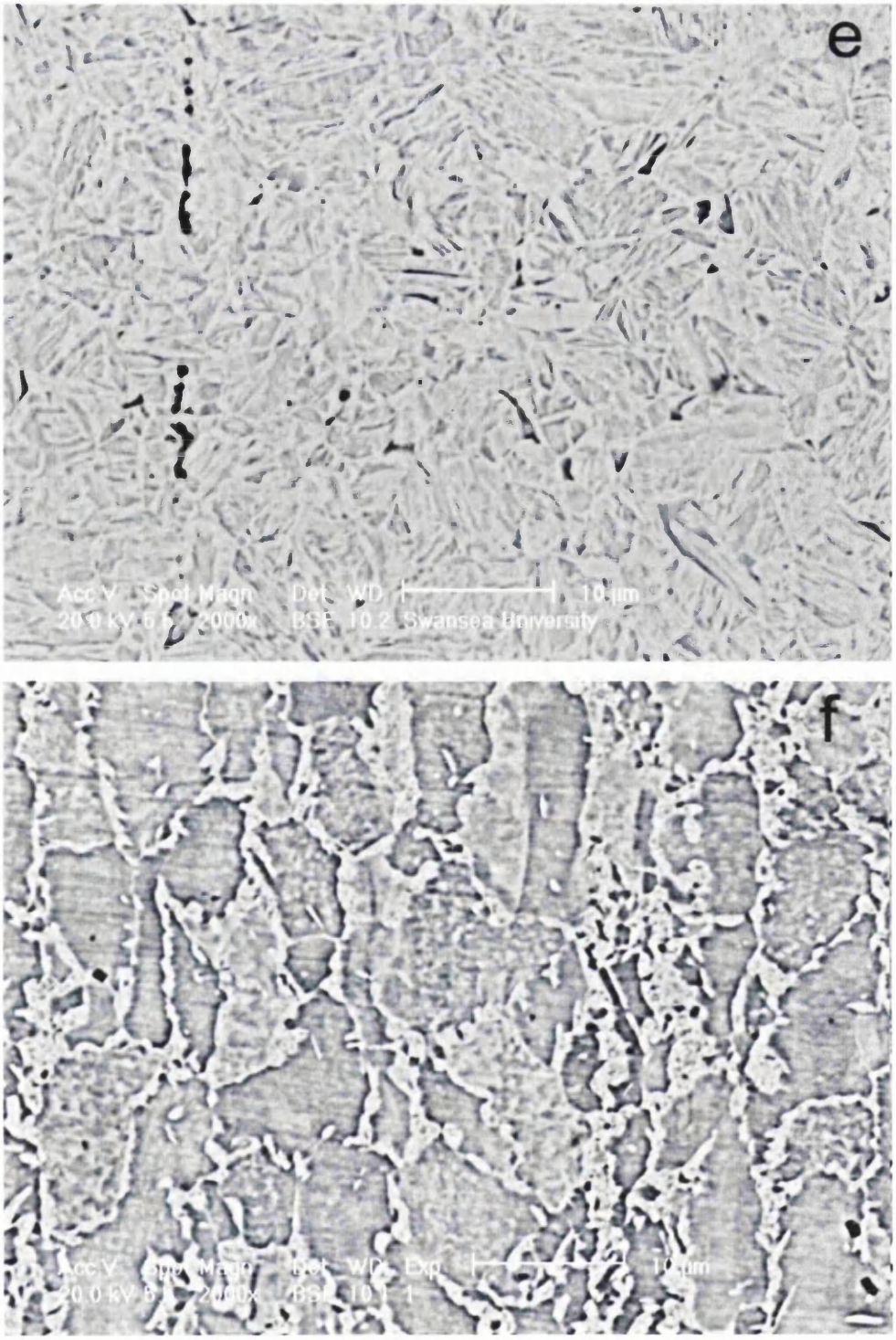

Fig.5.16: Backscattered Electron Micrographs of DP800 intercritically annealed at (a) 775°C, (b) 800°C, (c) 825°C, (d) 850°C, and (e) 875°C followed by water quenching, and (f) as received.

5.4. Hardness Results

At a soaking temperature of 775°C for the water-quenched samples, the hardness started at 213, then increased as the soaking time is increased from 270s to 330s, and reached a peak value of 235, followed by a slightly decrease from 330s to 450s, and finished at 226. The highest hardness value obtained of 235 is roughly the same as that of the as received ones (Fig.5.17).

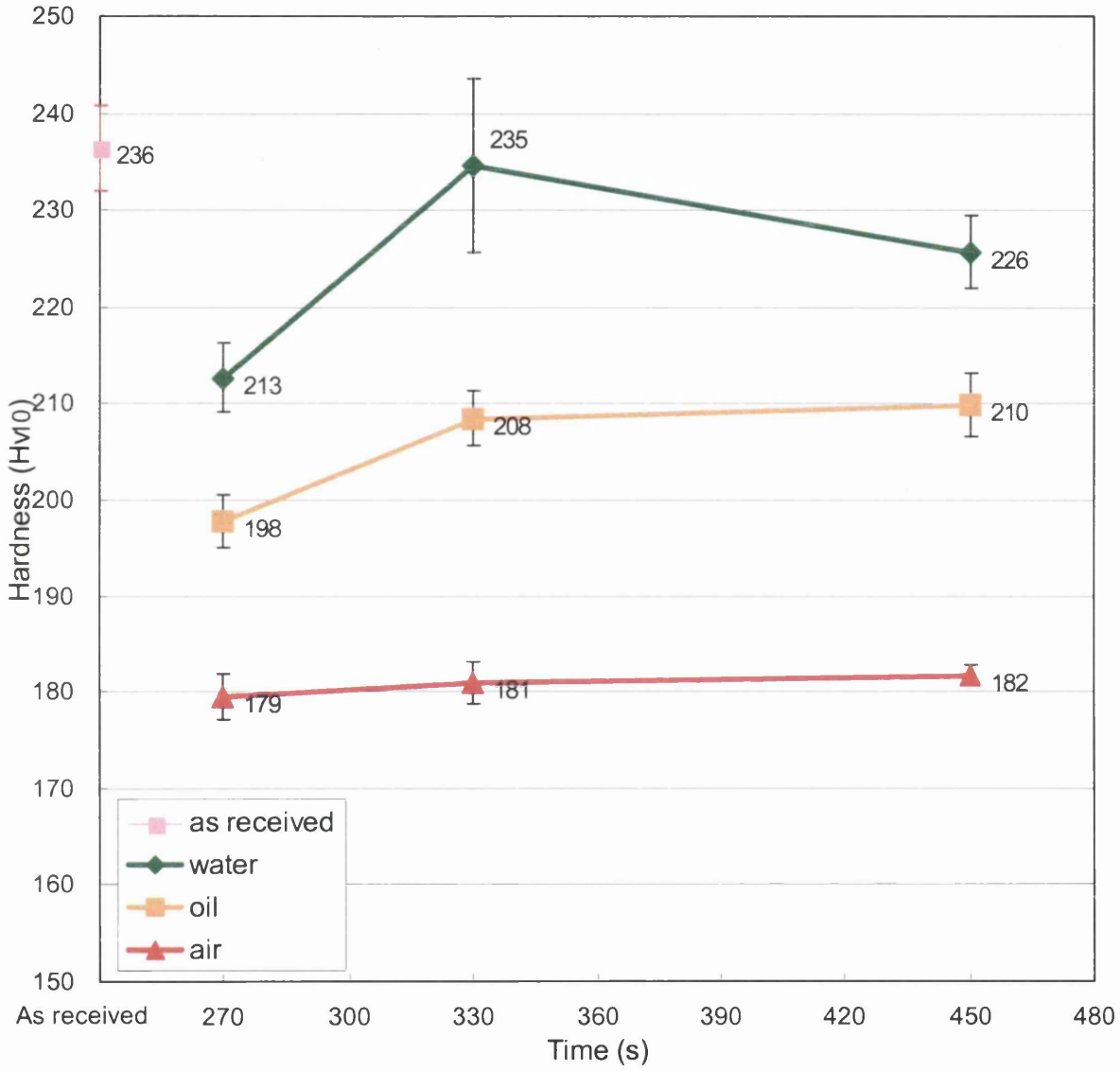

Fig.5.17: Evolution of hardness for the samples soaked at 775°C.

At a soaking temperature of 800°C for the water-quenched samples, the hardness

slightly decreases as the soaking time is increased from 270s to 330s, while hardness shows no marked change when the soaking time was increased from 330s to 450s (Fig.5.18).

At a soaking temperature of 825°C for the water-quenched samples, the hardness increases as the soaking time is increased from 270s to 330s, while the hardness shows no marked change when the soaking time was increased from 330s to 450s (Fig.5.19).

It's well known that the hardness increases with the increase of the volume fraction of martensite. However, the carbon content of martensite also plays a crucial role on its hardness. For low carbon grades, such as the DP800, the carbon content is defined, so when the volume fraction of martensite exceeds a given limit, the carbon content of martensite will decrease and affect the sample's overall hardness. Therefore, when the martensite volume fraction is increased, the hardness does not appear to always increase. And it seems for the DP800 samples, the "best" soaking time to get the highest hard ability is between 300s and 330s, which is the best combination of martensite volume fraction and carbon concentration in martensite for maximum hardness (Figs.5.17-5.21).

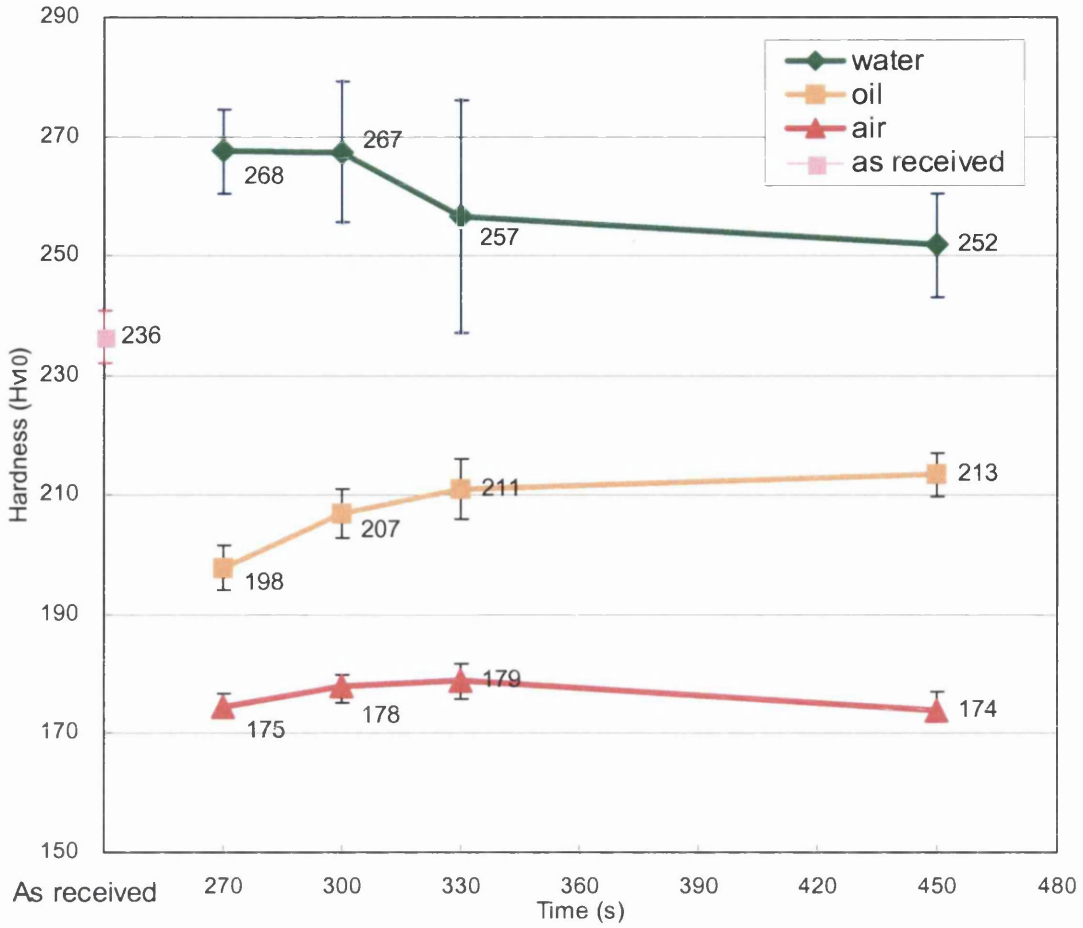

Fig.5.18: Evolution of hardness for intercritically annealed samples at a soaking temperature of 800°C followed by various cooling regions.

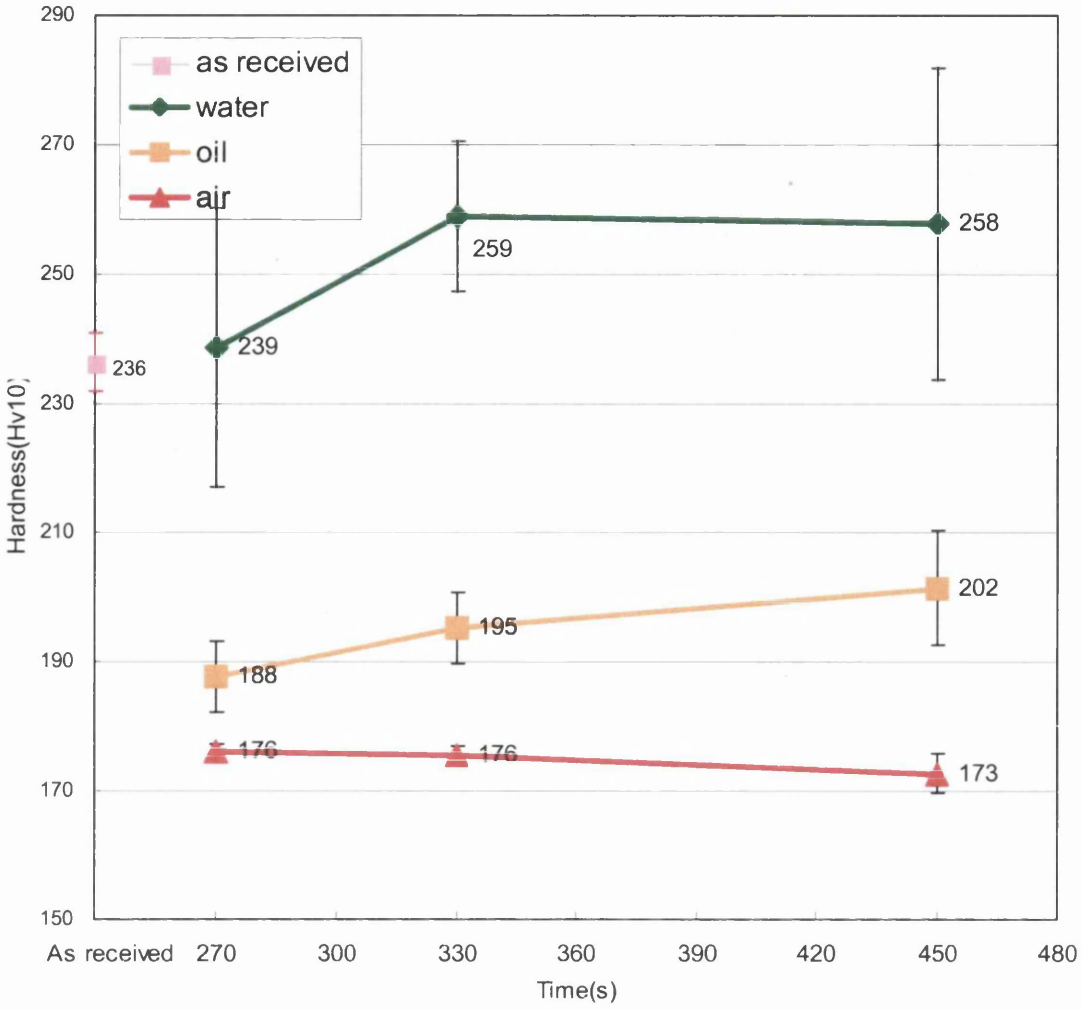

Fig.5.19: Evolution of hardness for an intercritically annealing soaking temperature of 825°C followed by water quenching.

At a the soaking temperatures of either 850°C or 875°C, for water quenched samples, the lowest hardness value reached was at 330s, while a slight increase was observed when the soaking time was increased to 450s (Figs.5.20, 5.21). Though the average carbon content within martensite would have decreased from 330s to 450s, the increase of the volume fraction of martensite is the defining factor contributing to the highest hardness values observed.

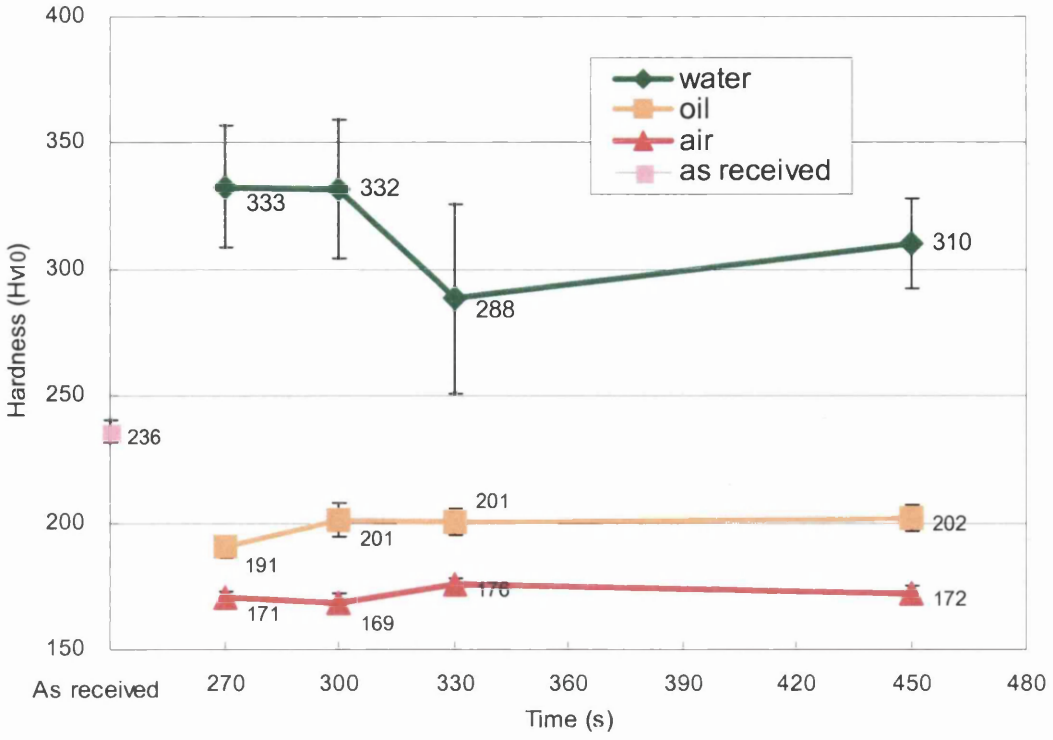

Fig.5.20: Evolution of hardness for an intercritical annealing temperature of 850°C.

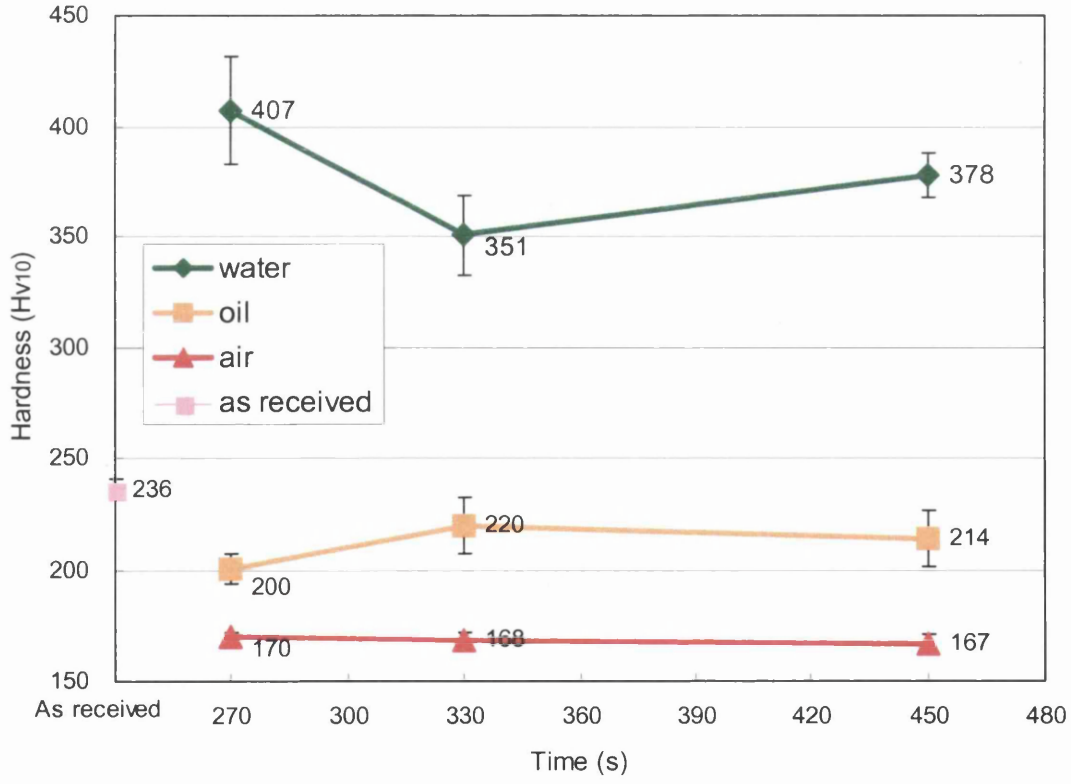

Fig.5.21: Evolution of hardness for an intercritical annealing temperature of 875°C.

Basically, at a given soaking time, the hardness is increased as the soaking temperature is increased (Fig.5.22). This is due to the increase of the second phase volume fraction, as well as the increase of martensite volume fraction, which is the result of the increase of austenite volume fraction as the soaking temperatures are increased. However, the hardness of the oil-quenched and air-cooled samples did not change significantly. This illustrates that it is the evolution of martensite volume fraction mainly responsible for the overall hardness of the samples. The obtained microstructures of the oil-quenched and air-cooled samples also do not appear to contain sizeable amount of martensite.

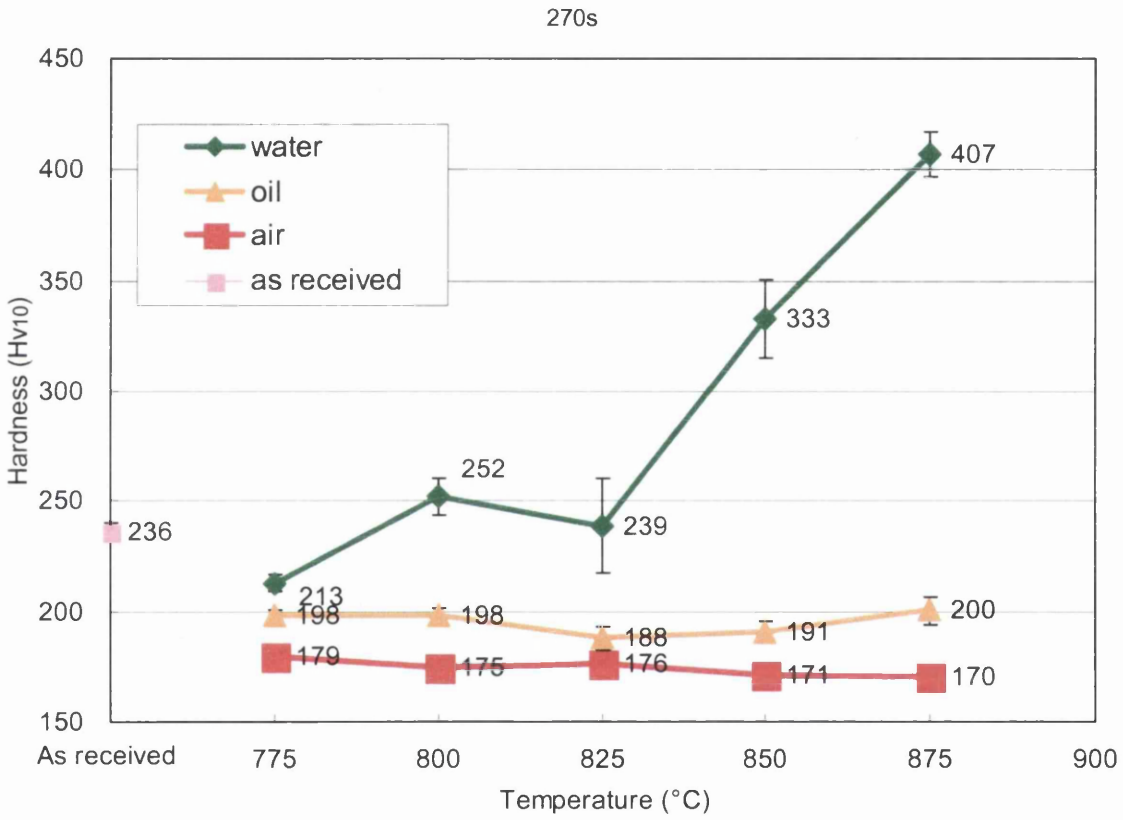

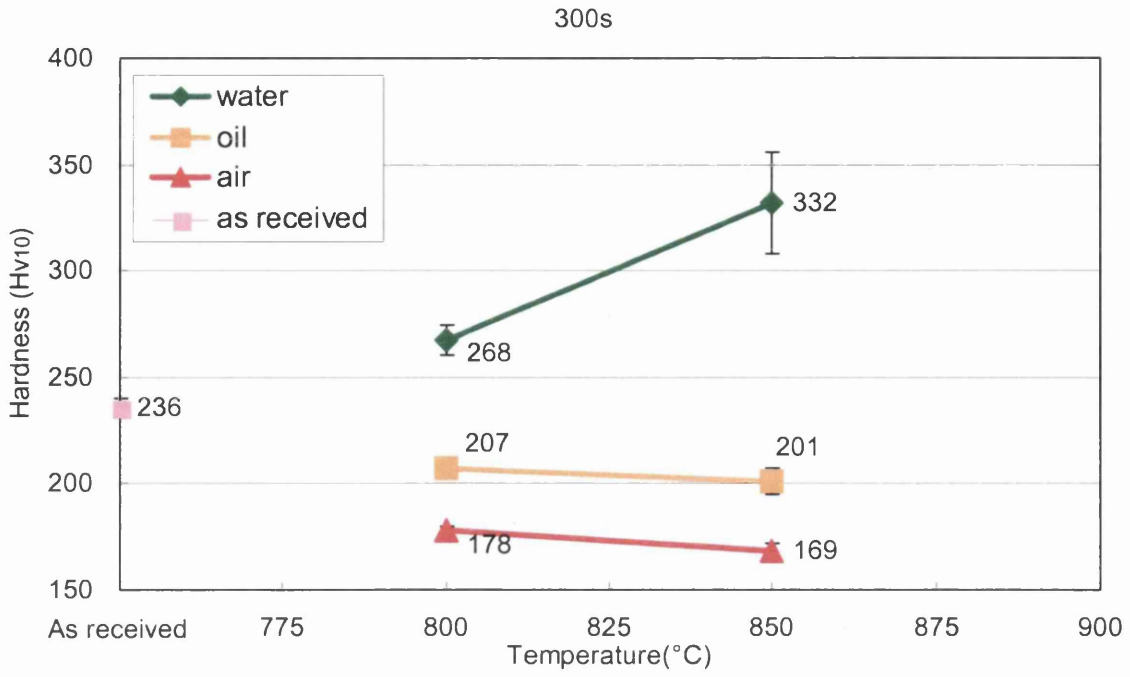
300s
water
oil
air
as received
Hardness (Hv10)
400
350
300
250
200
150
332
268
236
207
201
178
169
As received
775
800
825
850
875
900
Temperature(°C)

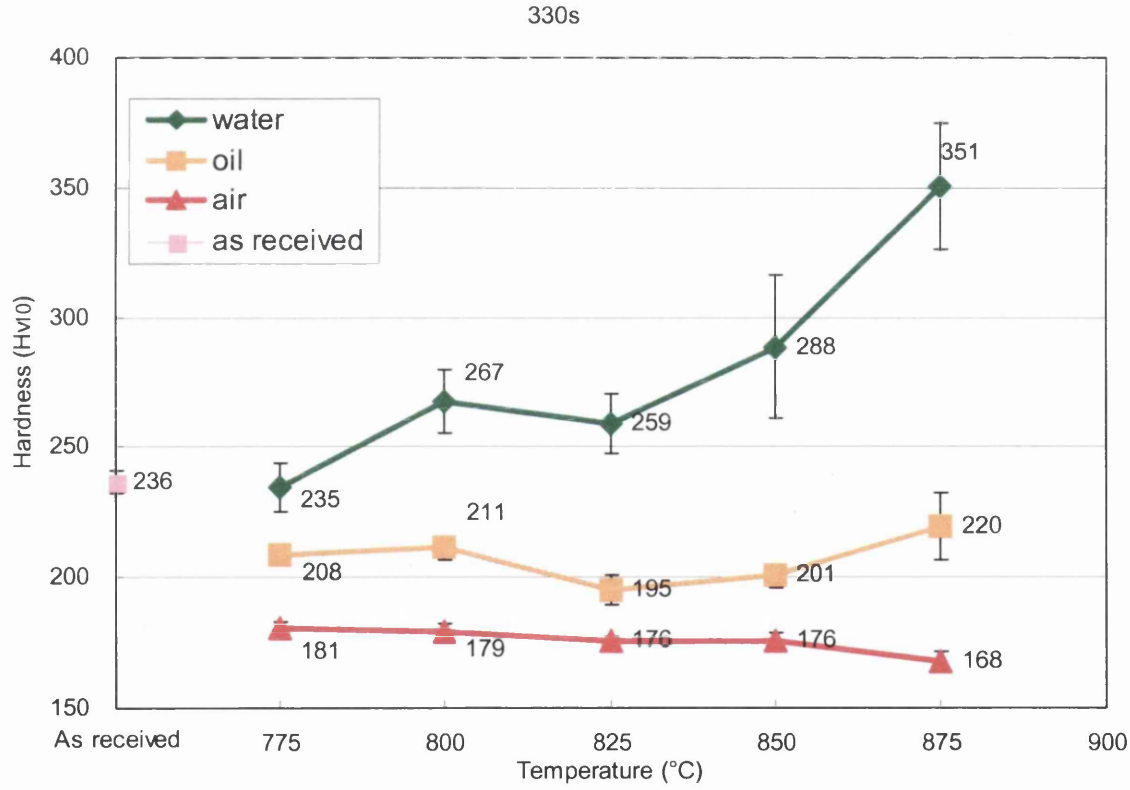
330s
water
oil
air
as received
Hardness (Hv10)
400
350
300
250
200
150
351
288
267
259
235
236
211
220
208
195
201
181
179
176
176
168
As received
775
800
825
850
875
900
Temperature (°C)

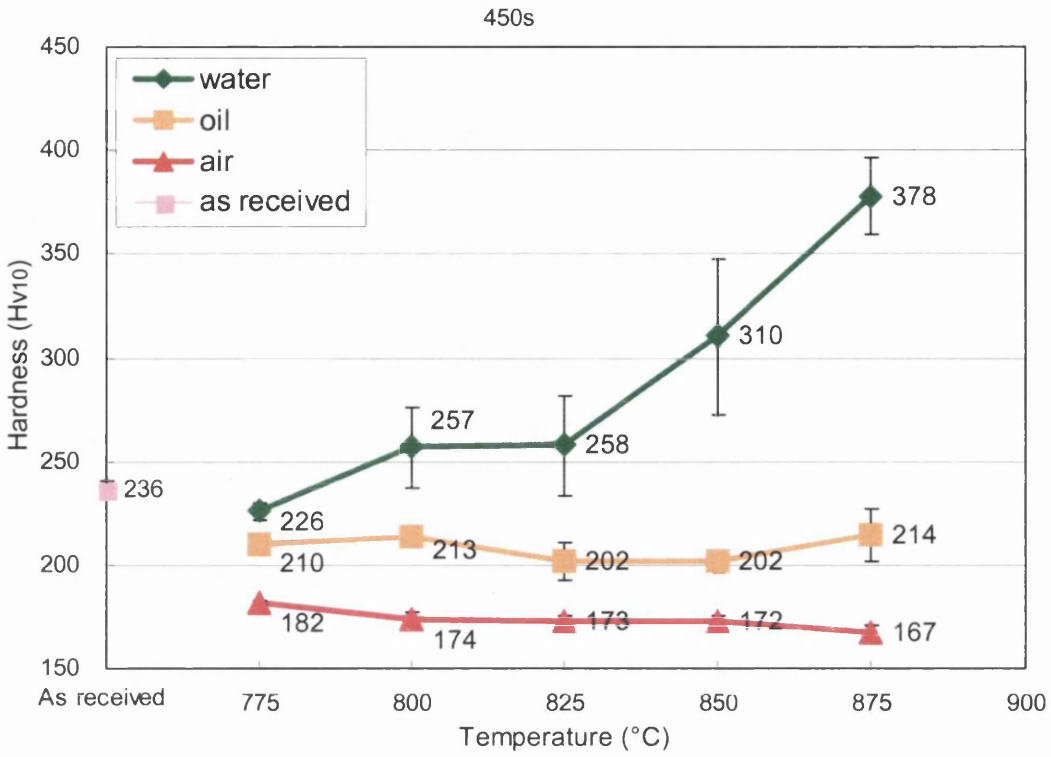

Fig.5.22: Hardness evolution versus intercritical annealing temperatures, for various soaking times.

5.5. Tensile Testing

5.5.1. Stress-Strain Curves

Tensile testing has been carried out on the following samples:

1) As received;
2) Soaked at 775°C for 330s followed by water quenching;
3) Soaked at 800°C for 330s followed by water quenching and oil quenching;
4) Soaked at 825°C for 270s, 450s followed by water quenching, and for 330s for both water and oil quenched samples.

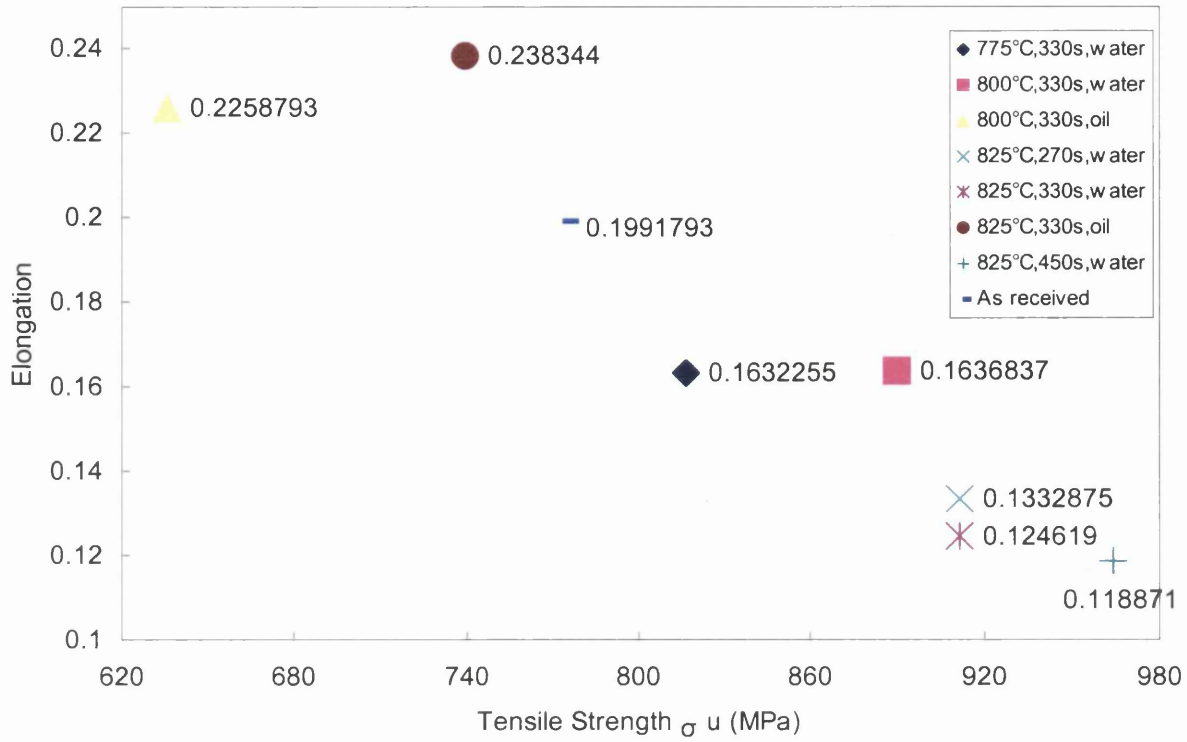

Fig.5.23: Comparison of elongation for DP800 as received and heat-treated conditions. (All data points are derived from the average of three different tensile tests)

The oil-quenched samples have the higher elongation valued measured, which were between 22% and 24%. Oil quenched samples have higher elongation rather than the as received samples, whose elongation value is approximately 20%. The elongation of the oil-quenched sample soaked at a higher temperature of 825°C is a little higher than that of the oil-quenched sample soaked at 800°C. For the water-quenched samples, those soaked at a lower temperature exhibit higher elongation values. For samples soaked at 775°C for 330s, the elongation was found to be approximately 16%. It is quite near the elongation value of samples soaked at 800°C for 330s. However, samples soaked at 825°C, are characterized by elongation values less than 14%. In addition, the elongation decreased as the soaking time was increased at 825°.

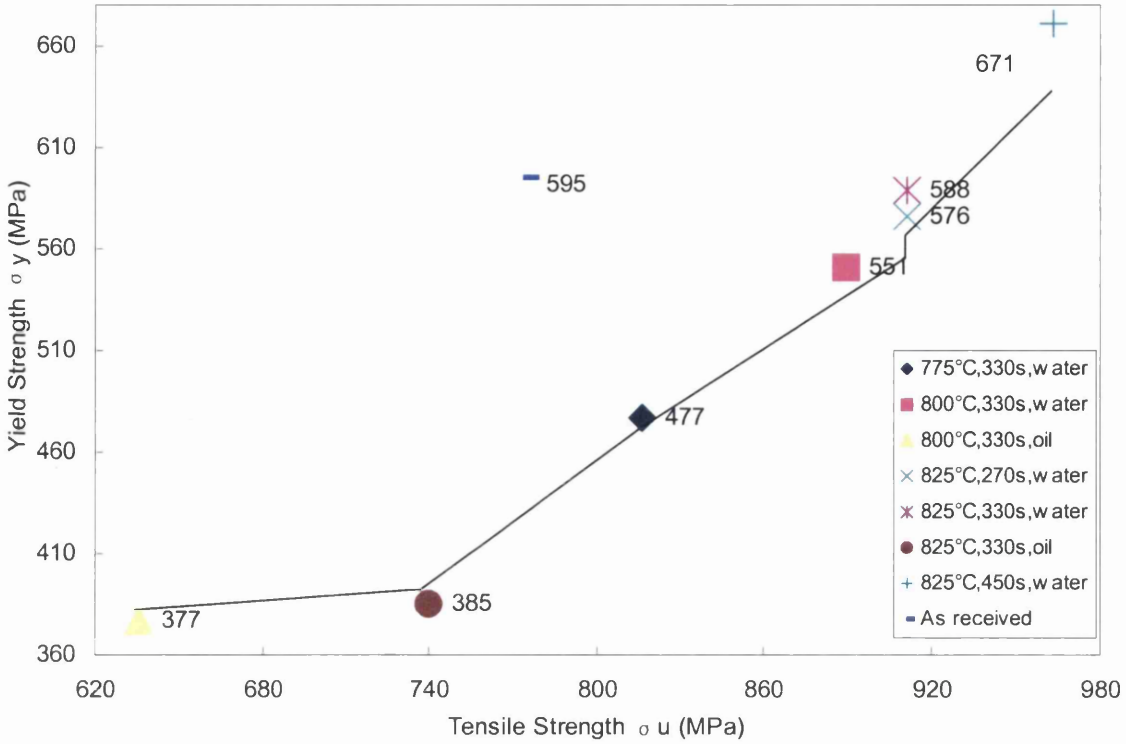

Fig.5.24: Comparison of yield strength for the DP800 steel, in the as received and heat-treated conditions. (All data points are derived from the average of three different tensile tests)

In contrast, for oil-quenched samples soaked at 800°C for 330s, the lowest yield strength values were obtained at 377MPa, coupled with the lowest tensile strength of 636MPa. This is followed by oil-quenched samples, initially annealed at 825°C for 330s, which had yield strength of 385Mpa, coupled with tensile strength values of 740MPa. Finally, the water quenched samples, initially soaked at the lower temperatures of 775°C and 800°C, exhibited yield strength values of 447MPa, 551Mpa, respectively, coupled with the tensile strength values of 816MPa and 890MPa, respectively. For an annealing temperature of 825°C, and soaking times of 270s and 330s, both the obtained yield strengths and tensile strengths are similar, namely yield strength values of approximately 580MPa and the tensile strength values approximately 920MPa. The yield strength was a little lower than that of the as received while the tensile strength significantly higher than that of the as received, for

samples annealed at 825°. Finally, for samples annealed at 825°C for 450s, the highest yield strength and tensile strength were obtained, namely 671MPa and 964MPa, respectively.

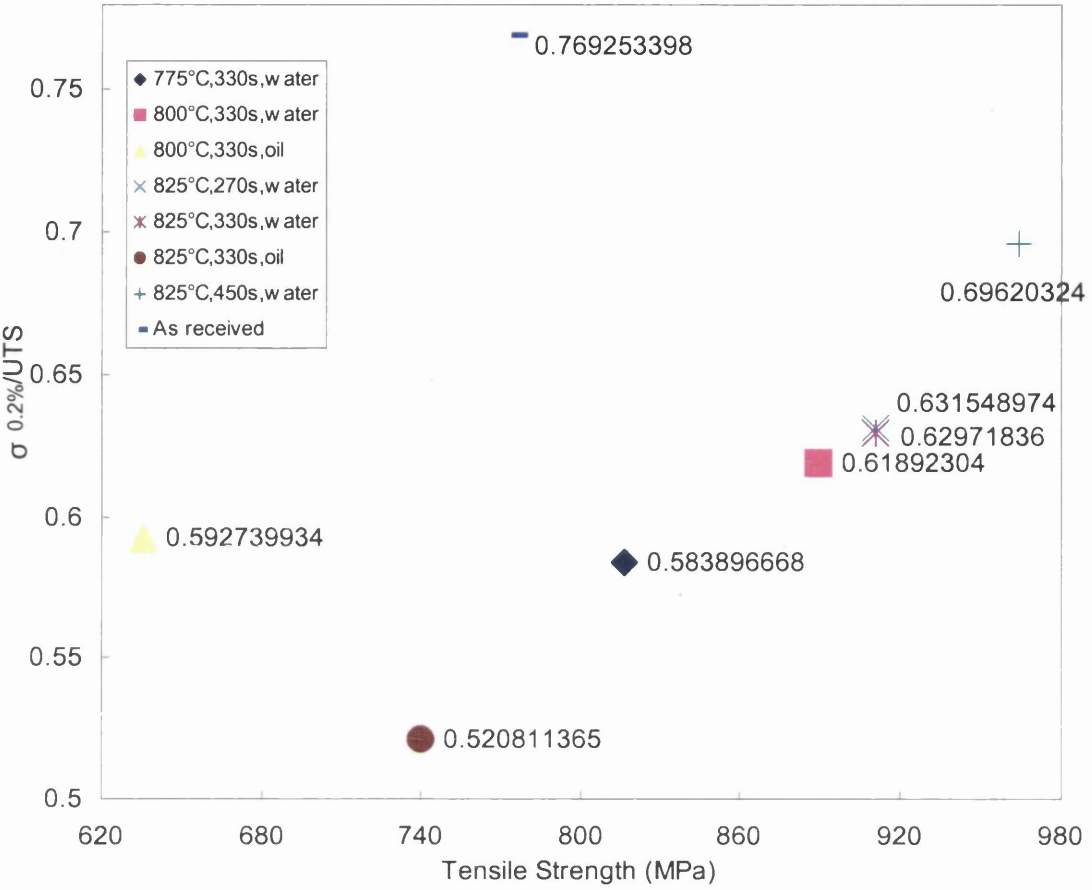

Fig.5.25: Comparison of yield/tensile strength ratios versus the tensile strength for as received and the heat-treated DP800 samples. (All data points are derived from the average of three different tensile tests)

Figs.5.23, 5.24 and 5.25 show the obtained tensile properties of tested samples. The oil-quenched samples possess higher elongation, as well as lower yield strength and tensile strength values, which implies that, the microstructures of oil quenched samples are not so "hard". They should have a relative lower martensite volume fraction. Moreover, for water-quenched samples, the elongation values decrease and the yield strength and tensile strength increase as the annealing temperature and the soaking time are increased. This can also be considered, in view of the fact that as the

annealing temperature and the soaking time are increased, the austenite volume fraction is increased as well, which results in the increased martensite volume fraction as well.

All these mechanical characteristics can also be seen in Figure 5.26 where the engineering stress versus the engineering strain for the as received and heat treated DP800 samples are presented. All samples exhibit continuous yielding behavior (no yield point) and all have high work hardening values with the exception of the oil-quenched samples.

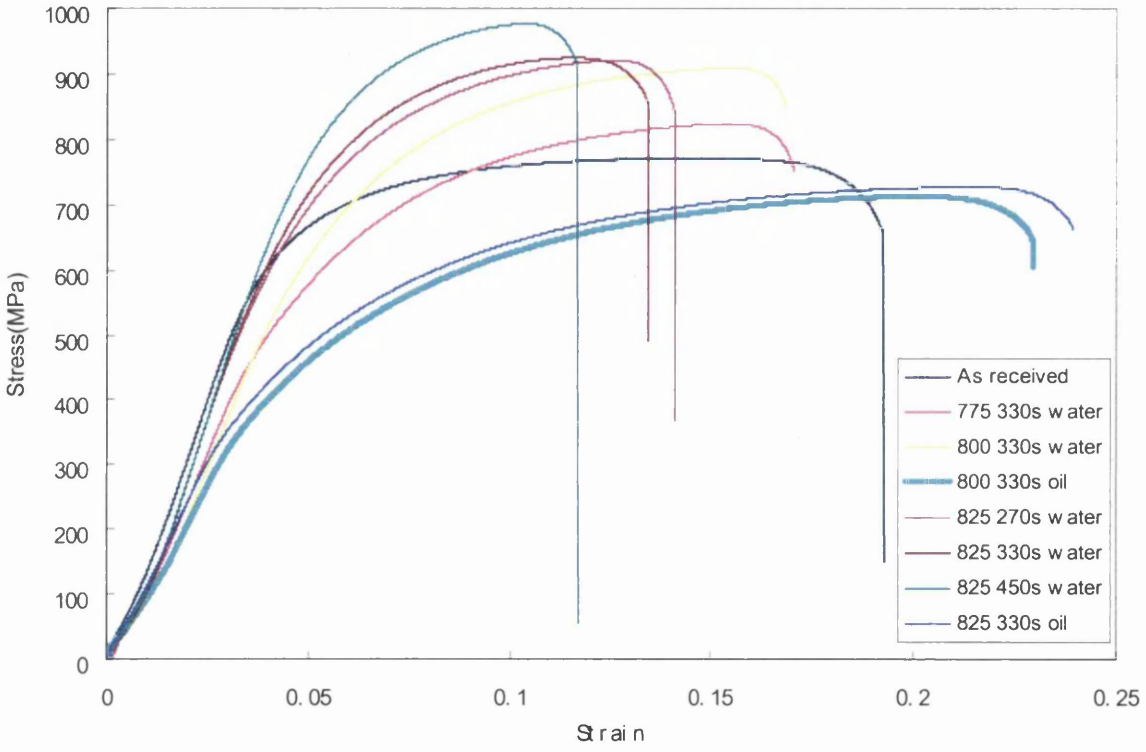

Fig.5.26: Engineering Stress versus Engineering Strain curves for all tested DP samples.

5.5.2. Microscopy of Fracture Surfaces

For an annealing temperature of 775°C, followed by water quenching, ductile fracture areas can be seen on the fracture surfaces of tensile samples (Fig.5.27). All the fracture surface exhibits similar ductile fracture characteristics.

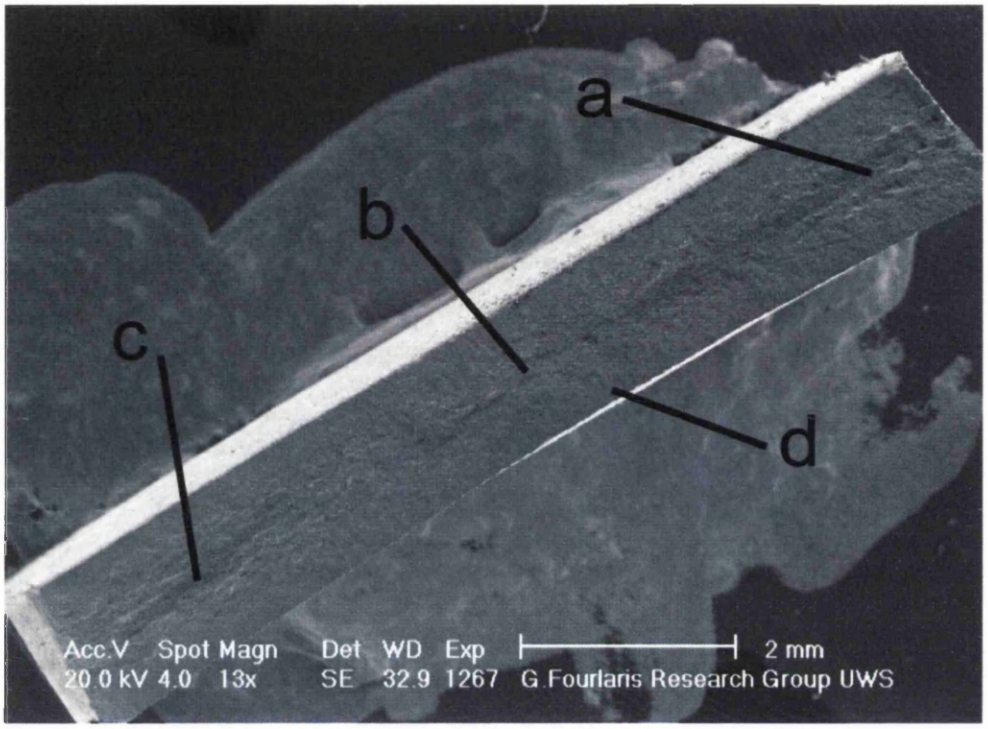

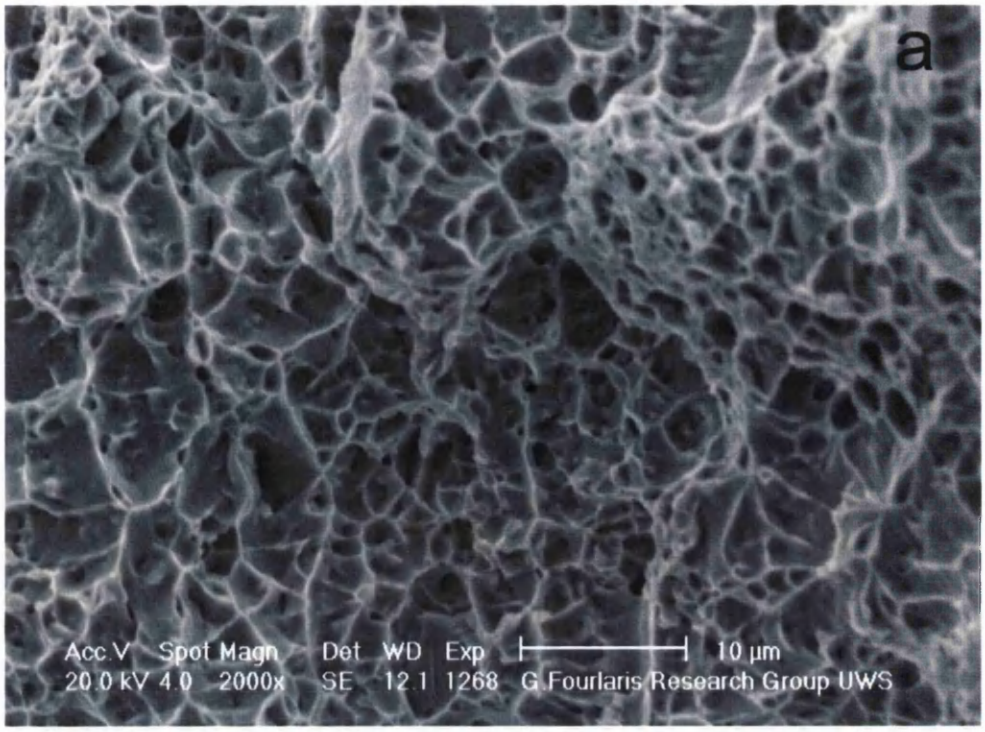
a
Acc.V Spot Magn Det WD Exp 10 µm
20.0 kV 4.0 2000x SE 12.1 1268 G.Fourlaris Research Group UWS

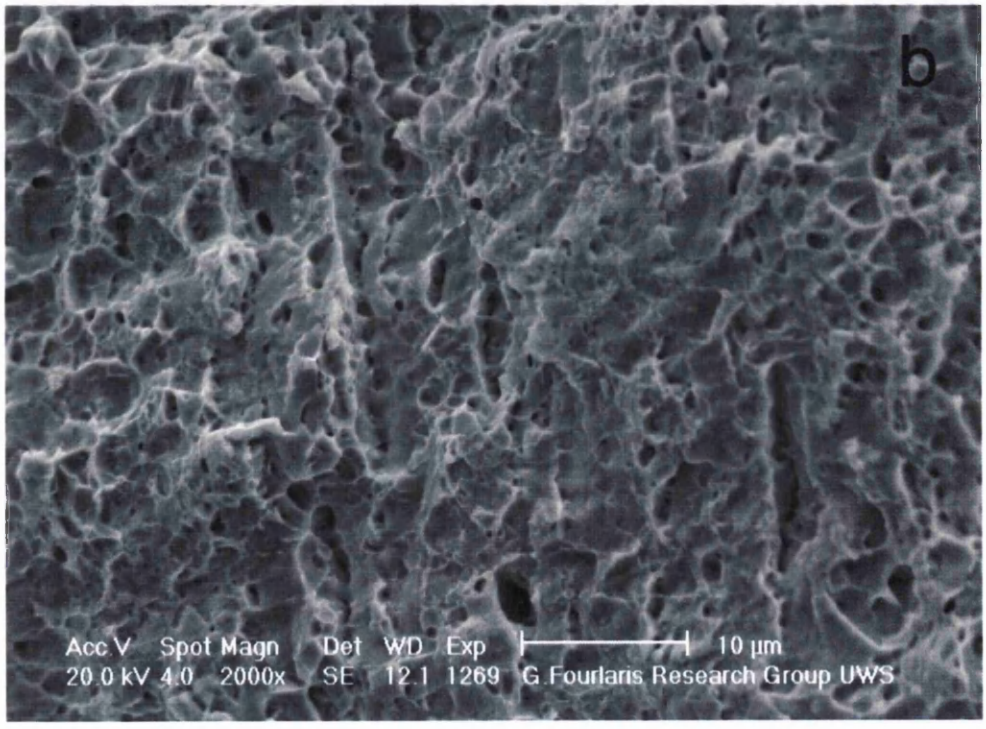
b
Acc.V Spot Magn Det WD Exp 10 µm
20.0 kV 4.0 2000x SE 12.1 1269 G.Fourlaris Research Group UWS

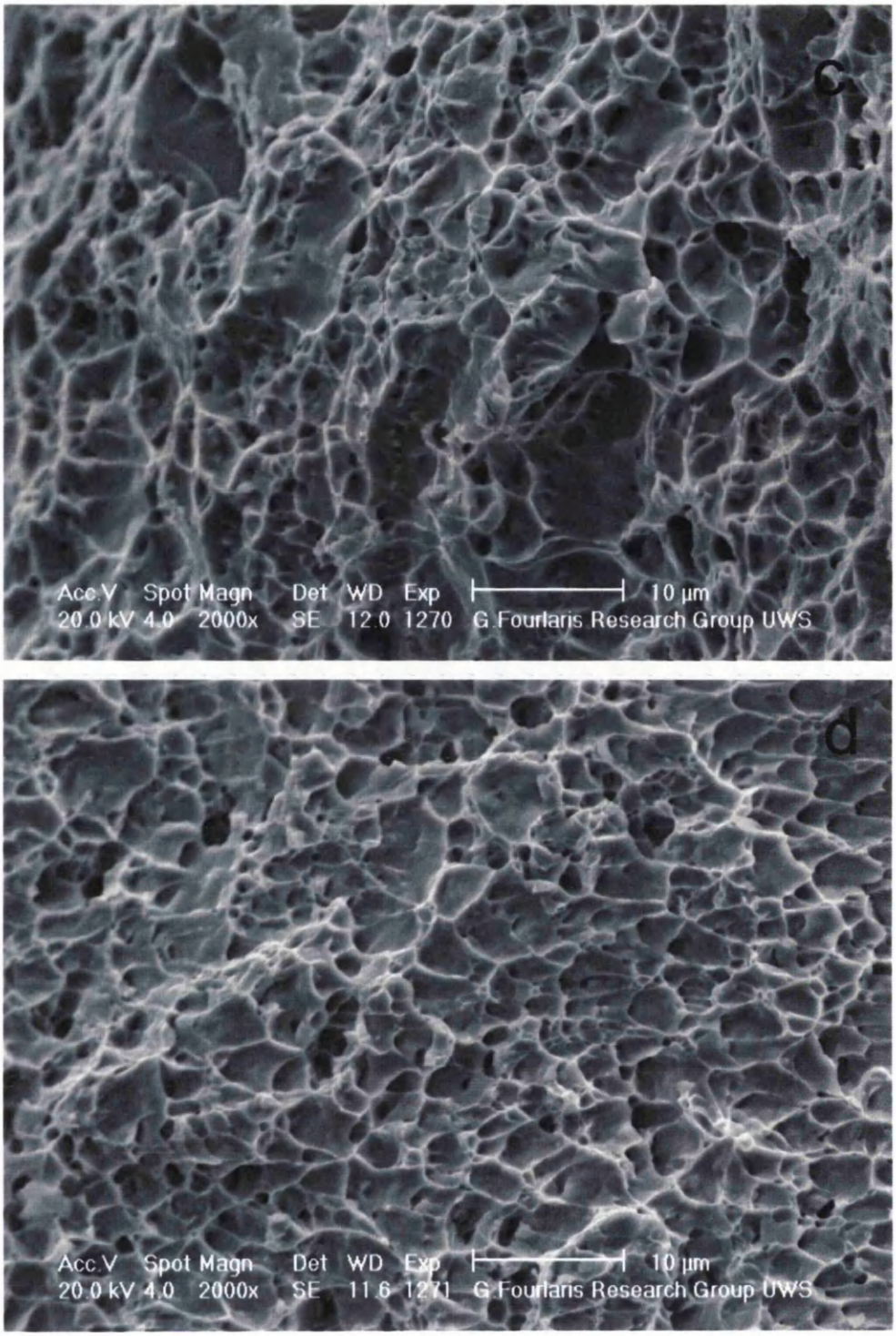

Fig.5.27: Secondary Electron micrographs of the fracture surface of a DP800 sample intercritically annealed at 775°C for 330s, followed by water quenching.

For an annealing temperature of 800°C for oil-quenched samples, all the fracture

surface exhibits typical ductile fracture characteristics (Fig.5.28).

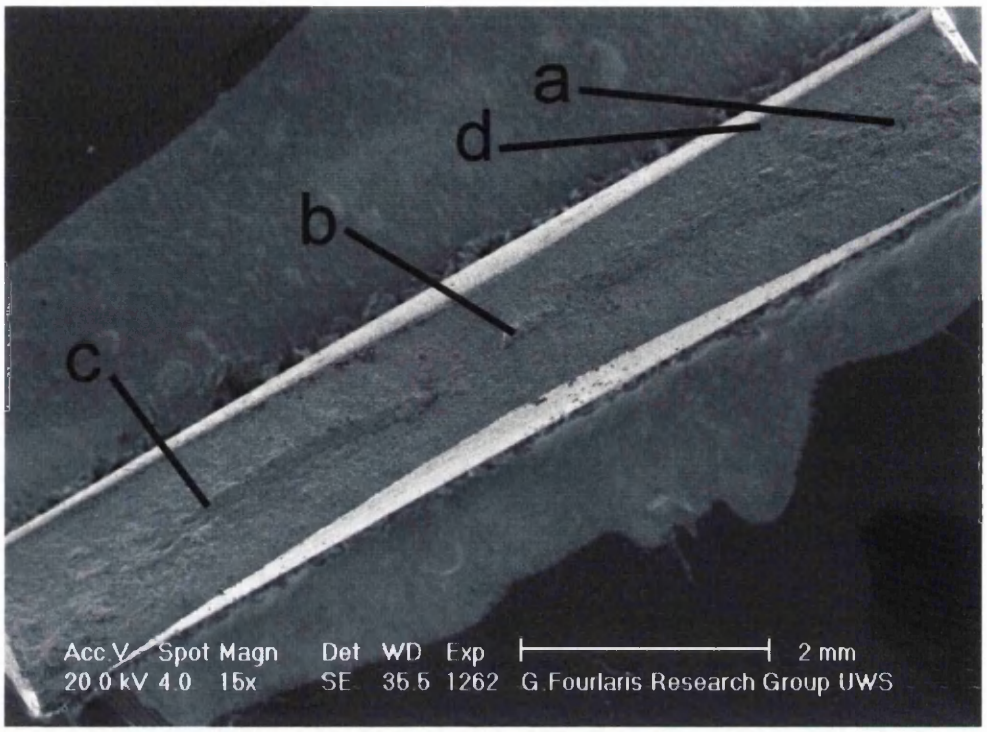

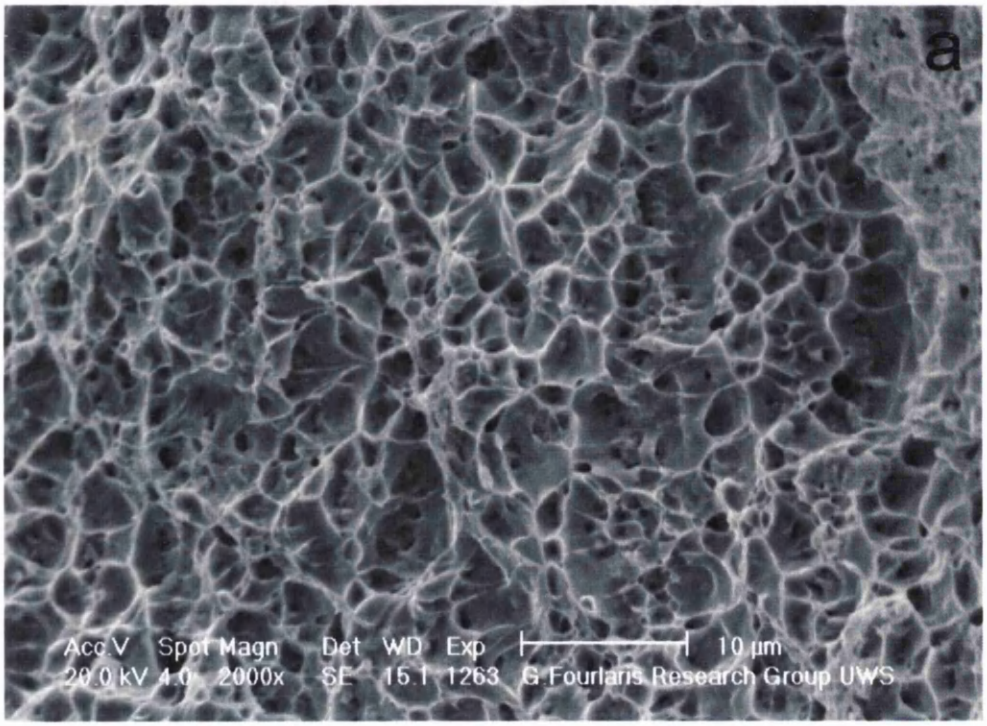

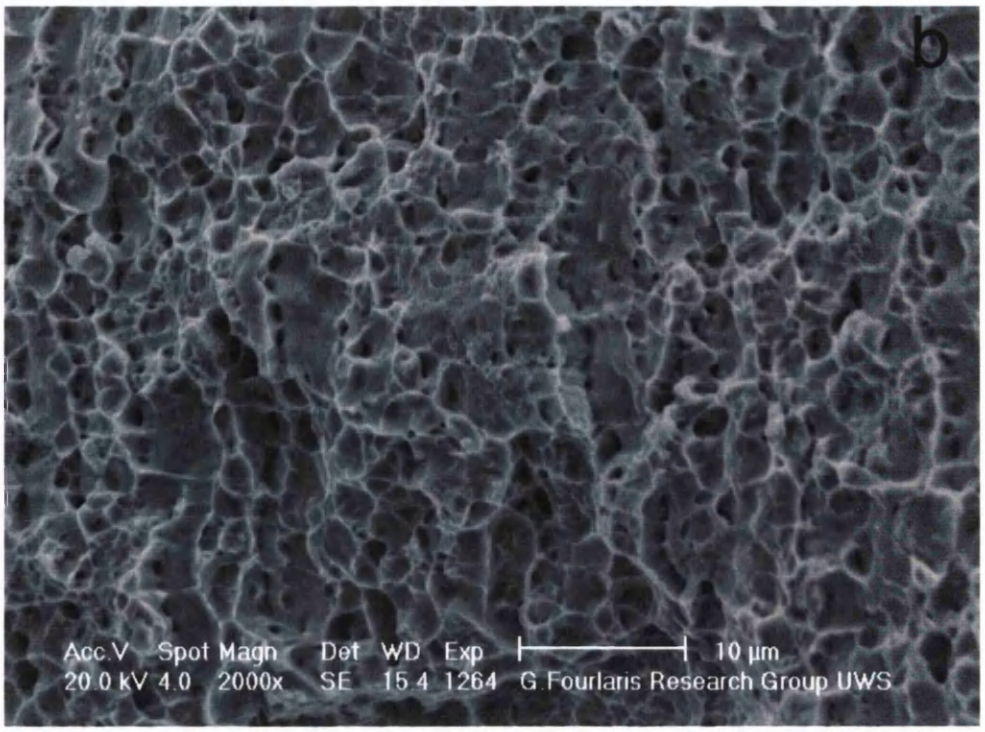
b
Acc.V Spot Magn Det WD Exp 10 µm
20.0 kV 4.0 2000x SE 15.4 1264 G Fourlaris Research Group UWS

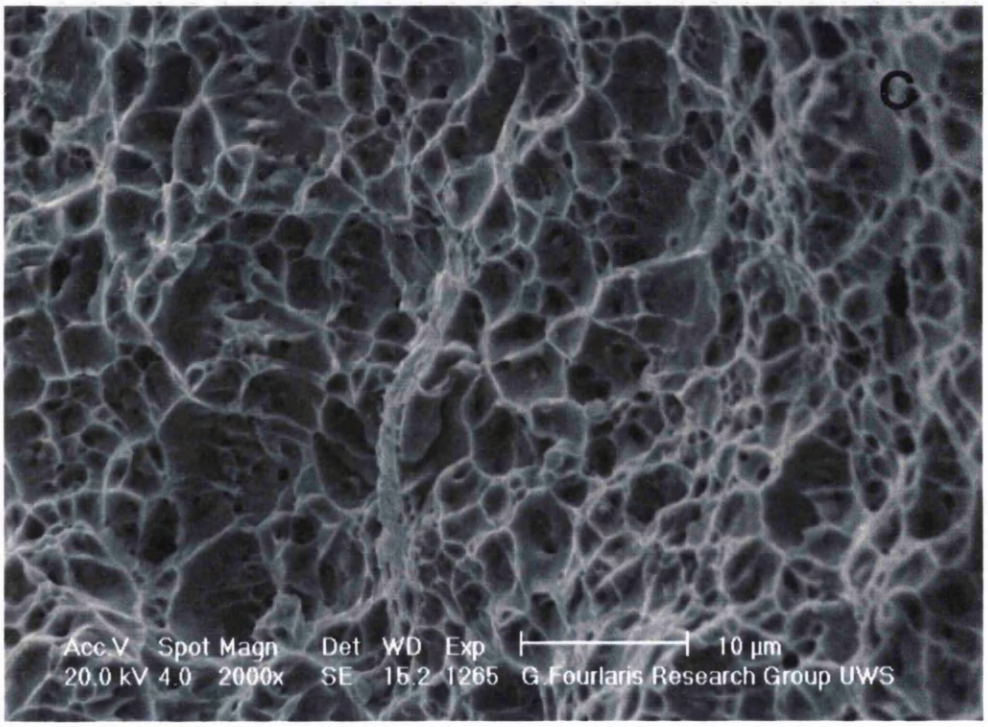
c
Acc.V Spot Magn Det WD Exp 10 µm
20.0 kV 4.0 2000x SE 15.2 1265 G.Fourlaris Research Group UWS

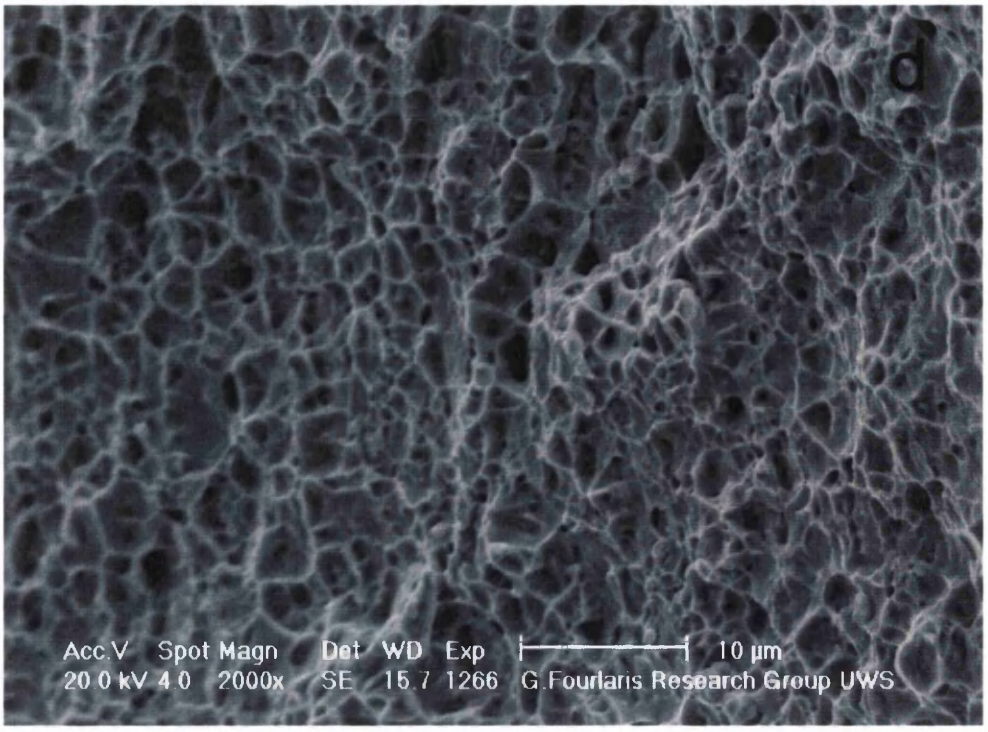

Fig.5.28: Secondary Electron micrographs of the fracture surface of DP800 samples intercritically annealed at 800°C for 330s, followed by oil quenching.

However, for the same soaking temperature and for the same soaking time, but for samples subjected to water quenching, brittle fractures can be observed in certain areas such as those marked with "d" in Figure 5.29.

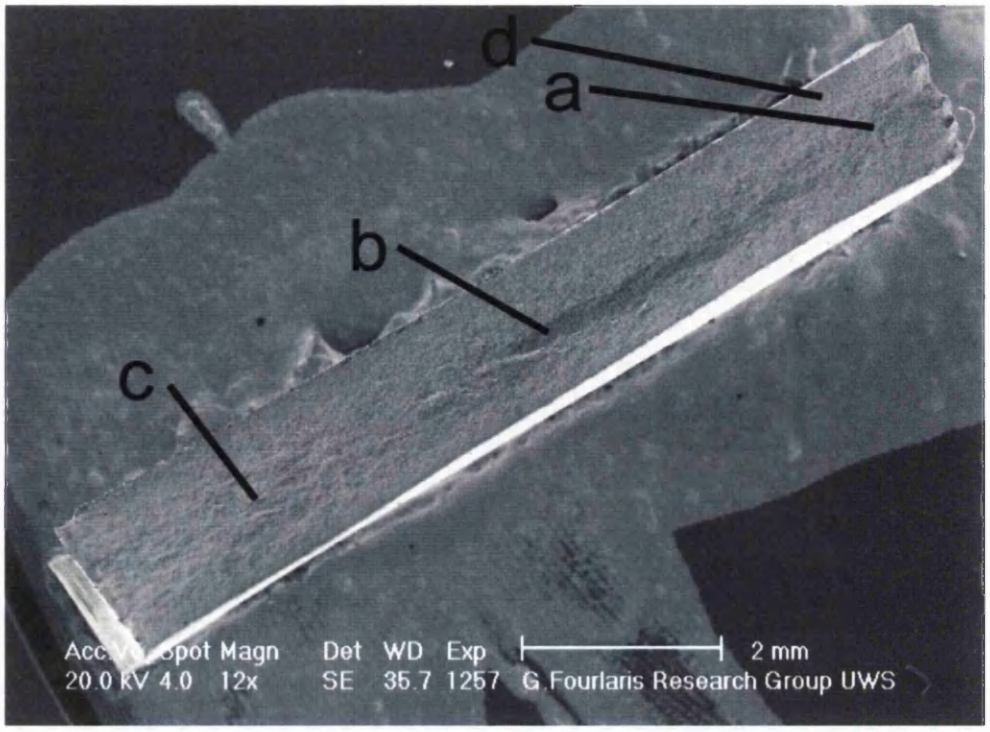
d
a
b
c
Acc.V Spot Magn Det WD Exp 2 mm
20.0 kV 4.0 12x SE 35.7 1257 G.Fourlaris Research Group UWS

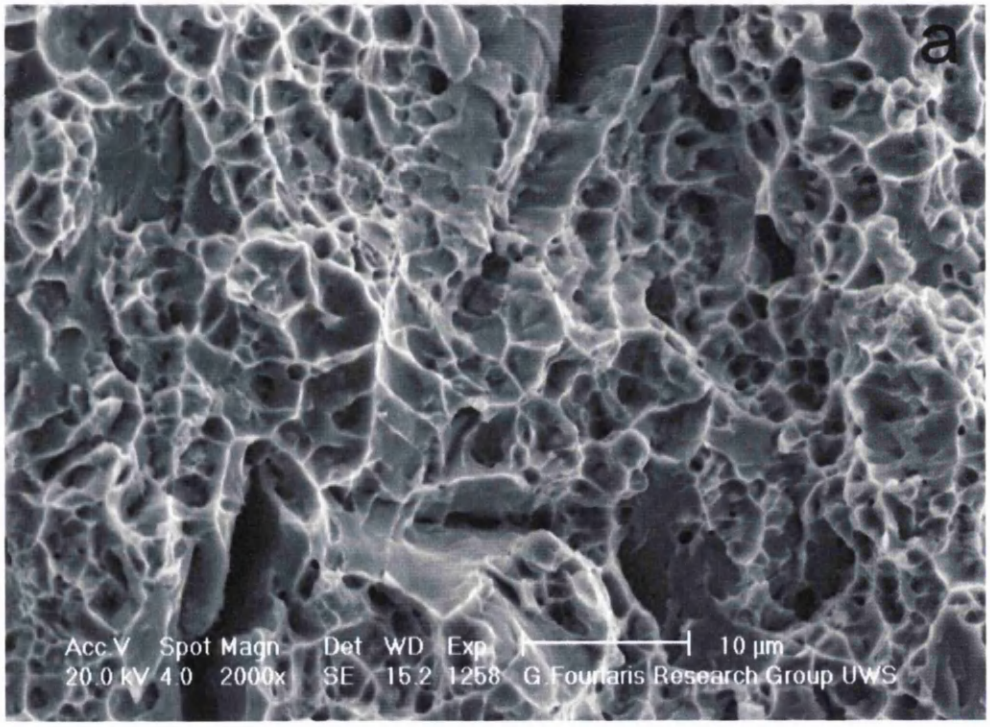
a
Acc.V Spot Magn Det WD Exp 10 µm
20.0 kV 4.0 2000x SE 15.2 1258 G.Fourlaris Research Group UWS

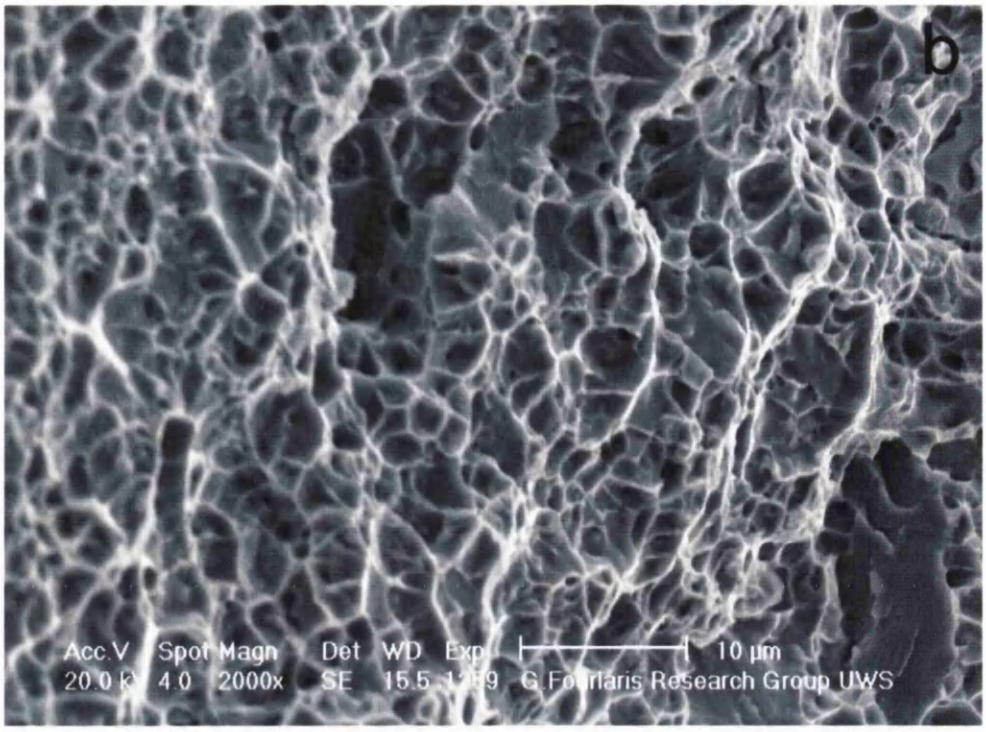
b
Acc.V Spot Magn Det WD Exp 10 µm
20.0 k 4.0 2000x SE 15.5 1259 G.Fourlaris Research Group UWS

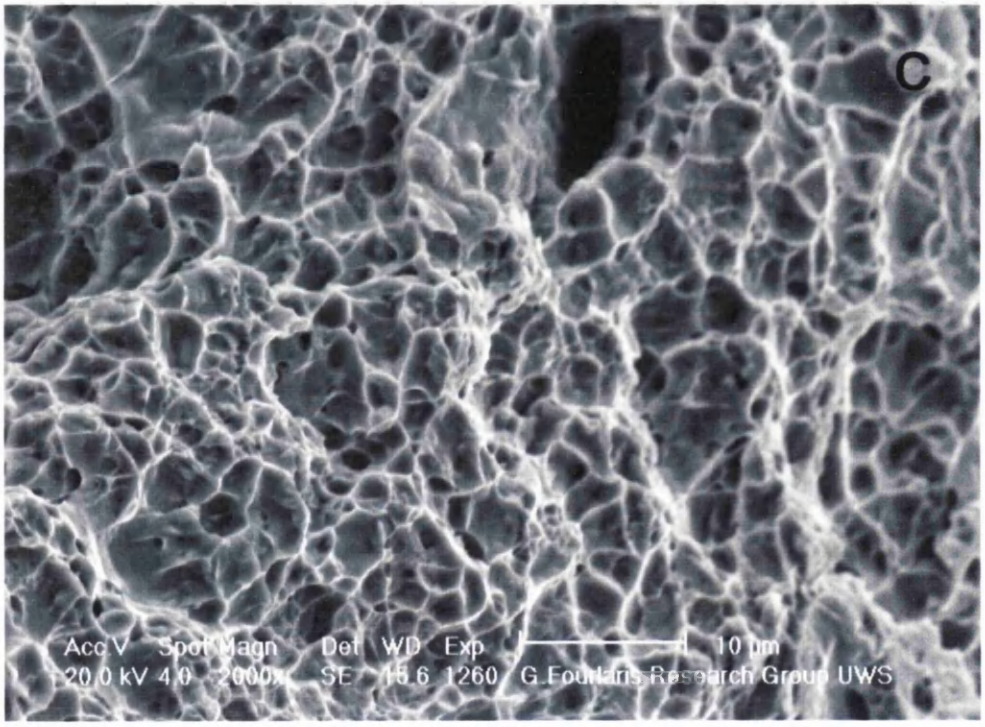
c
Acc.V Spot Magn Det WD Exp 10 µm
20.0 kV 4.0 2000x SE 15.6 1260 G.Fourlaris Research Group UWS

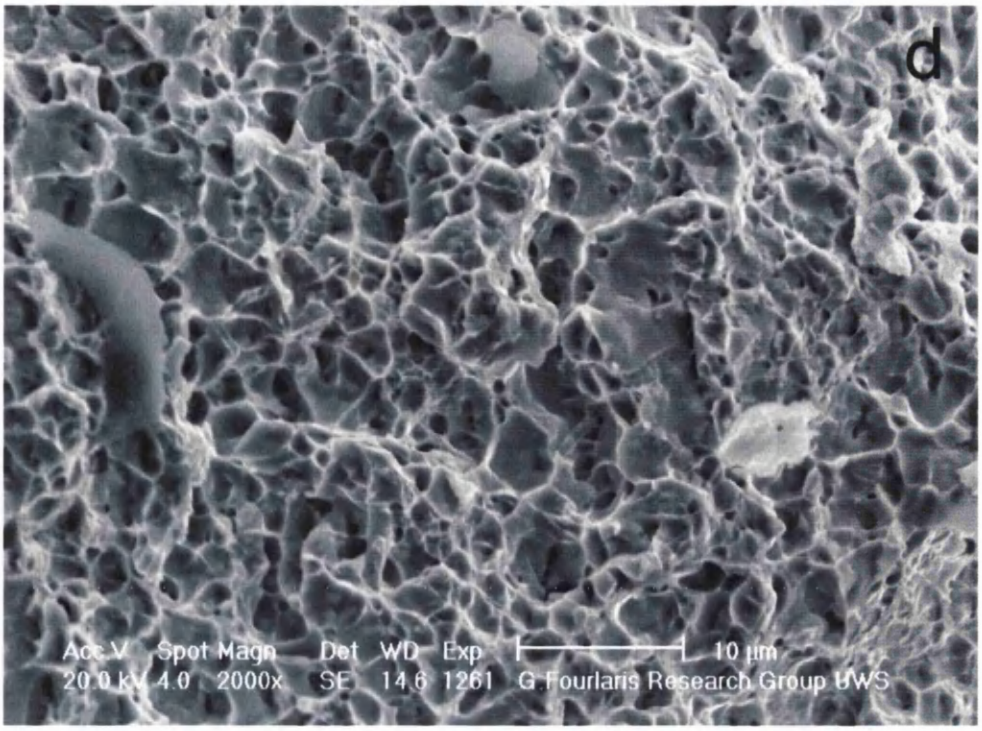

Fig.5.29: Secondary Electron micrographs of the fracture surface of DP800 samples intercritically annealed at 800°C for 330s followed by water quenching.

As the soaking temperature was increased to 825°C, for all soaking times studied (i.e. 270s, 330s and 450s), water-quenched samples exhibit brittle fracture areas. Meanwhile, the longer the sample is kept at a given soaking temperature, the more evident the brittle facture areas are (Fig.5.30). At a soaking temperature of 825°C, for a soaking time of 330s, oil-quenched samples also exhibit brittle facture characteristics (Fig.5.31). All the above indicate the samples became harder as the soaking time and soaking temperature are increased, which is attributed to the increased amounts of martensite present in the microstructure.

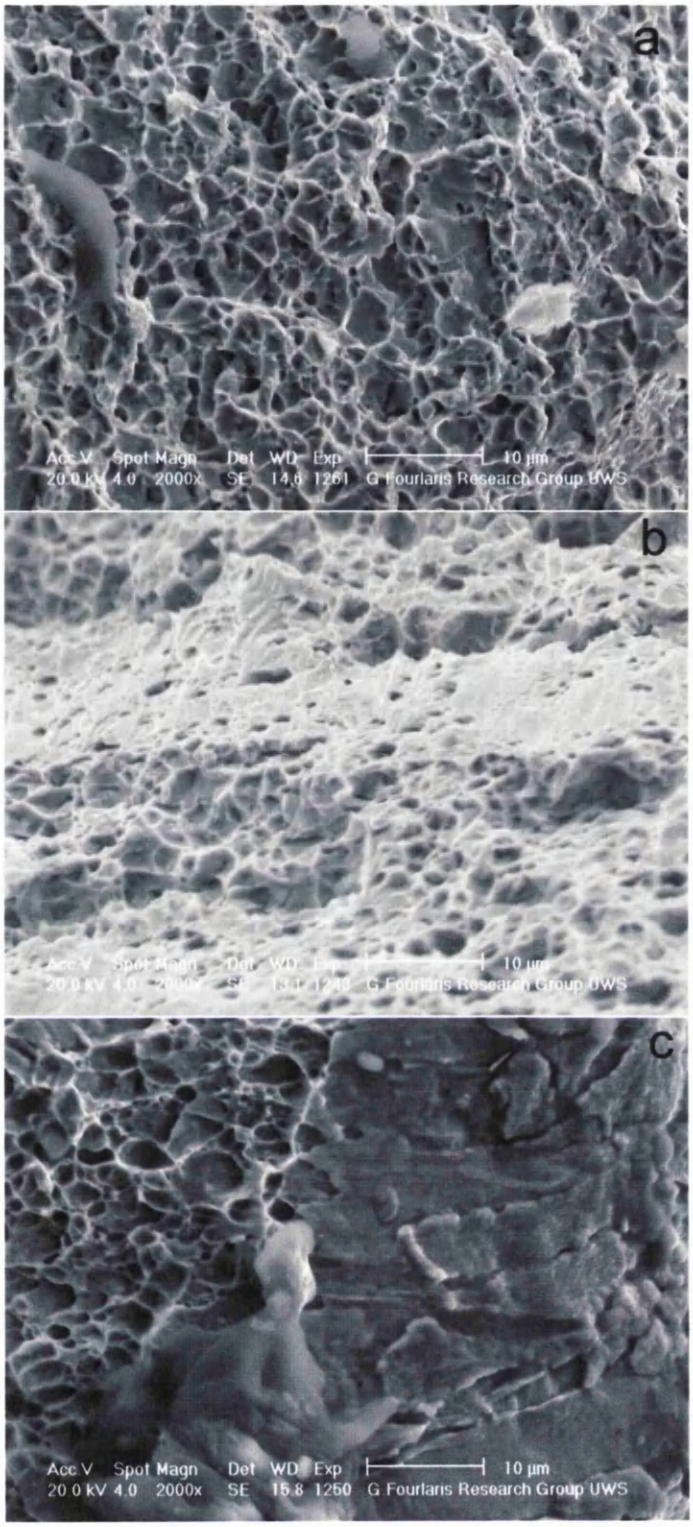

Fig.5.30: Brittle areas of DP800 samples annealed at 825°C for a soaking time of (a) 270s, (b) 330s, and (c) 450s, followed by water quenching.

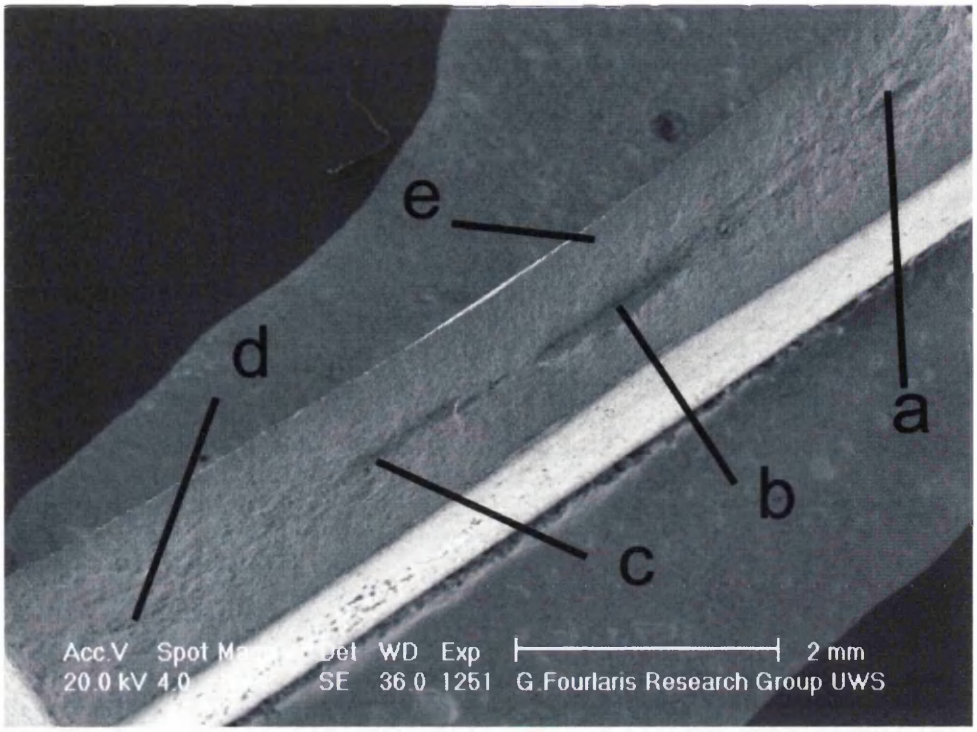
e
d
a
b
c
Acc.V Spot Ma Det WD Exp 2 mm
20.0 kV 4.0 SE 36.0 1251 G.Fourlaris Research Group UWS

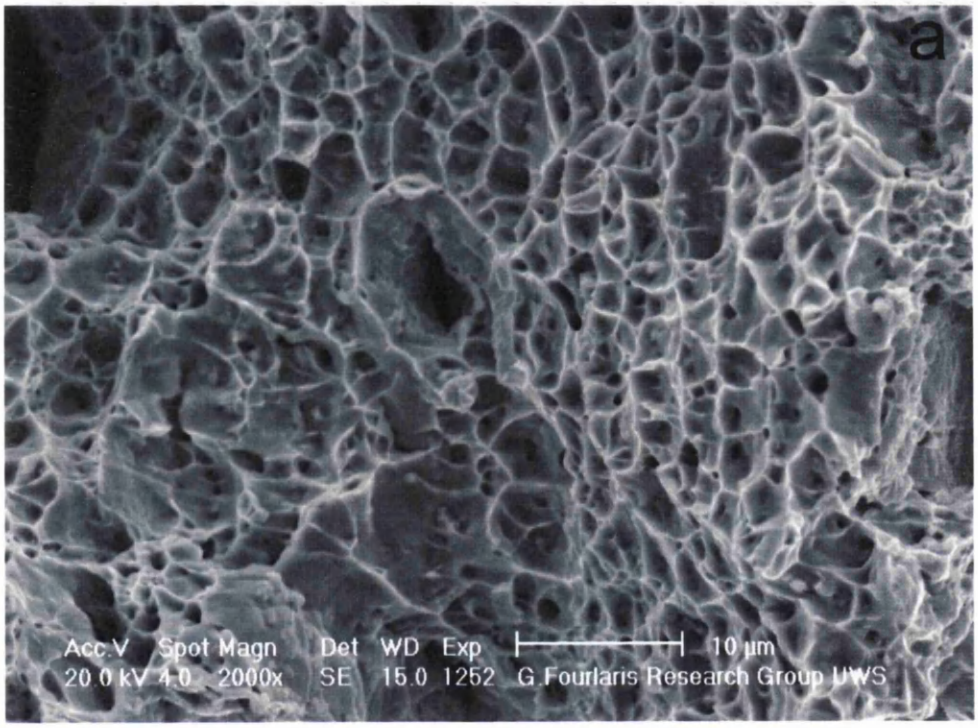
a
Acc.V Spot Magn Det WD Exp 10 µm
20.0 kV 4.0 2000x SE 15.0 1252 G.Fourlaris Research Group UWS

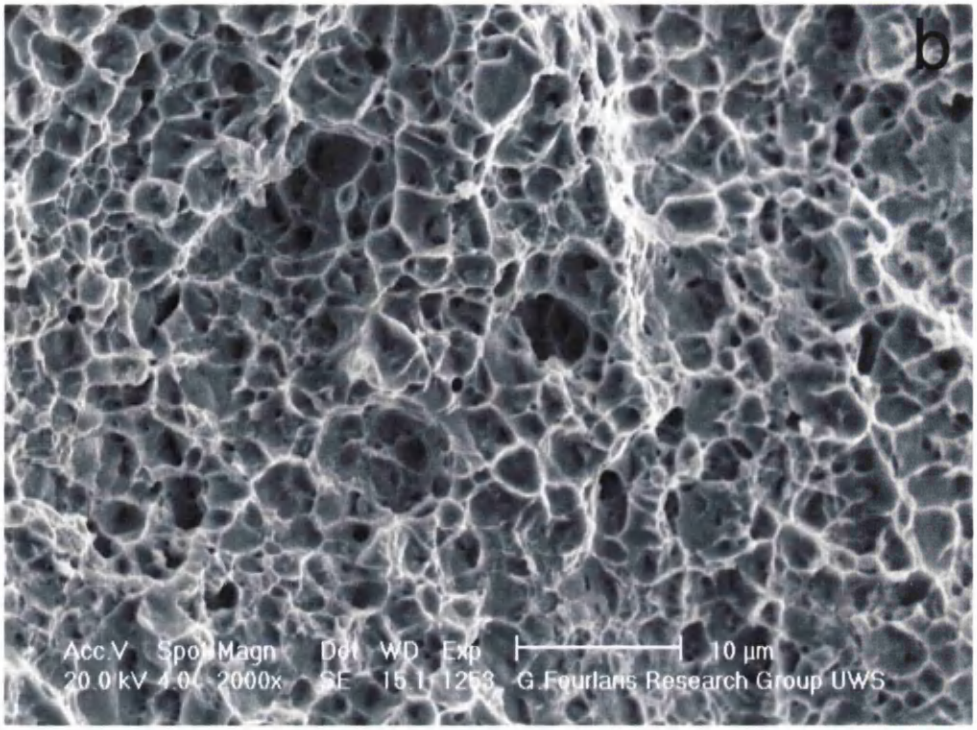
b
Acc.V Spot Magn Det WD Exp 10 µm
20.0 kV 4.0 2000x SE 15.1 1253 G.Fourlans Research Group UWS

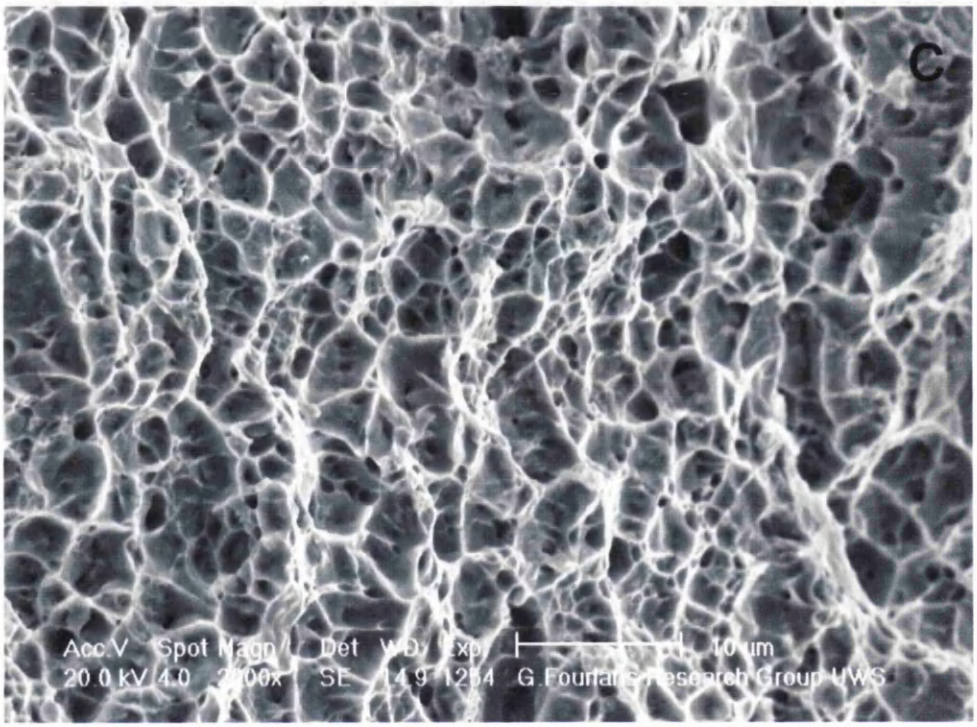
c
Acc.V Spot Magn Det WD Exp 10 µm
20.0 kV 4.0 2000x SE 14.9 1254 G.Fourlans Research Group UWS

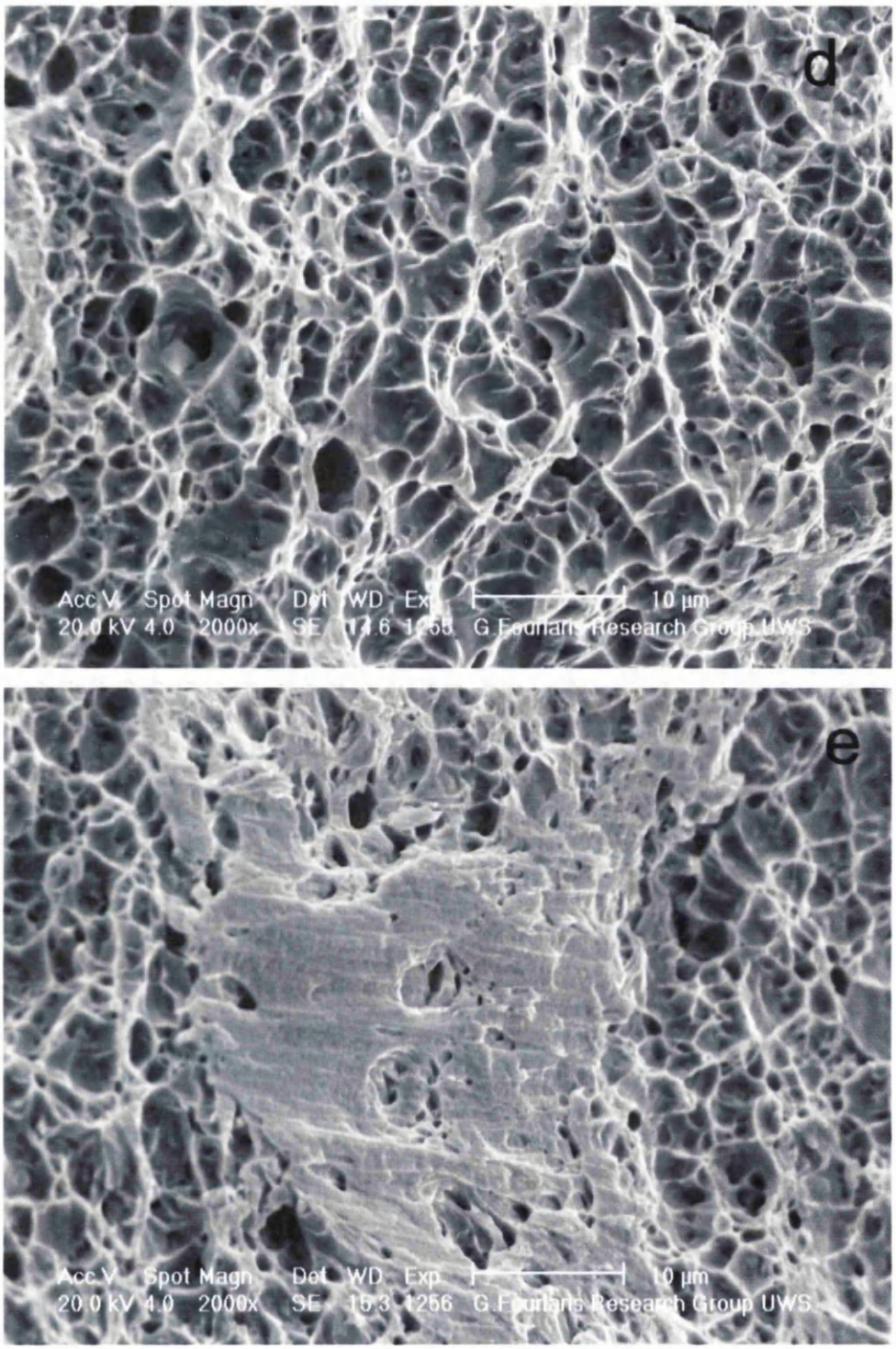

Fig.5.31: Secondary Electron micrographs of the fracture surface of the DP800 samples intercritically annealed at 825°C, followed by oil quenching for a soaking time of 330s.

The as received samples of DP800 when tensile tested and their fracture surfaces examined exbit only ductile characteristics (Fig.5.32).

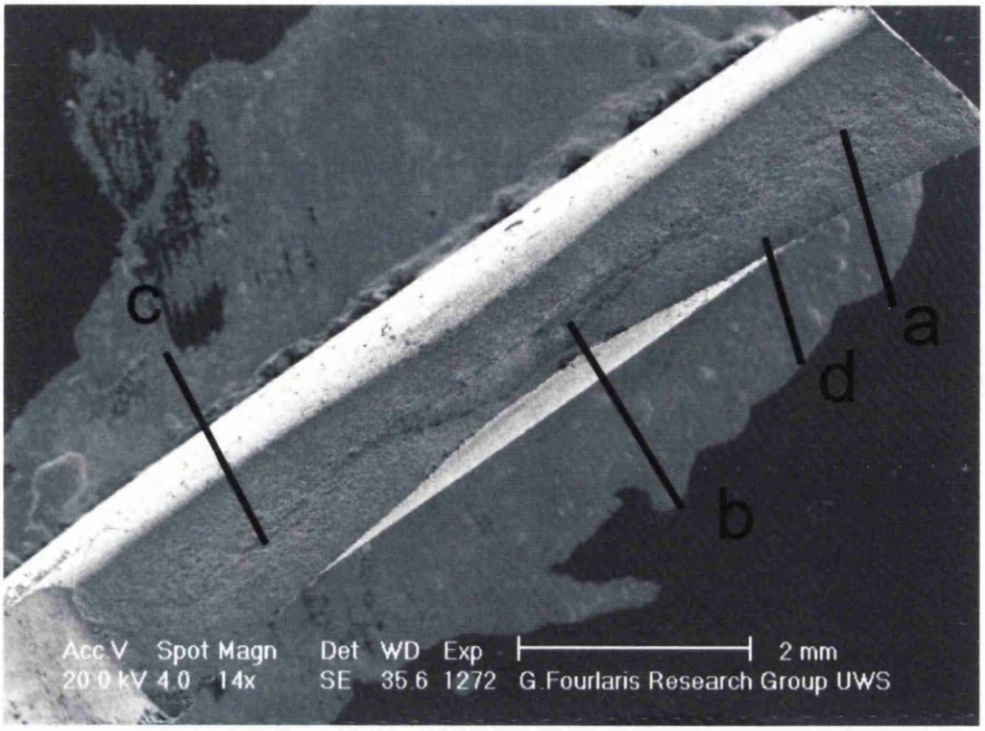

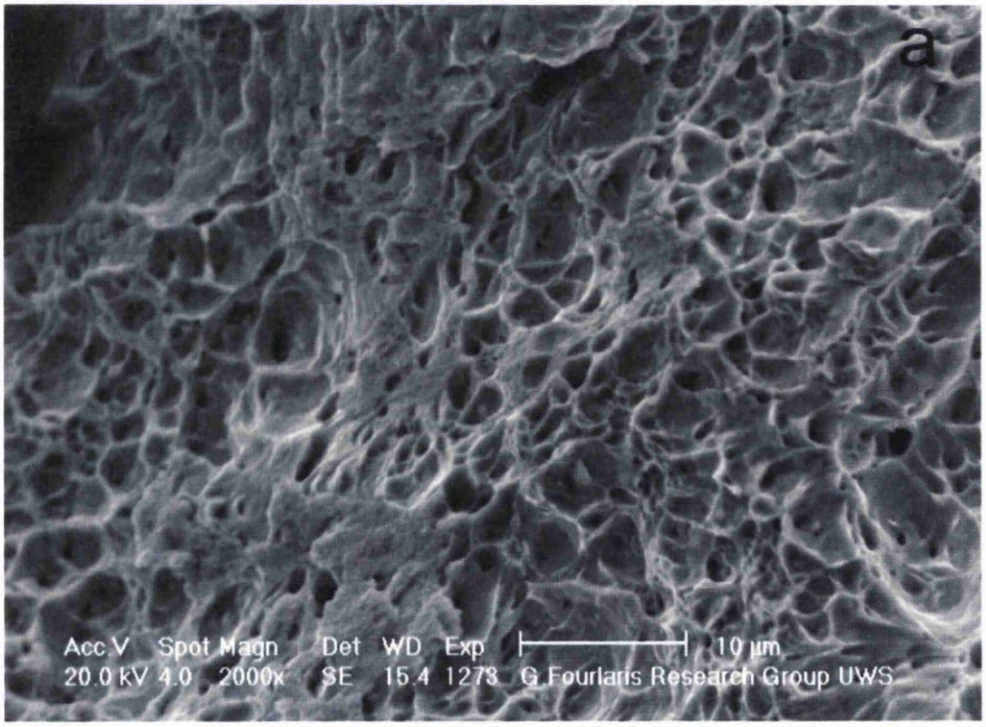

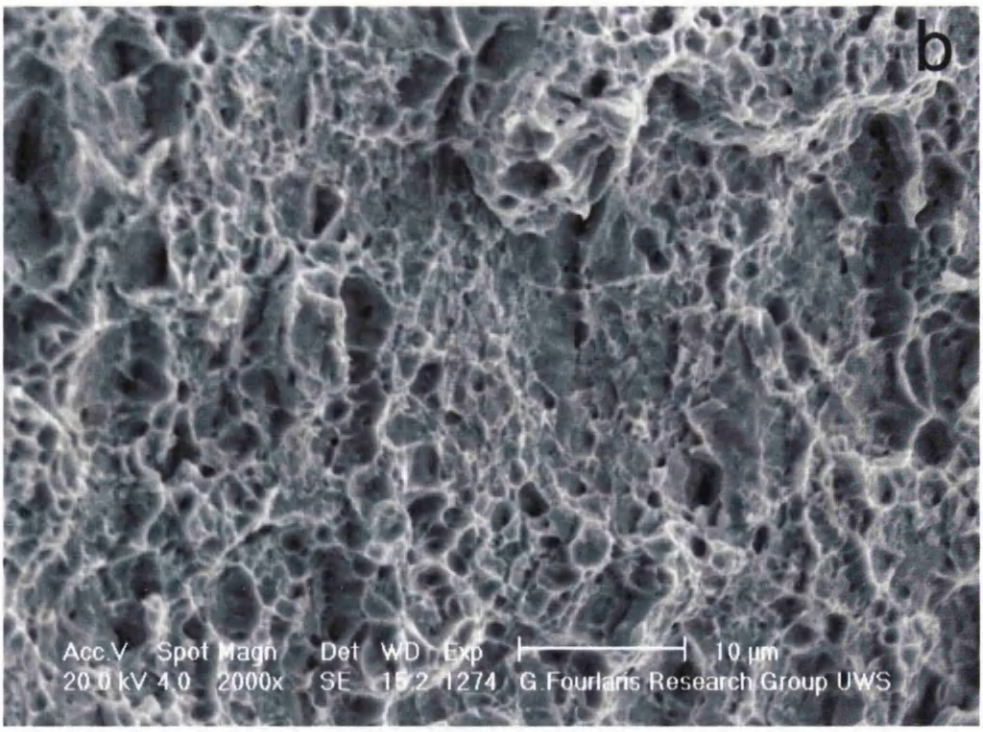
b
Acc.V Spot Magn Det WD Exp 10 µm
20.0 kV 4.0 2000x SE 15.2 1274 G Fourlaris Research Group UWS

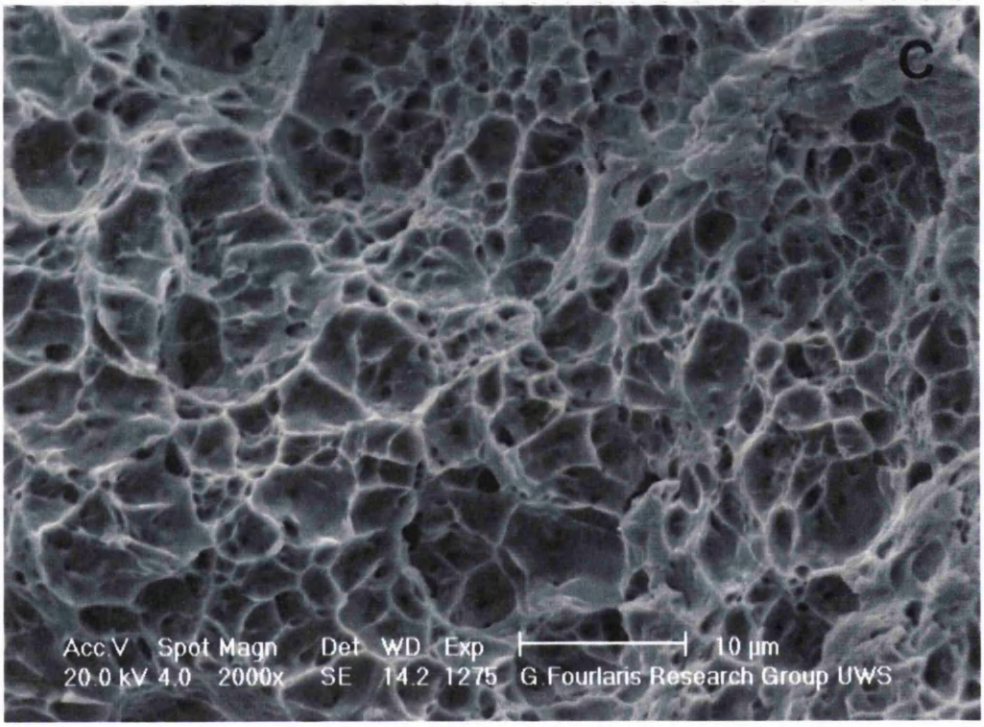
c
Acc.V Spot Magn Det WD Exp 10 µm
20.0 kV 4.0 2000x SE 14.2 1275 G Fourlaris Research Group UWS

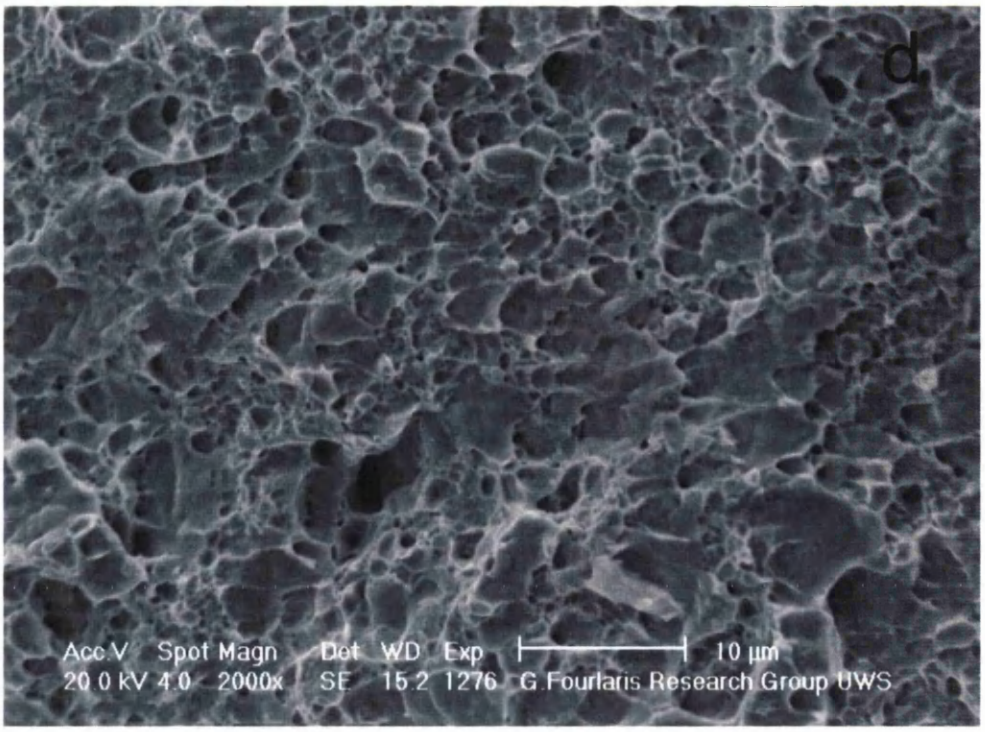

Fig.5.32: Secondary Electron micrographs of the fracture surface of the as received DP800 samples.

5.5.3. Through Thickness Microstructural Examination

The rolling direction can be easily identified from the secondary electron micrographs of the DP800 in the as received condition (Fig.5.33). It is evident the presence of some banding, especially in the central region of the samples which may have formed during the rolling process.

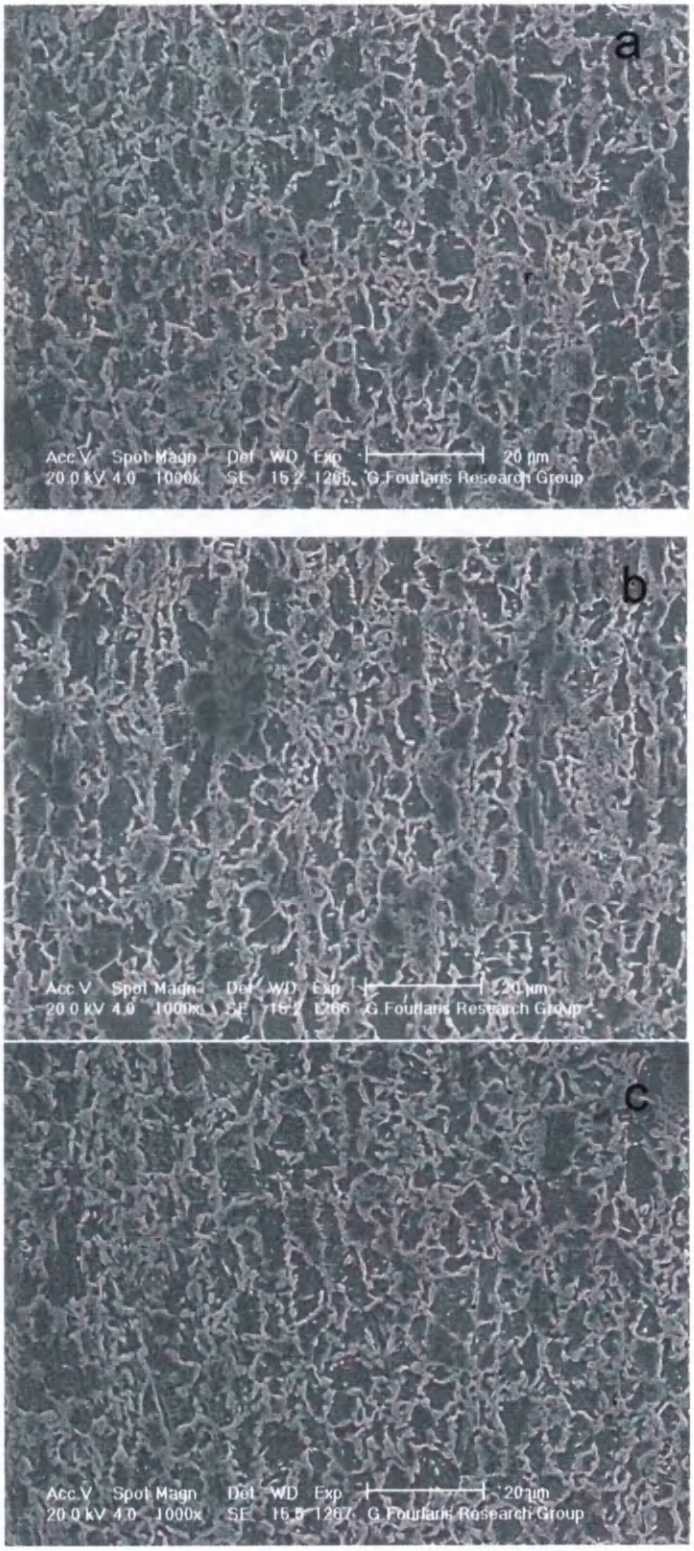

Fig.5.33: Secondary Electron Micrographs of the DP800 as received samples through thickness. (a) Area close to the edged of sample, (b) Central zone, (c) Area close to the opposite edge of the sample.

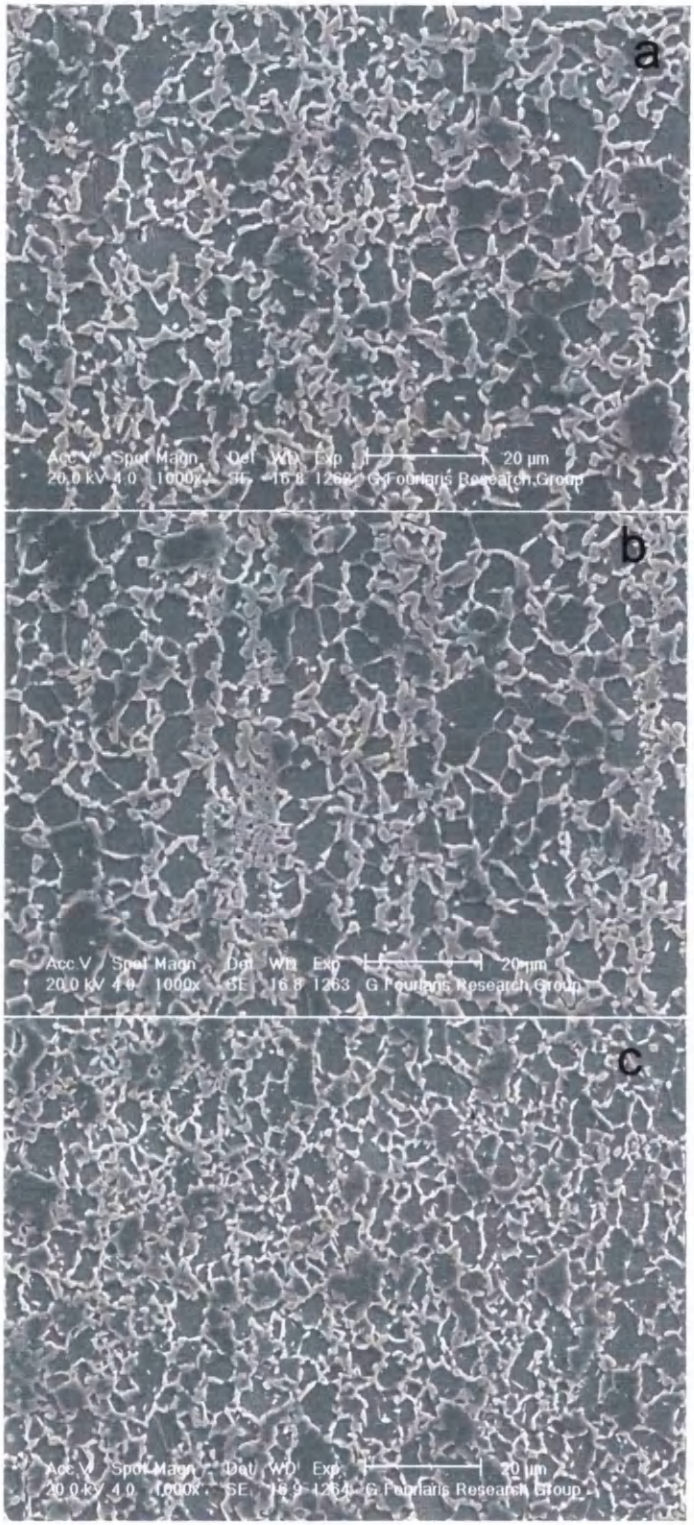

Fig.5.34: Secondary Electron micrographs of the DP800 samples intercritically annealed at 775°C for a soaking time of 330s, followed by water quench through the thickness. (a) Area close to the edged of sample, (b) Central zone, (c) Area close to the opposite edge of the sample.

For samples intercritically annealed at 775°C for 330s, and followed by water quenching, the rolling direction is no longer so evident in the micrographs of studied samples. However, some banding can still be observed in the central region of the samples. (Fig.5.34) This 'residual' banding may be due to the fact that when samples are heated under this condition, the central portions of the sample did not fully transform as those close to the edges. Longer times or higher annealing temperatures might be required to obtain homogeneous microstructures. The second phase 'islands' in the central area are more scattered than those close to the edges of the sample. This can be understood by considering the cooling rate at the surfaces is higher than that of the centre of the sample, which results in finer martensite dispersions in areas adjacent to the surface of the sample. Balliger [36] reported that void nucleation occurred preferentially at the larger second phase islands. Therefore, the ductile fracture process is generally considered to occur in three sequential stages, namely, void nucleation, void growth and void coalescence. The voids nucleate at second phase particles and form either by cracking of the particle or by decohesion of the particle/matrix interface [37]. For the DP800 samples examined, the coarse and scattered second phase always existed in the central region of the samples. All the above observation could provide an explanation for crack initiation in the central area of the tensile samples.

For a higher annealing temperature of 800°C and for a soaking time of 330s, although the rolling direction can still be identified, the banding is no longer clear, even in the central regions of water quenched samples. In addition, martensite island dispersions are also more scattered in the middle area (Fig.5.35). For the same annealing temperature and soaking time, but for oil-quenched samples, the rolling direction can be easily found, and the banding can still be seen in the central regions of the sample (Fig.5.36).

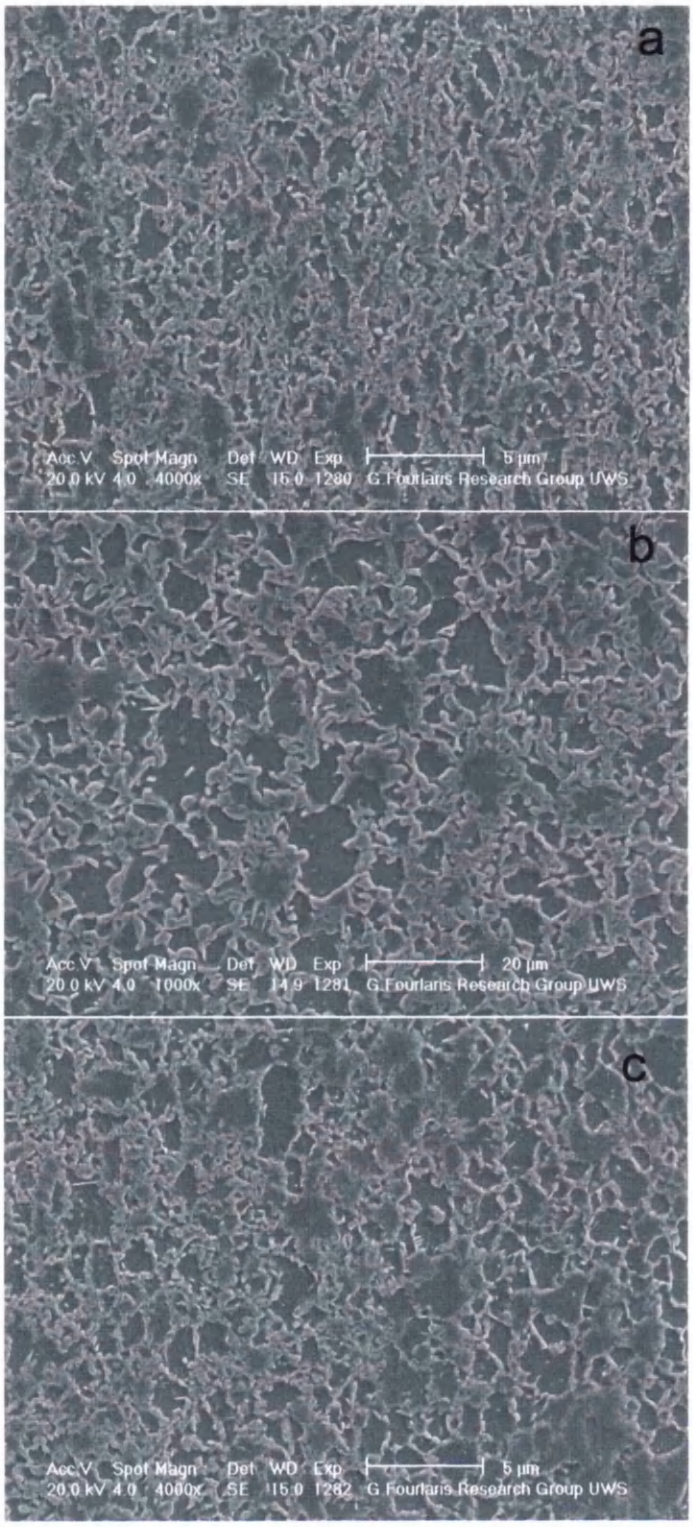

Fig.5.35: Secondary Electron micrographs of the DP800 samples intercritically annealed at 800° C for a soaking time of 330s, followed by water quench through the thickness. (a) Area close to the edged of sample, (b) Central zone, (c) Area close to the opposite edge of the sample.

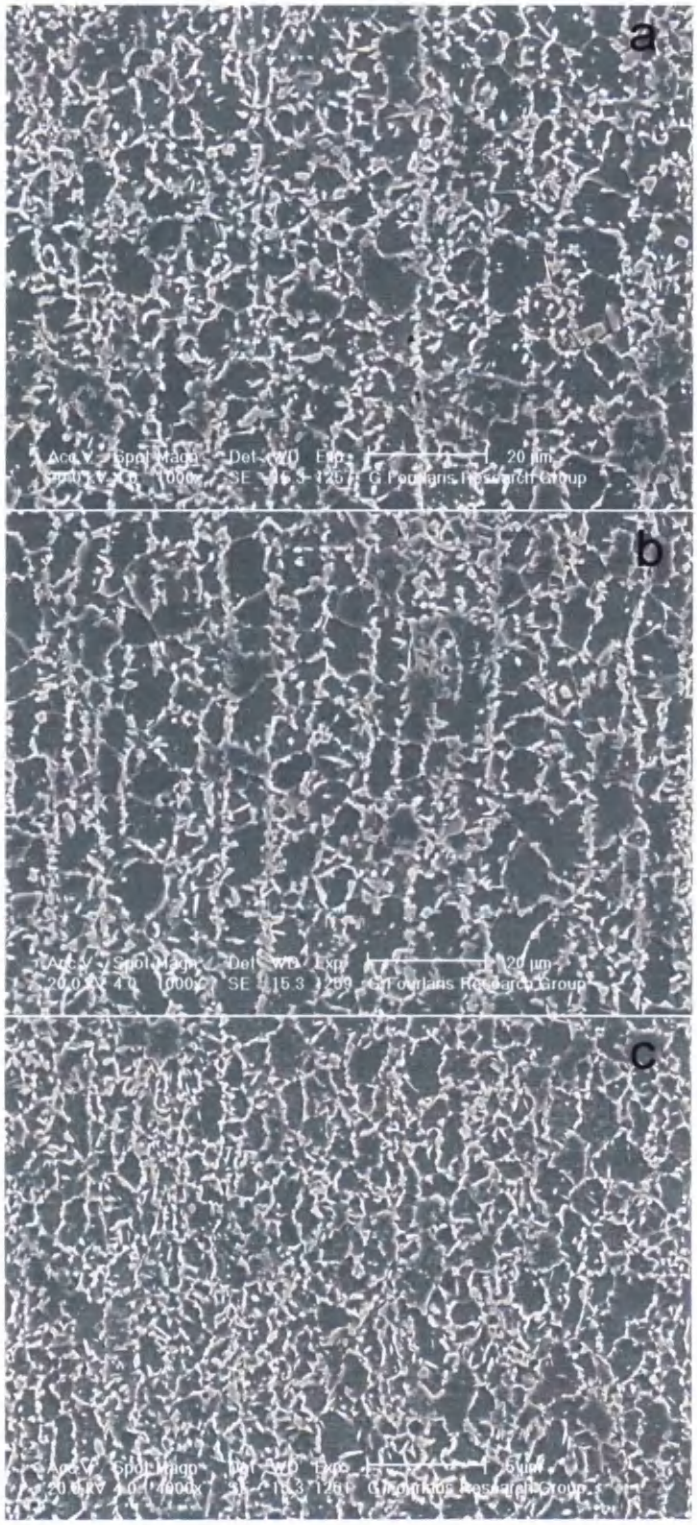

Fig.5.36: Secondary Electron micrographs of the DP800 samples intercritically annealed at 800°C for a soaking time of 330s, followed by oil quench through the thickness. (a) Area close to the edged of sample, (b) Central zone, (c) Area close to the opposite edge of the sample.

When the annealing temperature was increased to 825°C, for a soaking time of 270s or 330s water-quenched samples, the obtained microstructures look similar as those obtained at an annealing temperature of 800°C for a soaking time of 330s, followed by water quenching. The rolling direction can also be defined while the presence of a banding is no longer clear (Figs.5.37, 5.38).

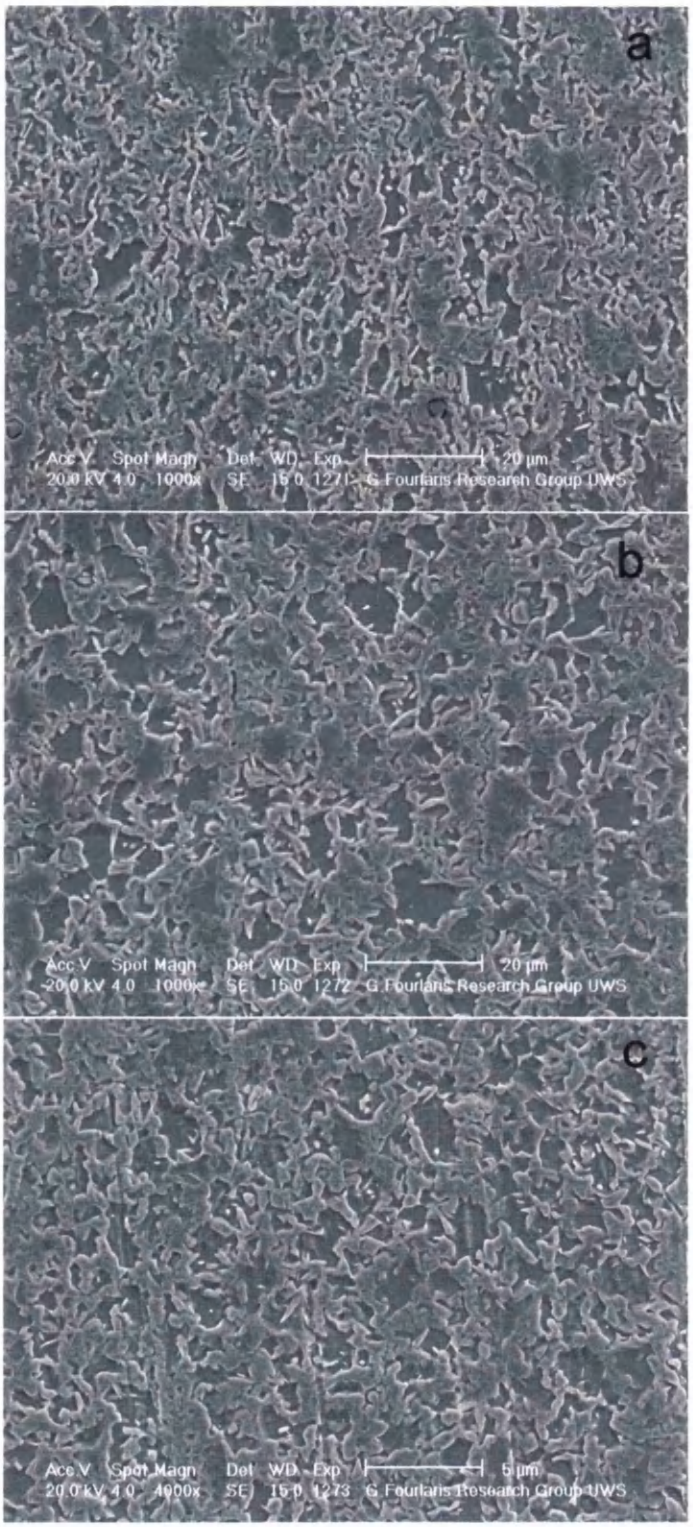

Fig.5.37: Secondary Electron micrographs of the DP800 samples intercritically annealed at 825°C for a soaking time of 270s, followed by water quench through the thickness. (a) Area close to the edged of sample, (b) Central zone, (c) Area close to the opposite edge of the sample.

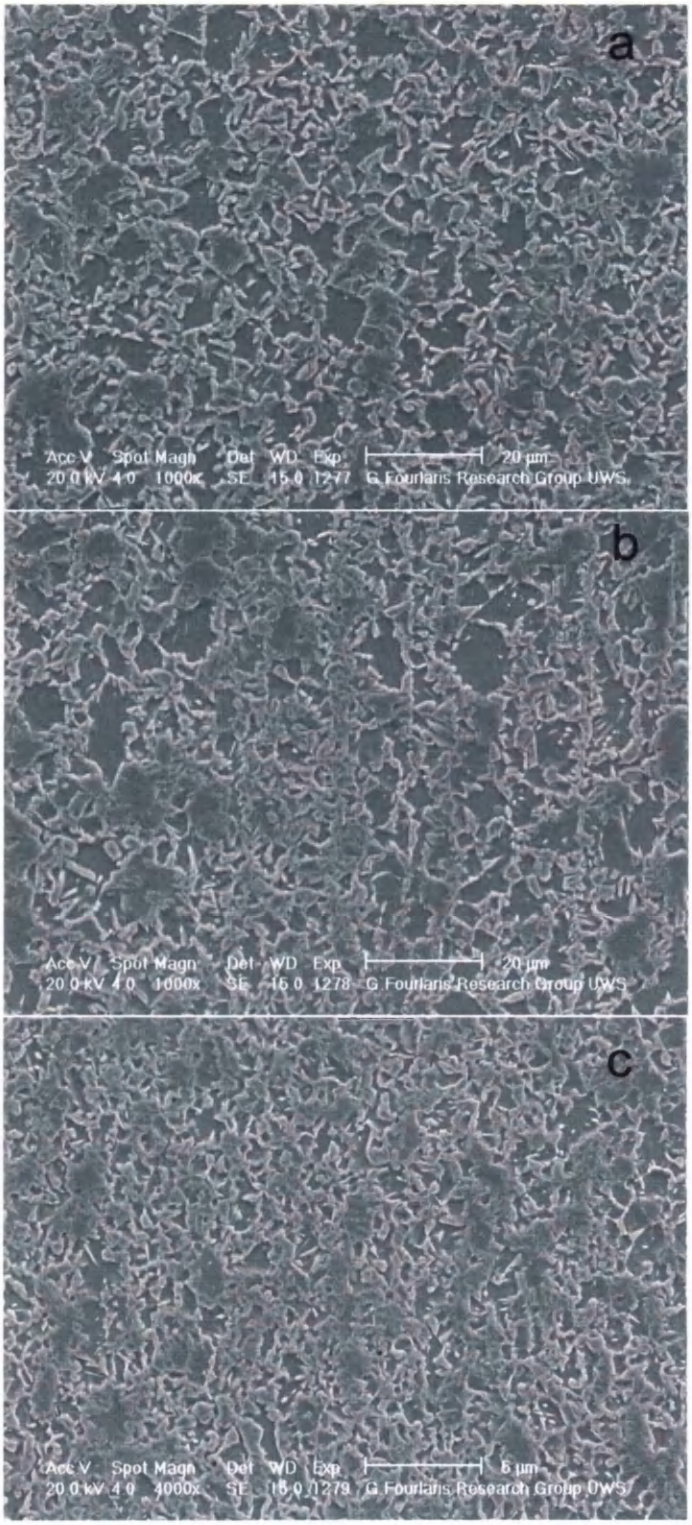

Fig.5.38: Secondary Electron micrographs of the DP800 samples intercritically annealed at 825° C for a soaking time of 330s, followed by water quench through the thickness. (a) Area close to the edged of sample, (b) Central zone, (c) Area close to the opposite edge of the sample.

However, when the soaking time was increased to 450s, the banding is completely eliminated. It indicates that at such a high annealing temperature, this soaking time is sufficient to let the phase transformation reach its completion (Fig.5.39).

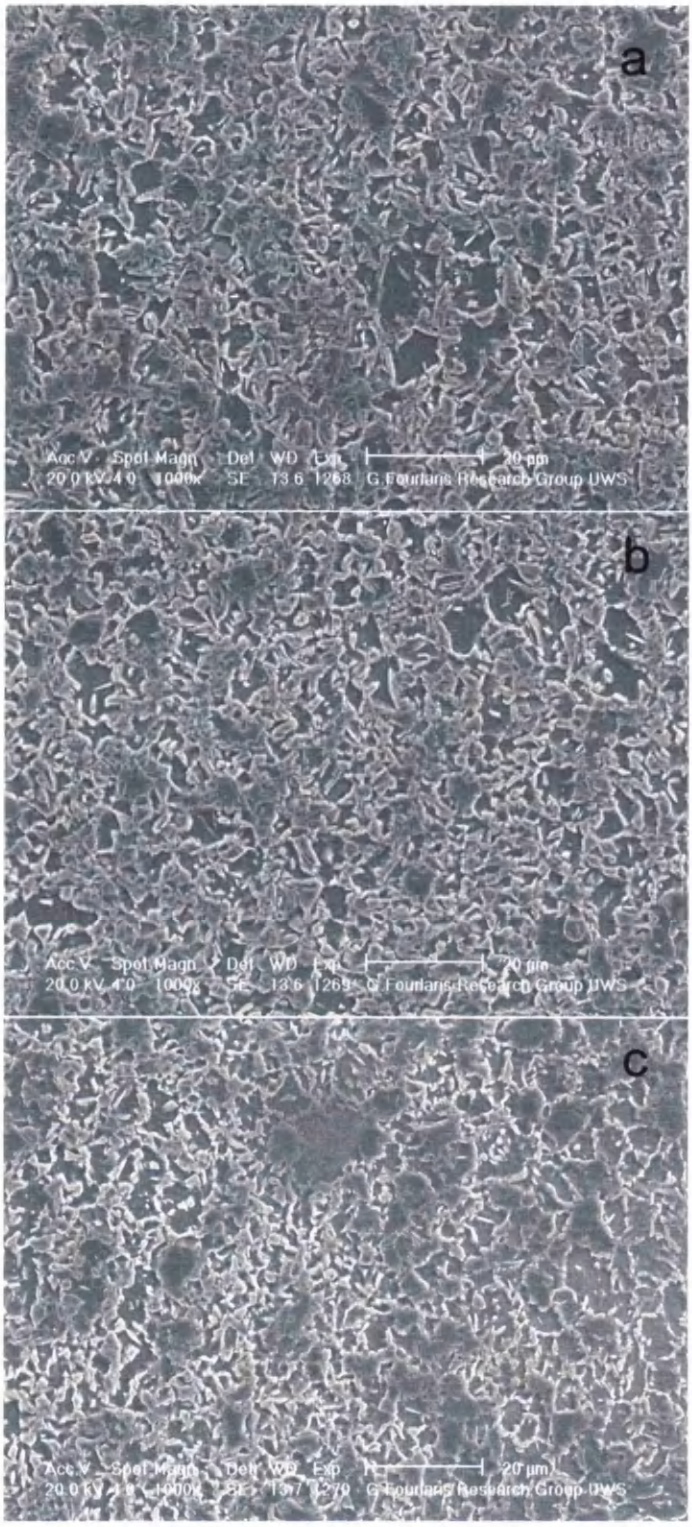

Fig.5.39: Secondary Electron micrographs of the DP800 samples intercritically annealed at 825°C for a soaking time of 450s, followed by water quench through sample the thickness. (a) Area close to the edged of sample, (b) Central zone, (c) Area close to the opposite edge of the sample.

5.6. General Discussion

The results of the present study have highlighted several effects of the heat treatment parameters on the microstructure and mechanical properties of DP800 samples. It is evident that higher annealing temperatures and longer soaking times increased the austenite volume fraction, which consequently caused the increase of the volume fraction of second phase, when identical cooling rates were employed. For water-quenched samples, the high volume fraction of second phase resulted in higher hardness, higher tensile strength, higher yield strength, and lower elongation values. Meanwhile, a longer soaking time can partially or even totally eliminate the prior bands present in the microstructure, appearing in the middle area of the as received cold rolled samples. These bands are observed along the rolling direction, which implies that its formation took place during the rolling process. A high annealing temperature can increase the austenite growth rate (kinetic considerations), and a longer soaking time could result in a complete phase transformation. To obtain the harder microstructures required for a DP800 product, a soaking time between 300s and 330s is required. To efficiently eliminate the banding, at temperatures above 800°C, a soaking time of 330s was sufficient. However, at lower annealing temperatures such as 775°C, a longer soaking time is required to efficiently eliminate this banding. In addition, as the volume fraction of second phase is increased, the more evident the brittle fracture characteristics of tested tensile specimens. As previously mentioned, void nucleation occurred preferentially at the larger second phase islands. For the DP800 samples examined, the banding and the coarse and scattered second phase always existed in the central region of the samples. This could provide an explanation for crack initiation in the central area of the tensile samples.

Optimized DP800 strips are obtained by intercritically annealing the as received samples at 775°C for 330s, followed by water quenching. Compared to the as received DP800 samples, these modified strips have a tensile strength of approximately 816MPa, significantly higher than 774MPa (as received sample). In

addition, the modified via heat treatment samples retain a relative high elongation, approximately 16%. Both modified and as received samples have a hardness value of approximate 236. The most important aspect of this modification via heat treatment approach is that the modified sample has an excellent ratio of $\delta 0.2\%$/UTS of approximate 0.58, which is less than the "ideal" DP ratio of 0.6, and much less than 0.77, obtained in the as received DP800 samples. Consequently, samples intercritically annealed at 775°C for 330s, followed by water quenching, have the best dual phase properties for producing a DP800 steel product among all tested samples.

6.0. CONCLUSIONS

- The cooling rate from the intercritical annealing temperatures appears to be the most important factor influencing the microstructure developed during heat treatment procedures applied on the DP800 samples.

- Higher intercritical annealing temperatures and longer soaking times can increase the volume fraction of hard second phase. For temperatures above 825°C, the microstructures are already too coarse to identify the presence of any ferrite in the predominately martensitic microstructure.

- Higher hardness, higher tensile strength, higher yield strength and lower elongation are obtained from the intercritically annealed and water quenched DP800 strips as the volume fraction of second phase is increased.

- At the lower annealing temperatures studied, e.g. 775°C and 800°C, the observed fracture characteristics of tensile tested samples exhibited ductile fracture facts. While at higher intercritical annealing temperatures, predominantly brittle fractures took place during tensile tests.

- For DP800 strip steels, a soaking time between 300s and 330s should be used to obtain the harder microstructures during intercritical annealing.

- For DP800 samples intercritically annealed at 775°C for 330s and followed by water quench, the optimum mechanical properties were obtained among all tested samples. These intercritically modified DP800 samples exhibited a yield strength of 477MPa, a tensile strength of 816MPa and a elongation of 16%. This compares favourable with the yield and tensile strength values of the as received DP800 samples, while retaining a reasonable elongation. Most important, the modified of

775°C DP800 strips have a ratio of $\delta_{0.2\%}$/UTS at approximate 0.58, which is less than the "ideal" DP ratio of 0.6.

7.0. REFERENCES

1. Rocha, R.O., et al., *Microstructural evolution at the initial stages of continuous annealing of cold rolled dual-phase steel.* Materials Science and Engineering a-Structural Materials Properties Microstructure and Processing, 2005. **391**(1-2): p. 296-304.
2. Rao, B.V.N. and M.S. Rashid, *Direct observations of deformation-induced retained austenite transformation in a vanadium-containing dual-phase steel (Reprinted from Metallography, vol 16, pg 19-37, 1983).* Materials Characterization, 1997. **39**(2-5): p. 435-453.
3. Saleh, M.H. and R. Priestner, *Retained austenite in dual-phase silicon steels and its effect on mechanical properties.* Journal of Materials Processing Technology, 2001. **113**(1-3): p. 587-593.
4. Takahashi, M., *Development of High Strength Steels for Automobiles.* Nippon Steel Technical Report, 2003. **88**.
5. Eberle, K., P. Cantinieaux, and P. Harlet, *New thermomechanical strategies for the production of high strength low alloyed multiphase steel showing a transformation induced plasticity (TRIP) effect.* Steel Research, 1999. **70**(6): p. 233-238.

6. G.R.Speich. *Physical Metallurgy of Dual-phase Steels*. in *Fundamentals of dual phase steels*. 1981. Chicago, IL: TMS-AIME.

7. Zaefferer, S., J. Ohlert, and W. Bleck, *A study of microstructure, transformation mechanisms and correlation between microstructure and mechanical properties of a low alloyed TRIP steel.* Acta Materialia, 2004. **52**(9): p. 2765-2778.

8. Shoujin Sun, M.P., *Properties of thermomechanically processed dual-phase steels containing fibrous martensite.* Materials Science and Engineering A-Structural Materials Properties Microstructure and Processing, 2002. **335**: p. 298-308.

9. Hong, S.C. and K.S. Lee, *Influence of deformation induced ferrite transformation on grain refinement of dual phase steel.* Materials Science and Engineering a-Structural Materials Properties Microstructure and Processing, 2002. **323**(1-2): p. 148-159.

10. Van der Zwaag, S., et al., *Thermal and mechanical stability of retained austenite in aluminum-containing multiphase TRIP steels.* ISIJ International, 2002. **42**(12): p. 1565-1570.

11. Erdogan, M. and S. Tekeli, *The effect of martensite particle*

size on tensile fracture of surface-carburised AISI 8620 steel with dual phase core microstructure. Materials & Design, 2002. **23**(7): p. 597-604.

12. Hillis, D.J., *Rapid Annealing of Dual Phase Steels*. 1999, University of Wales Swansea.
13. Haight, B., *Living in a material world: advanced technologies are opening doors for new materials - Product: Materials - materials in automotive industry - Industry Overview.* Automotive Industries, 2003. **April.**
14. Fan Yunchang, D.Z., QiHaibo, *Dual-Phase Steels and the Prospects for Their Applications in Manufacturing of Railway Stocks.* Journal of Shijiazhuang Railway Institute, 1999. **12**(3).
15. I. A. El-Sesy, Z.M.E.-B., *Influence carbon and/or iron carbide on the structure and properties of dual-phase steels.* Materials Letters, 2002. **57**: p. 580-585.
16. N.K.BALLIGER, D.J.N., C. DASARATHY, R.HUDD, A. JONES and J.D.HESSEY. *Developments in dual phase steels by the British Steel Corporation.* in *Advances in the physical metallurgy and applications of steels*. 1981. University of Liverpool: The Metals Society.
17. Eldis, G.T. *The Influence of Microstructure and Testing Procedure on the Measured Mechanical Properties of*

Heat-Treated Dual-Phase Steels. in *Structure and Properties of Dual-Phase Steels*. 1979. New York: AIME.

18. Rigsbee, J.M.a.V., P. J. *Laboratory Studies of Microstructures and Structure-Property Relationships in Dual -Phase Steels*. in *Formable HSLA and Dual-Phase Steels*. 1979. New York: AIME.
19. Dabkowsky, D.S.a.S., G. R. *Transformation Products and the Stress-Strain Behavior of Control-Rolled Mn-Mo-Cr Line-Pipe Steels*. in *Proc. Mechanical Working and Steel Processing Conf. XV*. 1977. New York: AIME.
20. Baird, J.D., *Strain Aging of Steel--A Critical Review.* Iron and Steel, 1963. **63**: p. 186-191.
21. U.Liedl, S.T., E.A Werner, *An unexpected feature of the stress-strain diagram of dual-phase steel.* Computational Materials Science, 2002. **25**: p. 122-128.
22. books, D.o.d., *Dialog on disk books*. 2001, The dialog corporation.
23. Andrews, K.W., *Empirical formula for the calculation of some transformation temperatures.* Journal of the Iron and Steel Institite, 1965. **July**: p. 721-727.
24. Steel, U.S., *Dual Phase Steel.* http://ussautomotive.com/auto/, 2005.

25. Datta, N.R.B.a.S., *Effect of Manganese Partitioning on Transformation Induced Plasticity Characteristics in Microalloyed Dual Phase Steels.* ISIJ International, 2004. **44**(5): p. 927-934.

26. Seung Chul BAIK, S.K., Young Sool JIN and Ohjoon KWON, *Effects of Alloying Elements on Mechanical Properties and Phase Transformation of Cold Rolled TRIP Steel Sheets.* ISIJ International, 2000. **41**(3): p. 290-297.

27. P. J. Jacques, E.G., A. Mertens, B Verlinden, J. van Humbeeck and F. Delannay, *The Developments of cold-rolled TRIP-assisted Multiphase Steels. Al-alloyed TRIP-assisted Multiphase Steels.* ISIJ International, 2001. **41**(9): p. 1068-1074.

28. DATTA, N.R.B.a.S., *Effect of Manganese Partitioning on Transformation Induced Plasticity Characteristics in Microalloyed Dual Phase Stells.* ISIJ International, 2004. **44**(5): p. 927-934.

29. Sun, S.J. and M. Pugh, *Manganese partitioning in dual-phase steel during annealing.* Materials Science and Engineering a-Structural Materials Properties Microstructure and Processing, 2000. **276**(1-2): p. 167-174.

30. Shunichi HASHIMOTO, S.I., Koh-ichi SUGIMOTO and

Syugo MIYAKE, *Effects of Nb and Mo Addition to 0.2%C-1.5%Si-1.5%Mn Steel on Mechanical Properties of Hot Rolled TRIP-aided Steel Sheets.* ISIJ International, 2004. **44**(9): p. 1590-1598.

31. S.YUE, A.Z.-H.a., *Ferrite Formation Characteristics in SI-Mn TRIP Steels.* ISIJ International, 1997. **37**(6): p. 583-589.
32. S. JIAO, F.H., R. L. DONABERGER, E. ESSADIQI and S. YUE, *The Effect of Processing History on a Cold Rolled and Annealed Mo-Nb Microalloyed TRIP Steel.* ISIJ International, 2001. **42**(3): p. 299-303.
33. M. De Meyer, D.V.a.B.C.D.C., *The Influence of the Substitution of Si by Al on the Properties of Cold Rolled C-Mn-Si TRIP Steels.* ISIJ International, 1999. **39**(8): p. 813-822.
34. Chang Gil Lee, S.-J.K., Tae-Ho Lee, Sunghak Lee, *Effects of volume fraction and stability of retained austenite on formability in a 0.1C-1.5Si-1.5Mn-0.5Cu TRIP-aided cold-rolled steel sheet.* Materials Science and Engineering A-Structural Materials Properties Microstructure and Processing, 2004. **371**: p. 16-23.
35. P. J. Jacques, K.E., Ph. Harlet and F. Delannay. *Development and Characterization of a Cold-Rolled Low Silicon*

TRIP-Assisted Multiphase Steel: a New Opportunity for the Automotive Steel Industry. in *40TH MWSP CONF. PROC., ISS.* 1998.

36. N.K.BALLIGER. *Ductile fracture of dual phase steels*. in *Advances in the physical metallurgy and applications of steels*. 1981. University of Liverpool: The Metals Society.